International
Progress Report

IPR-04-22

Äspö Hard Rock Laboratory

Prototype Repository

Hydromechanical behaviour of fractures due to excavation and thermal load

Ingvar Rhén
Patrik Alm

SWECO VIAK AB

May 2004

Svensk Kärnbränslehantering AB
Swedish Nuclear Fuel
and Waste Management Co
Box 5864
SE-102 40 Stockholm Sweden
Tel 08-459 84 00
+46 8 459 84 00
Fax 08-661 57 19
+46 8 661 57 19

Äspö Hard Rock
Laboratory

Report no.	No.
IPR-04-22	F63K
Author	Date
Patrik Alm Ingvar Rhén	2004-05-03
Checked by	Date
Lars-Olof Dahlström Rolf Christiansson	2004-05-25
Approved	Date
Christer Svemar	2004-10-07

Äspö Hard Rock Laboratory

Prototype Repository

Hydromechanical behaviour of fractures due to excavation and thermal load

Ingvar Rhén
Patrik Alm

SWECO VIAK AB

May 2004

Keywords: Fractures, fractures deformation, normal stress, transmissivity, THM-processes

Abstract

The Prototype Repository is an international, EC-supported activity with the objective to investigate, on a full-scale, the integrated performance of engineered barriers and near-field rock of a simulated Deep Repository. This is done in crystalline rock with respect to heat evolution, rock mechanics, water flow, water chemistry, gas evolution and microbial processes under natural and realistic conditions at approximately 450 m depth below the ground surface.

One of the issues that will be investigated is the hydromechanical behaviour of fractures in crystalline rock as a result of increased temperature induced by the electrical heaters, simulating heat generated from radioactive waste.

This report investigates if any significant response is to be expected during the heating phase. The hydromechanical behaviour of fractures is investigated by a literature review, a detailed study of a numerical modelling work and analytical calculations.

The modelling work gives a good picture of stress situation in the rock mass at different stages of the construction work and after 5 and 10 years of heating.

By using analytical relationship the change of fracture widths (due to the alteration of the principal stress) is calculated. The calculations consider the orientation of the fracture plane compared to the strike and dip of the principal stress.

Furthermore, the change of fracture transmissivity, as a result of change of fracture width, is also estimated.

The scoping calculations indicate that minor decrease in fracture transmissivity near the prototype tunnel can be expected due to increased mechanical stress caused by the increased temperature.

Sammanfattning

Prototypförvaret är ett internationellt, EC-stött projekt med syfte att i full skala undersöka den integrerade funktionen hos ingenjörsbarriärer och närfältsberg i ett simulerat slutförvar i kristallint berg med hänsyn till värmeutveckling, bergmekanik, vattengenomströmning, vattenkemi, gasbildning, och mikrobiologi under naturliga och realistiska förhållanden på ca 450 meters djup.

En av frågeställningarna som skall belysas är sprickors (i kristallint berg) hydromekaniska beteende till följd av den ökade temperaturen (från elektriska värmare) som simulerar värme som avges från radioaktivt avfall.

I den här rapporten utreds huruvida någon tydlig respons är att vänta under uppvärmningsfasen. Det hydromekaniska beteendet hos sprickor är belyst genom en litteraturstudie, en noggrann analys av ett numeriskt modelleringsarbete samt analytiska beräkningar.

Den numeriska modelleringen ger en god bild av spänningssituationen i bergmassan vid olika skede under byggandet och efter 5 respektive 10 års uppvärmning.

Med hjälp av analytiska samband har sprickviddsförändringar (till följd av förändringar av huvudspänningarna) beräknats.

Dessutom har förändringen i spricktransmissiviteten (till följd av ändrade sprickvidder) uppskattats.

Överslagsberäkningar indikerar att spricktransmissiviteten kan förväntas minska något i Prototyptunnelns närhet på grund av den ökade mekaniska spänningen orsakad av temperaturökningen.

Executive Summary

The Prototype Repository is an international, EC-supported activity with the objective to investigate, on a full-scale, the integrated performance of engineered barriers and near-field rock of simulated deep repository. This is done in crystalline rock with respect to heat evolution, rock mechanics, water flow, water chemistry, gas evolution and microbial processes under natural and realistic conditions at approximately 450 m depth below the ground surface.

The test site is a 65 m long TBM-bored drift from which six 1.75 m diameter deposition holes are extended downwards to about 8 m depth in accordance with the KBS-3 concept. The test site is divided in two parts, an inner 40 m long section (Section I) with 4 deposition holes and an outer section (Section II) with two deposition holes. Stiff and tight plugs will separate the sections and Section II from the rest of the Äspö Hard Rock Laboratory (ÄHRL).

A large number of boreholes have been drilled in order to characterize the rock mass. These boreholes will be used for the long-term monitoring of the Prototype Repository.

One of the issues that will be investigated is the hydromechanical behaviour of fractures in crystalline rock as a result of increased temperature due to the electrical heaters.

The scopes of this report are mainly three:

- Summarise the state of the art concerning Thermo-, Hydro-and Mechanical processes (THM-processes) related to fractures in crystalline rock.
- Estimate, by using data from a numerical model, the hydromechanical effects on the fractures due to excavation and thermal load.
- Evaluate, if any, relevant responses would affect a forthcoming repository.

The heat from the spent fuel will cause an expansion of the rock mass that will increase the stresses. As a result of the expansion the fractures will be exposed to compression forces, which tend to close the fractures (fracture deformation) and thereby reduce the ability to transmit water.

A typical fracture deformation curve can be described by a logarithmic or a power function, i.e. the fracture will become stiffer and stiffer the further the loading continues.

The deformation is a function of:

- Applied stress
- In-situ stresses before any changes
- Conditions of the fracture surfaces such as:
    - Contact area
    - Spatial geometry of the contact area
    - Roughness
    - Presence of fracture filling
    - Mated or unmated surfaces
- Rock type

The literature shows that a change in effective stress has a significant influence on the hydraulic properties of the fracture.

Numerical modelling

Four different stages for inducing stress changes during the construction and running of the prototype repository were studied with numerical modelling. These stages are:

1. After completing the tunnel excavation.
2. After completing the tunnel excavation and a deposition hole.
3. After completing the tunnel excavation and a deposition hole and 1 year of heating.
4. After completing the tunnel excavation and a deposition hole and 10 years of heating.

The effect of the excavation and heating decrease the longer out from the tunnel and heater the observation point is. The effect also depends on which principal stress is considered and where the observation point is positioned in space in relation to the tunnel and heater.

Results from the numerical modelling are used as input in the analyses of the fracture behaviour.

Estimate of hydromechanical effects

In order to estimate the hydromechanical effects, the magnitudes of the principal stresses from the numerical modelling are used. For this purpose three fictitious boreholes are placed in different directions in the rock mass (see Figure 1). At five points (with increasing distance out from the tunnel wall/floor) the magnitudes of the principal stresses are obtained by studying the results from the numerical modelling.

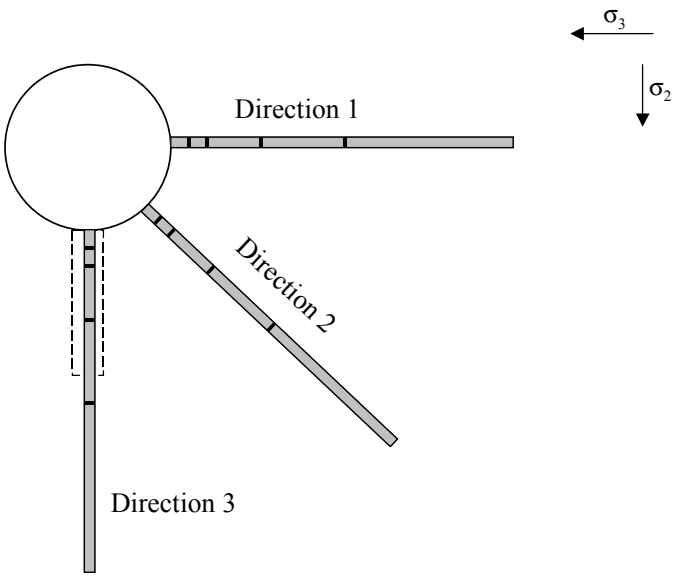

Figure 1. *The figure shows the three fictitious boreholes. The dark lines represent the "observation points" at 1, 2, 5,10 and 20 metres out from the tunnel wall.*

The different effective stress levels after stage 4 are summarised in Table 1. It is notable that the increases of each principal stress from in-situ stress are in the same range independent of which direction is considered.

Table 1. A summary of the effective stress levels (after stage 4) obtained from the analyses of the numerical modelling done by Claeson et al. (2001).

	σ'_1 [MPa]	σ'_2 [Mpa]	σ'_3 [MPa]
Direction 1	56-64	38-44	14-32
Direction 2	56-66	36-44	15-36
Direction 3	56-90	36-45	16-36

The deformation depends, among other things, on the magnitude of increase of the thermally induced stress and the in-situ stresses, i.e. it is not obvious which fracture plane (according to the orientation) that will be exposed to the largest deformation.

Three cases have been chosen in order to estimate the fracture deformation and the changes in transmissivity. The three fictitious fractures and their relation to the principal stress are:

1. Vertical fractures which strikes perpendicular to the maximum principal stress. The normal stress to these fractures is the maximum principal stress (see Figure 2 a).
2. Vertical fractures which strikes parallel to the maximum principal stress. The normal stress to these fractures is the minimum principal stress (see Figure 2 b).
3. Horizontal (or sub-horizontal) fractures where the intermediate principal stress acting as the normal stress to the fracture plane (see Figure 2 c).

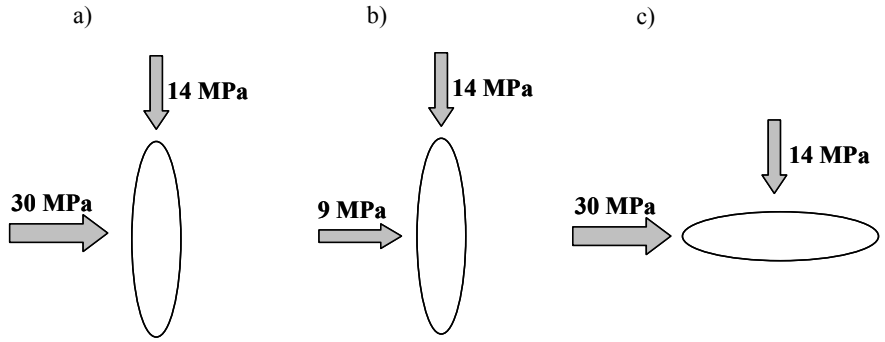

Figure 2. *Three cases that are considered when the fracture deformation and hydraulic change are estimated.*

The estimation of the mechanical responses are made by using a relationship where the fracture deformation ($\Delta\delta$) is described as a logarithmic closure law (a function of fracture stiffness (K_n) and effective stress (σ')), and the transmissivity (T) change expressed as function of the change in effective stress (σ_0'= initial level):

$$-\Delta\delta = \left(\frac{dK_n}{d\sigma'}\right)^{-1} \ln\left(\frac{\sigma'}{\sigma_0'}\right)$$

$$\frac{T}{T_0} = \left(\frac{\sigma'}{\sigma_0'}\right)^{-\beta}$$

In Figure 3 the relationships are plotted. The different curves in the deformation plot represent different values of the fracture stiffness and the values of β represent the minimum value (0.2), maximum (2.0) and an intermediary value (1.0) in the transmissivity plot. In the figure the factor β is denoted with the letter B.

A detailed analyse of each observation point in each direction is reported in Appendix A.

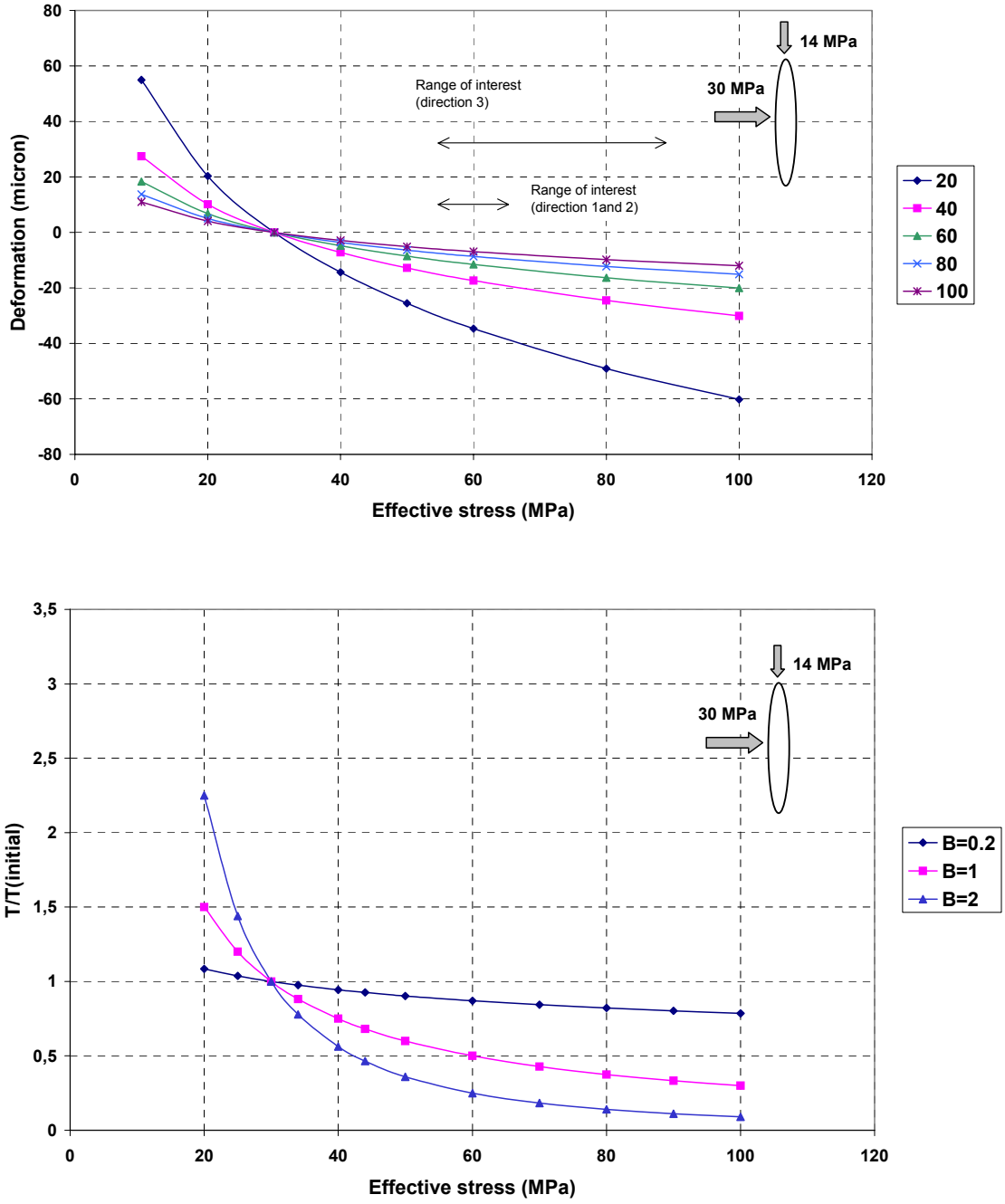

Figure 3. *Mechanical and hydraulic response due to a change in stress. The responses refer to a fictious fracture that strikes perpendicular to the maximum stress (30 MPa). "Range of interest" corresponds to the final stress level after 10 years.*

At this stage the predictions are uncertain since values of the fracture stiffness are based on values from the literature. In Table 2 the predicted fracture deformation for all observation points is summarised. The predicted fracture deformation for fractures that strike perpendicular to σ_2 and σ_3 is in the same range. Slightly larger are the prediction concerning fractures that strike perpendicular to σ_1.

Table 2. Summary of the expected effective stresses after 10 years of heating as well as the fracture deformation and change in transmissivity that will occur at fracture that strikes perpendicular to each principal stress.

	σ_1	σ_2	σ_3
Direction 1 [MPa]	56-64	38-44	14-32
Direction 2 [MPa]	56-66	36-44	15-36
Direction 3 [MPa]	56-90	36-45	16-36
Expected deformation [μm]	20-65	10-50	5-70
Expected change in transmissivity [T/T(initial)]	0.1- 0.9	0.1- 0.8	0.2- 0.9

The conclusions are:

- The hydraulic response will in general be decreased transmissivity. The decrease will be larger the closer the fractures are to the canisters.
- The transmissivity will be reduced to something between 10 and 80 percent of the in-situ values.
- The fracture closure will be in the range of 5-70 micrometer.
- The hydraulic and mechanical responses on the fracture depend on the orientation of the fracture relative the stress field.
- Major part (~80%) of the increase in stress and temperature is reached within two years.

The temperature load will be uniformly distributed in the rock mass. This implies that the ratio between σ_1 and σ_3 will be more or less constant and the risk of shearing will be low in the rock mass.

Contents

List of Figures

List of Tables

1 Introduction

The Äspö Hard Rock Laboratory is an essential part of the research, development and demonstration work performed by SKB in preparation for construction and operation of the deep repository for spent fuel. Within the scope of SKB:s programme for RD&D 1995, SKB has decided to carry out a project with the designation "Prototype Repository Test". The aim of the project is to test important components in SKB:s deep repository system in full scale and in a realistic environment.

The Prototype Repository Test is focused on testing and demonstrating the function of SKB:s deep repository system. Activities aimed at contributing to development and testing of the practical, engineering measures required to rationally perform the steps of a deposition sequence are also included. However, efforts in this direction are limited, since these matters are addressed in the Demonstration of Repository Technology Project and to some extent in the Backfill and Plug Test.

1.1 Scope of this report

The scopes of this report are mainly three:

- Summarise the state of the art concerning Thermo-, Hydro-and Mechanical processes (THM-processes) related to fractures in crystalline rock.
- Estimate, by using data from a numerical model, the hydromechanical effects on the fractures due to excavation and thermal load.
- Evaluate if any relevant responses would affect the prototype test.

1.2 Stress increase in the rock mass due to the heat from the spent fuel

The heat from the spent fuel will cause an expansion of the rock mass that will increase the stresses. As a result of the expansion the fractures will be exposed to compression forces, which tend to close the fracture and thereby reduce the ability to transmit water.

The mechanical behaviour of a fracture have been investigated in laboratory scale by many researches e.g. Goodman (1976), Bandis et al. (1983), Witherspoon et al. (1980), Raven & Gale (1985) and Sun et al. (1985). Typical stress-deformation curves are shown in Figure 1-1.

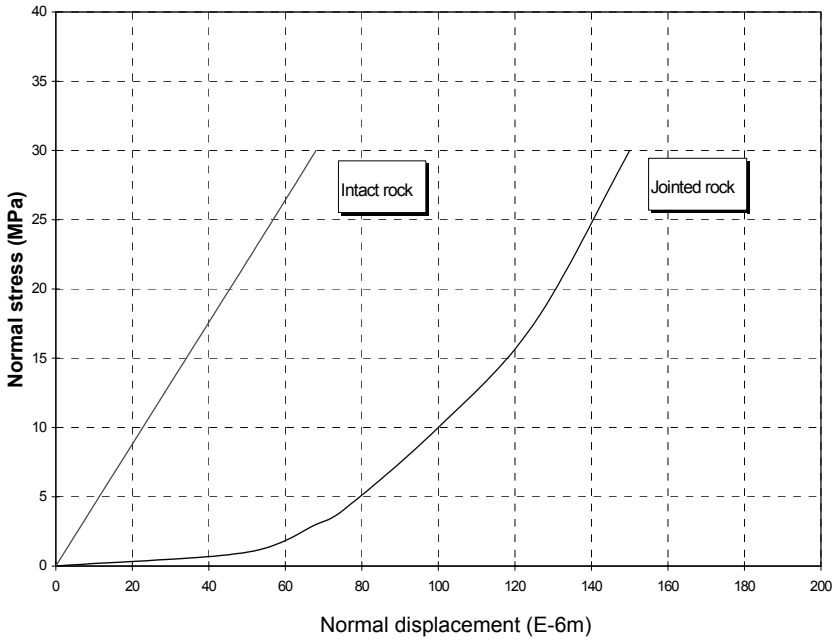

Figure 1-1. *Typical normal stress-deformation curves for a core with a fracture and a core of intact rock, respectively (after Tsang and Witherspoon, 1981).*

At low stresses the deformation modulus for jointed rock is much lower than for intact rock. With increased stress the modulus increases and approaches the value of the intact rock.

The difference in deformation behaviour between intact rock and jointed rock is explained by the topology and deformation characteristic of the fracture surfaces. Fractures consist of two rough opposite surfaces. The roughness is composed of asperities of varying heights. Where these asperities stay in contact (with the opposite surface) a contact area is created (see Figure 1-2).

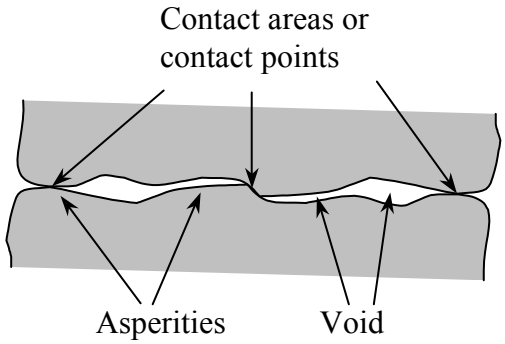

Figure 1-2. *A schematic figure of a fracture*

Two different conceptual models (of fracture deformation) are found in the literature. The first one interpreted the deformation as deformation of the contact points (see Figure 1-3) while the second models interpreted it as deformation of the voids between the contact points (see Figure 1-4).

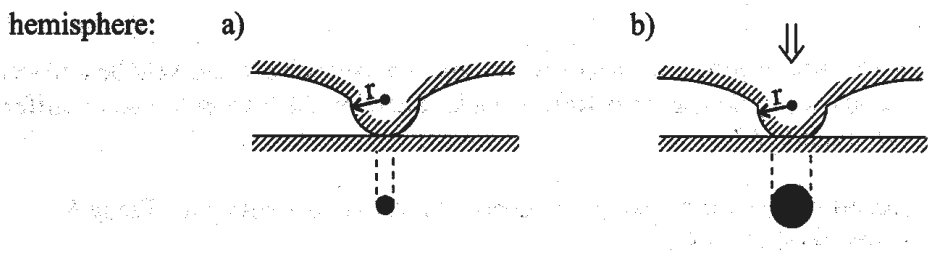

Figure 1-3. *A conceptual model of how the contact points will deform during a loading phase (modified after Alm, 1999)*

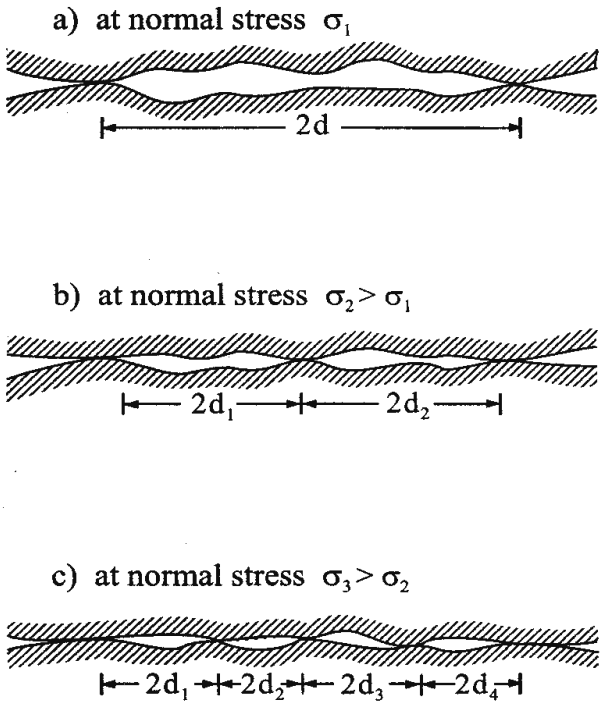

Figure 1-4. *Deformation of voids in a sequence of increasing normal stress (after Tsang & Witherspoon, 1981)*

The actual deformation of a fracture exposed to a load has been well known for a long time even if discussions continue regarding the conceptual description. The last decade great efforts have been made to investigate of the effects of coupling temperature gradient, hydrologic flow and mechanical deformation in fractured rock, e.g. Stephansson et al (1996). The increase in interest of these problems is due to the concern of solute transport through a rock mass hosting a heat-releasing nuclear waste repository.

Temperature (T), hydraulics (H) and mechanical deformation (M) are closely linked to each other. For example, if the temperature increases in the rock mass it will cause an expansion of the rock mass that will cause stress increase and possible deformation of fractures, which will reduce the fluid flow.

Some laboratory tests indicate that the deformation modulus is dependent of the temperature. The modulus decreases while the temperature increase. That implies that if a fracture is subjected to a constant load the deformation will increase if the specimen is heated.

1.3 Basic definitions and concepts

Stresses:
The stresses, which exist in an undisturbed rock mass, are related to the weight of the overlying strata and the geological history of the rock mass. Amadei & Stephansson (1997) did a resume of different types of rock stresses and their origin (see Table 1:1).

Table 1:1. Classification of rock stresses according to Amadei & Stephansson, 1997.

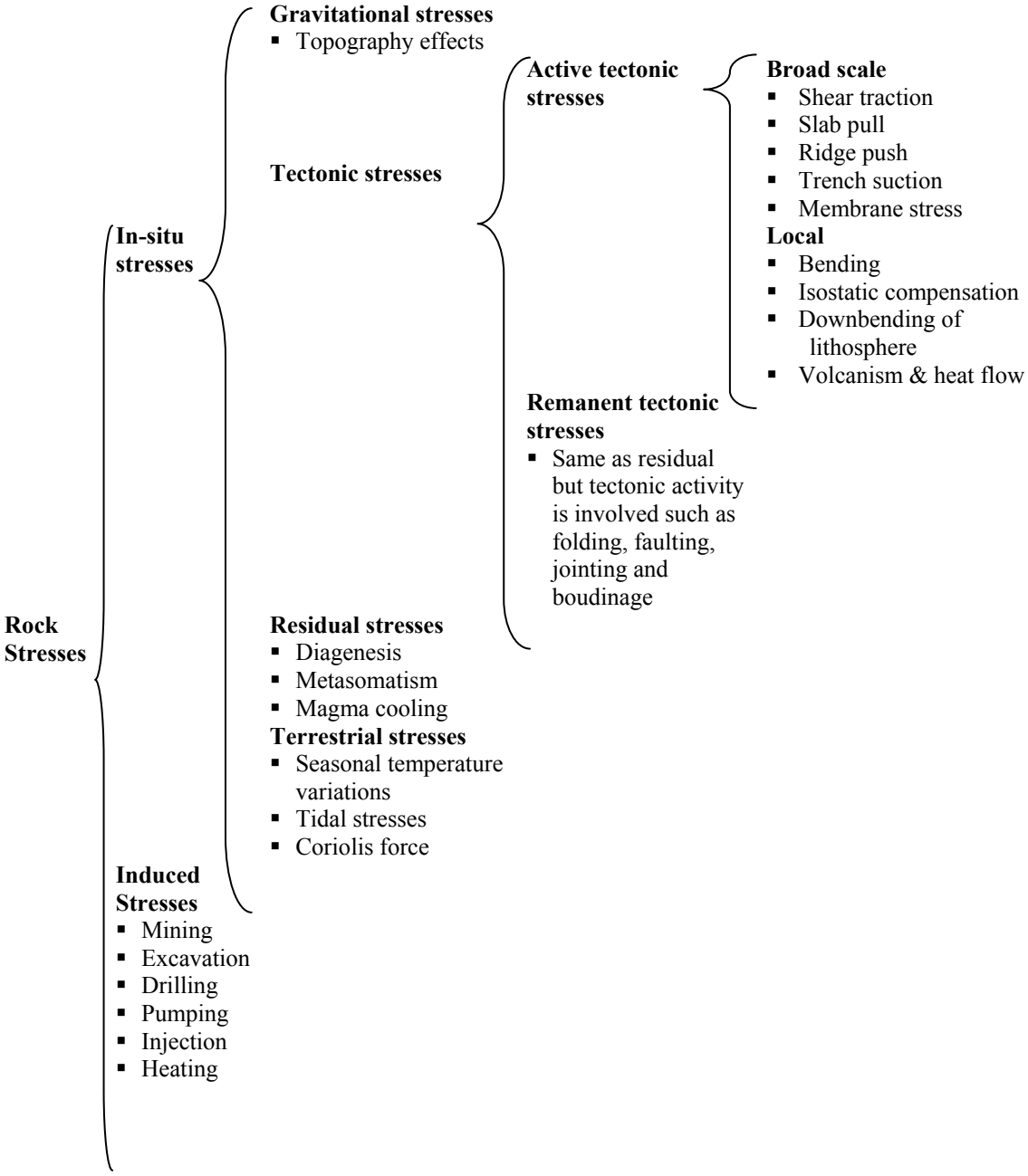

The rock mass is normally intersected by fractures in different directions. If a rock core with a fracture is exposed to a loading test, the stresses will be affected and, as a result, a deformation will take place. The value of the deformation depends on the magnitude of the stresses and the stiffness of the fracture (see Figure 1-5).

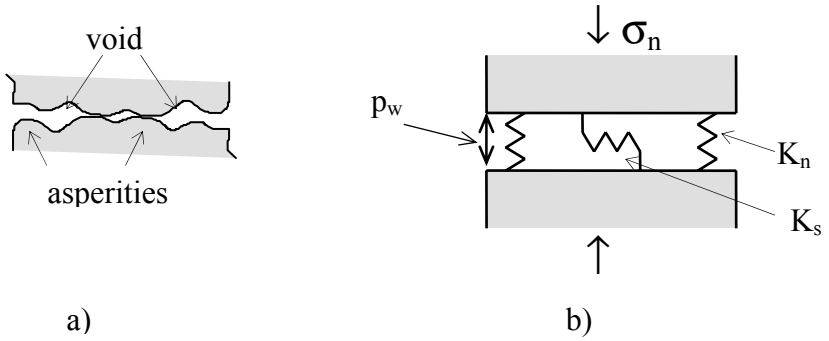

Figure 1-5. *a) A schematic and b) a conceptual model of a fracture (modified after Alm, 1999).*

The relationship between stress, stiffness and deformation can be expressed as (Bandis et al., 1983):

$$\begin{pmatrix} \sigma_n \\ \tau \end{pmatrix} = \begin{vmatrix} K_n & 0 \\ 0 & K_s \end{vmatrix} \begin{pmatrix} u_n \\ u_s \end{pmatrix} \qquad \textbf{Eq. 1-1}$$

where σ_n= normal stress [MPa]

τ = shear stress [MPa]

K_n = normal stiffness [MPa/ mm]

K_s = shear stiffness [MPa/ mm]

u_n = normal displacement [mm]

u_s = shear displacement [mm]

Normal and shear stiffness:
The normal and shear stiffness measures the amount of force necessary to produce a closure or a lateral movement between two fracture surfaces.

Thermal expansion coefficient:
The thermal expansion coefficient for intact rock (crystalline rock) is approximately 8×10^{-6} /°K.

Effective stress:
When the stresses are transferred from one block to another the stresses can be reduced if the fracture contain water. This is described by the effective stress concept. The effective stress, σ'_n, can be expressed as:

$$\sigma'_n = \sigma_n - \alpha\, p_w \qquad \textbf{Eq. 1-2}$$

where σ_n= normal stress [MPa]

p_w = fluid pressure [MPa]

α = fraction of fracture surface acted on by fluid pressure [-]

Young's modulus and rock mass modulus:
Since this report consider the deformation behaviour of intact rock as well as fractures it is necessary to distinguish the difference between Young's modulus and rock mass modulus (see Figure 1-6).

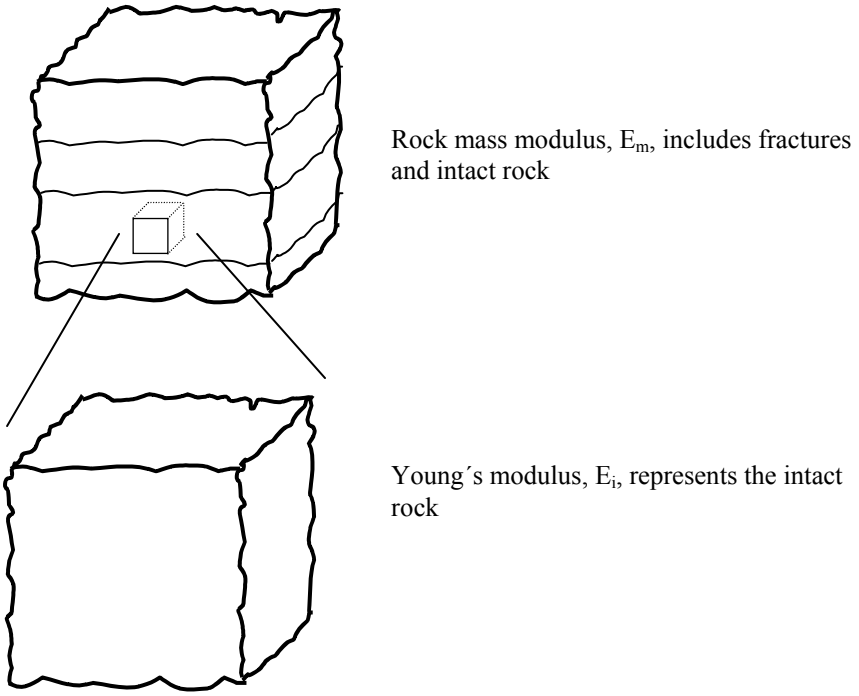

Figure 1-6. *A schematic figure that shows the difference between Young´s modulus and rock mass modulus.*

The difference between Young´s modulus and deformation modulus is that the fracture stiffness is included in the deformation modulus while the Young´s modulus represents the intact rock.

2 State of the art

The aim with this chapter is to make a short résumé of some laboratory as well as field tests concerning mechanical and hydromechanical behaviour of fractures (mainly in crystalline rocks) due to a change in stress level. The review will also pay attention to tests where thermal load has been studied.

The literature review will be focused on the following question: Does a change in effective stress caused by the thermal load, affect the conductivity of a fracture, or can it be neglected?

2.1 Literature review

Witherspoon et al. (1980) performed a number of hydromechanical laboratory tests on artificial fractures (created in the laboratory) in basalt, granite, and marble. The flow tests were performed with radial flow in cylinders and linear flow in block. When the samples were loaded with a successively increased load the fracture deformed non-linearly. The main part of the deformation took place in the beginning of the loading phase. They concluded that the cubic law was valid at these circumstances. The applied load was successively increased up to 20 MPa and the fracture apertures (estimated by cubic law and by closure measurements) were between 4 and 250 μm.

Sun et al. (1985) did compression and shear tests on fractures from granite and slate. Their results were in accordance the results obtained by Witherspoon et al. (1980). For example, the fracture becomes more and more stiff the further the normal loading continues. They described the behaviour with two explanations

1. for points initially in contact, the actual contact area increase during the loading phase, and
2. new points will successively brought into contact.

Furthermore they also noticed that fractures with larger aperture are less stiff than fractures with smaller apertures.

The magnitude of the normal displacement, due to shearing, is dependent of the normal stress. If the normal stress is low the normal displacement will be larger compared to if a higher normal stress is subjected to the fracture (see Figure 2-1). This is due to that the asperities seemed to ”climb” up on each other while the asperities will be sheared if the normal stress is high. Increasing normal stress increases the shear strength and increases the shear stiffness.

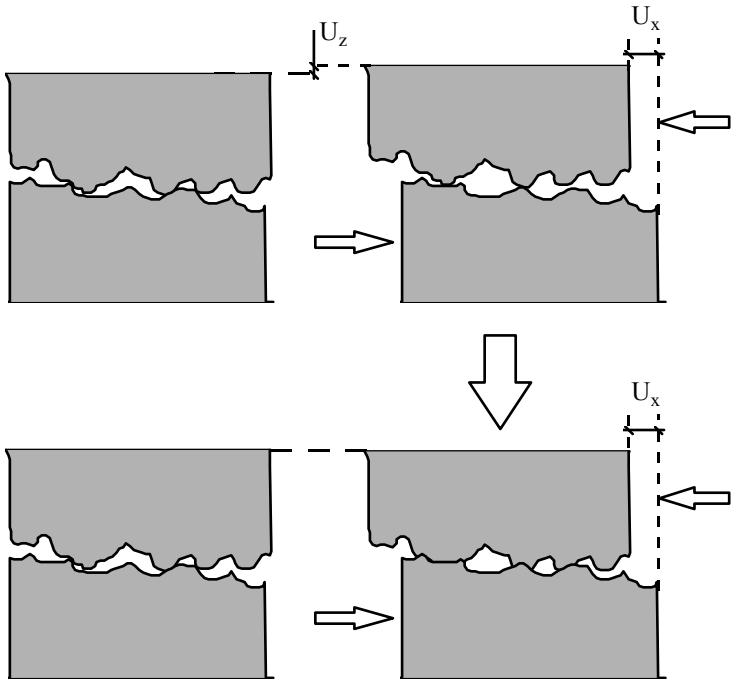

Figure 2-1. *Schematic figures that shows the effect of high and low normal stress at shearing.*

Yeo et al. (1998) conducted flow tests (both radial and linear) in rock fracture replicas made from epoxy resin. They performed the flow tests during different stages of shearing (0, 0.1 and 2.0 mm shear displacement). When the two surfaces moved relative each other they were allowed to "climb" i.e. no damages of the asperities occur. Application of the results on crystalline rock should be done with caution since they did their tests on replicas. Nevertheless, some of their conclusions are interesting:

- The number of contact points and contact area decreased successively during shearing.
- With increasing shear displacement, mean aperture and the standard deviation increased.
- Flow tests showed that with increasing shear displacement, the fracture become more permeable in the direction perpendicular to the shear displacement than in the direction parallel to the displacement.

Ahola et al. (1996) did a short résumé of a number of papers and they draw some general conclusions, namely:

- Normal loading of fractures creates little gouge material due to crushing of asperities compared to shear loading.
- Shear displacement has a much greater influence on fracture permeability than normal displacement. This is due to dilatancy and asperity degradation.
- Gouge formation may in same cases restrict the flow, thus reducing the hydraulic conductivity even though the fracture is undergoing dilation.
- The amount of asperity degradation and subsequent gouge production is dependent of the mechanical properties of the fracture as well as the applied load.

Furthermore Ahola et al. (1996) reported a laboratory test carried out at CNWRA (Centre for Nuclear Waste Regulatory Analyses, San Antonio, Texas). The test specimens were blocks of welded tuff with size of approximately 0.3x 0.2x 0.1 m^3 (note, the sheared area remained constant during the tests). The aim of the tests was to investigate the effects of coupled shear-flow tests under normal load of 2.0, 4.0, and 5.0 MPa. At each load phase the specimen was exposed to four shear cycles. During each shear cycle, the top block was sheared approximately 2.54 cm in forward direction followed by shearing in reverse direction back to the initial zero point. Some of the conclusions were that the joint dilation decreased with shear cycle, probably due to asperity degradation. During the forward shear movement the results show a clearly increase in hydraulic conductivity. After the reverse shear movement (to the initial zero point) at each cycle the hydraulic conductivity was significantly higher than at the start of the cycle.

Makurat et al (1990) performed both shear and conductivity tests on natural joints for different types of rock. They concluded that a relatively small shear displacement is enough to dilate hard rocks and thereby increase the fracture conductivity up to two orders of magnitude. They found out that the main parameters of importance were uniaxial compressive strength of the intact rock, joint compressive strength (JCS), joint roughness coefficient (JRC), normal stress, and shear displacement.

Experiments were conducted by Esaki et al. (1991) to investigate the shear-dilation-flow characteristics of granite fractures. Results show that the hydraulic conductivity increase by about one order of magnitude for the first 5 mm of shear displacement. The shearing continues up to 20-mm displacement, but this further shearing caused just a slightly increase in hydraulic conductivity. During reverse shearing, the hydraulic conductivity was found to be slightly lower than that during forward shearing (this conclusion is in accordance with experience reported by Ahola et al. (1996).

In the early 1980´s Terra Tek Engineering performed a THM in-situ test in an experimental mine belonging to the Colorado School of Mines, USA (Hardin et al., 1982). A number of tests were conducted on an 8-m^3 test block of granitic gneiss. The 2x2x2m block was released on all four vertical sides. Flatjacks were grouted in the slots.

The block consist of a sub-vertical joint set with a average spacing of 0.75m and foliation joints which strike is separated approximately 40° compared to the sub-vertical joints. The average spacing of the foliation joints is 0.60m. Five vertical boreholes were drilled along a centre line. Heaters were placed in these boreholes. The THM processes were registered in one sub-vertical fracture that strikes across the centre line.

The 8m^3 block was exposed to both biaxial stress and uniaxial stress. Four biaxial loading cycles (0 up to 6.9 MPa) were performed at an in-situ temperature of 12 °C, after latest loading cycle the temperature was increased in three steps (41, 56 and 74°C) while the stress was kept constant at 6.9 MPa. During this temperature increase the hydraulic aperture was decreased from 30.0 microns to 9.1 microns (see Figure 2-2). This indicates that the temperature increase itself will cause deformation of the fracture even if the stress is constant i.e. reduced deformation modulus.

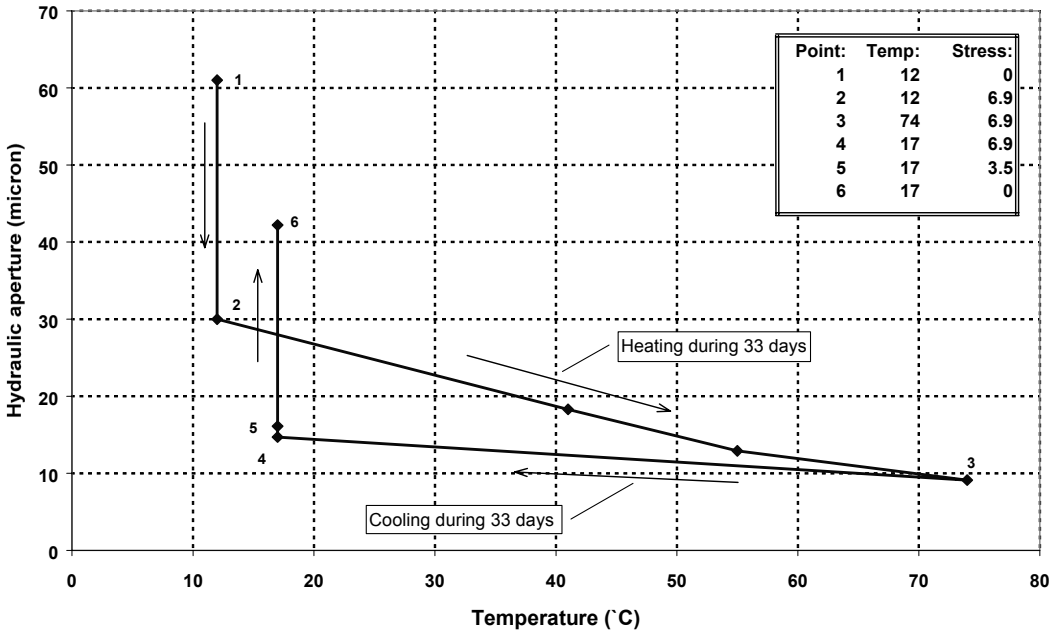

Figure 2-2. *A graphical presentation of the tests performed by Terra Tek in a mine belonging to the Colorado School of Mines, USA (after Hardin et al, 1982)*

If the hydraulic apertures are converted to fracture transmissivity and the relative decrease in fracture transmissivity is plotted the results showed that the transmissivity is decreased to approximately 15 % of the in-situ transmissivity (see Figure 2-2 and Figure 2-3).

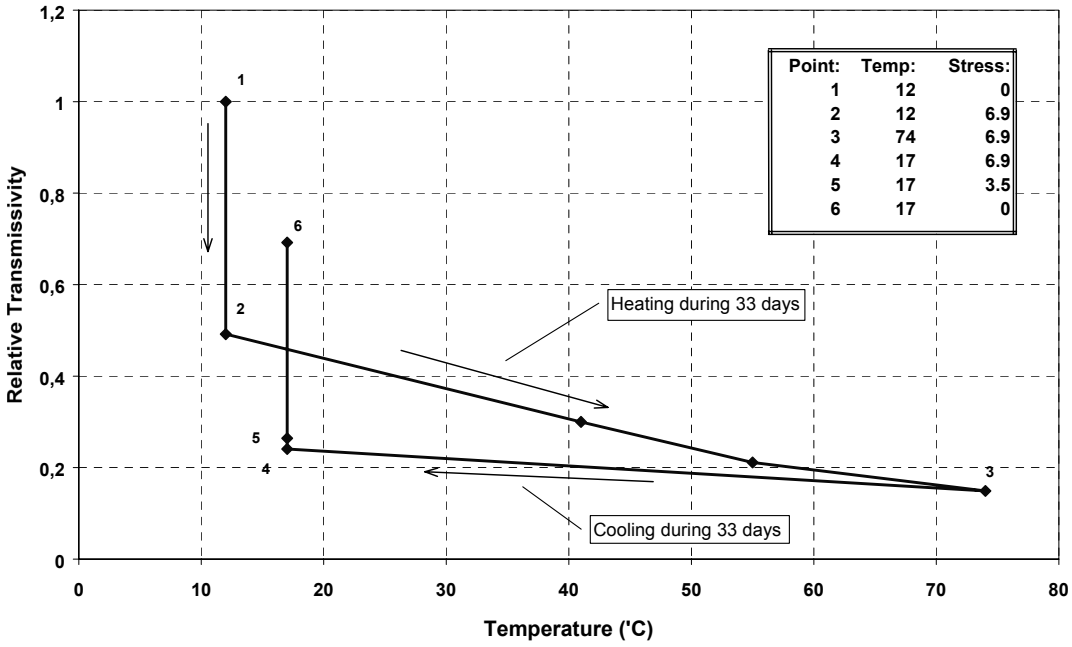

Figure 2-3. *The figure shows the change in relative fracture transmissivity during the different steps in the test (based on data from Figure 2-2).*

Samples cored from the block were triaxially tested in laboratory in order to investigate the relationship between the Young's modulus and temperature. The result shows that Young's modulus decrease during increase of temperature. With a confined stress of 6.9 MPa the modulus decreased from almost 69 GPa at 20°C to roughly 64 GPa at 140°C. The decrease is linear in this temperature range. These tests show that a relationship between the hydromechanical behaviour and the change in temperature as well as in stress exist.

Zhao (1993) reported some tests (TH) that were performed at Imperial College. The tests were conducted on natural fractures as well as artificially induced tension fracture in Carnmenellis granite. He states that the initial hydraulic aperture, e_0, is a function of temperature, T (°C). The relationship between temperature, initial hydraulic aperture and hydraulic aperture at elevated temperature, e_t, lies within the limits expressed:

$$0.0033\ \Delta T \leq \left(\frac{e_0 - e_t}{e_0} \right) \leq 0.0072\ \Delta T \qquad \textit{Eq. 2-1}$$

Dershowitz et al. (1991) summarised a number of laboratory studies concerning normal stress versus transmissivity. When the results of these tests were plotted the authors concluded that a change in normal stress generally produces changes in transmissivity according to the relationship expressed as:

$$\frac{T}{T_0} = \left(\frac{\sigma'}{\sigma'_0} \right)^{-\beta} \qquad \textit{Eq. 2-2}$$

Where T_0 is the fracture transmissivity [m^2/s] at a reference normal effective stress level, σ'_0 [MPa], and T is the transmissivity corresponding to the new normal effective stress level, σ' β is a coefficient which varies from 0.2 to 2.0 and with reasonable value of 1.0 according to Dershowitz et al. (1991) (see Figure 2-4). Experiences from field tests where hydraulic tests have been performed with different injection pressure shows that β can be more than 2 (e.g. Jung, 1989; Alm, 1999).

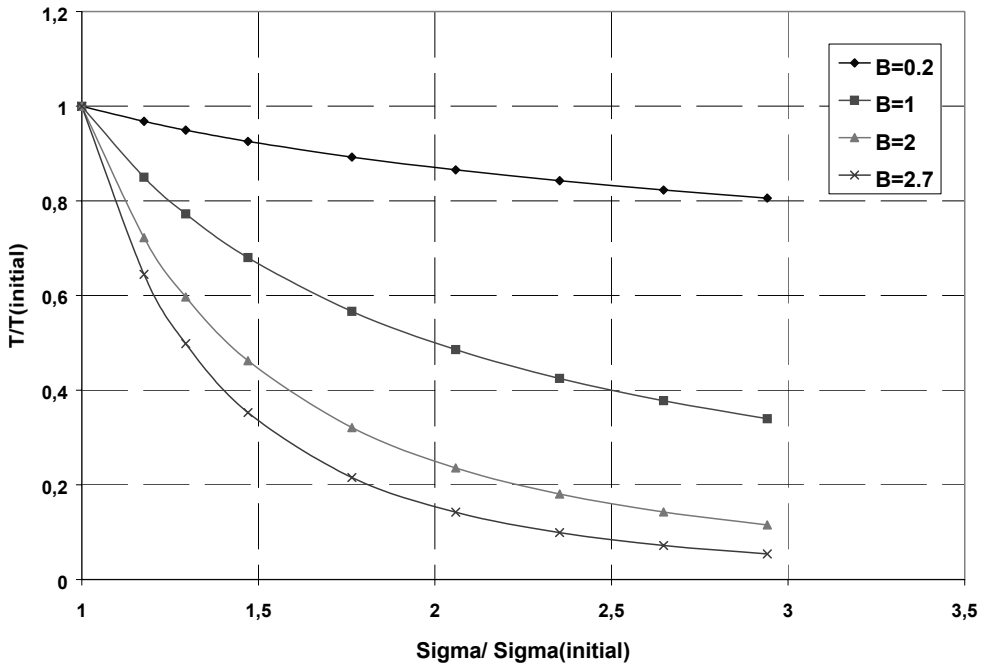

Figure 2-4. *The relationship between transmissivity and normal effective stress according to Dershowitz et al. (1991). Note that* B=β *and* Sigma=σ' *in Eq. 2-2.*

2.2 Experiences from other test sites

Several countries have during the last decades conducted field tests concerning disposal of nuclear waste. The field tests should simulate as many aspects as possible a real repository for example regarding geometry, materials, and rock environment.

Two of the field test projects are presented hereafter namely, Kamaishi mine in Japan (Chijimatsu et al. 1999) and Febex in Grimsel, Switzerland (FEBEX 2000).

2.2.1 Kamaishi mine, Japan

The Kamaishi mine is located 600 km north of Tokyo, Japan. The bedrock consists of sedimentary bedrock and igneous complexes. The test site is situated 260 metres below the surface (550m above sea level) in granodiorite. The principal stresses have been evaluated by using overcoring. The results from three boreholes placed at the test site are:

$$\sigma_1 = 19.2 \text{ MPa} \qquad \sigma_2 = 17.1 \text{ MPa} \qquad \sigma_3 = 6.0 \text{ MPa}$$

In the test site one deposition hole was excavated (1.7 m in diameter and 5.0 m in depth) and surrounded by fourteen boreholes planned for various sensors. In the deposition hole a heater, embedded in bentonite, was installed. The maximum temperature of the surface of the heater was 100 °C and was reached after 2-3 days. The temperature was kept constant throughout the whole heating phase. Duration of the heating phase was 260 days and the cooling phase was 180 days.

The temperature was measured in 63 different points in the rock mass. The temperature distribution in the rock mass, after 260 days, is showed in Figure 2-5.

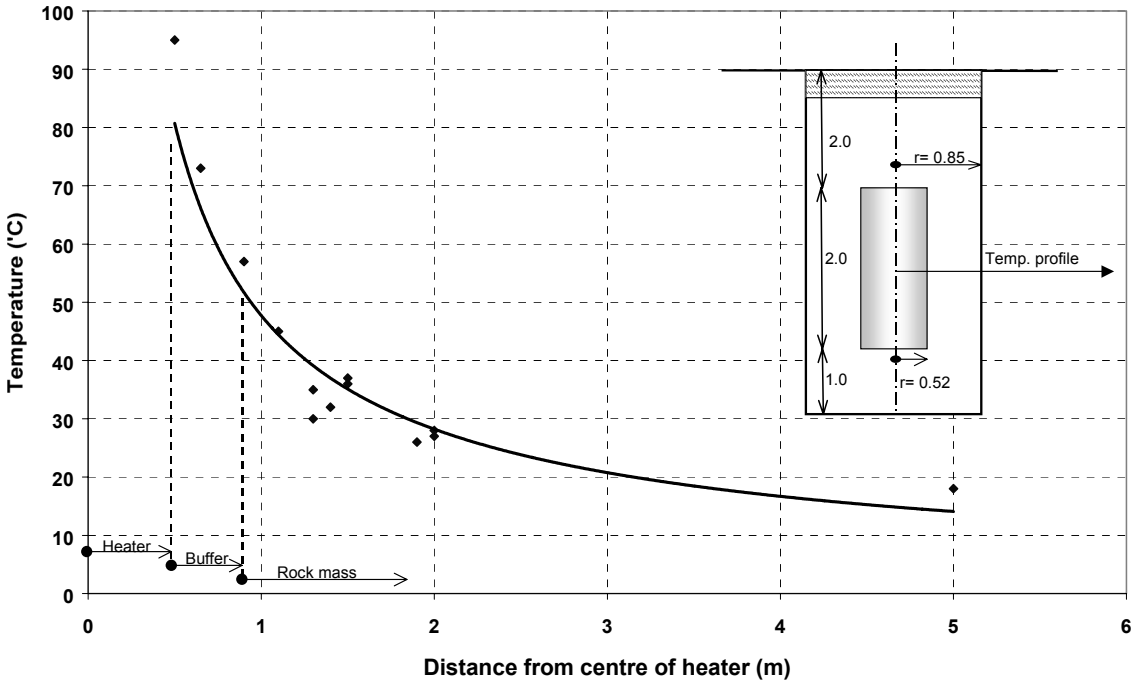

Figure 2-5. *Measured temperature profile in the rock mass at Kamaishi test site. The values represent the situation after 260 days of heating. The temperature on the surface of the heater was almost 100 °C and was reached after 2-3 days.*

Close (1.75 m) to the deposition hole two fractures were equipped with joint deformeters, which measured the displacement in two directions. The maximum closure of the fracture due to the heating was 0.2 mm. No information of the change in stress field was found in Chijimatsu et al. 1999.

The main conclusions, from a hydromechanical point of view, which are listed in the report, are:

- The rock was compressed both along the radial direction and vertical direction of the deposition hole.
- It was confirmed that the fractures were closing as a result of the thermal expansion of the rock mass.
- During the cooling phase the strain in the rock mass shows decompression and the fractures reopened.

2.2.2 FEBEX, Grimsel (Switzerland)

The FEBEX (Full-scale Engineered Barriers Experiment) project is aimed to demonstrate the technical feasibility and study the behaviour of near-field components of a high level radioactive waste repository in crystalline rock. The project is divided into three sub-projects whereas one concerns a full-scale test in Grimsel, Switzerland (FEBEX, 2000). The data considered is for period 1997-1999 but the project is still in operation.

The test site in Grimsel is situated 400 meters below ground surface at an elevation of 1700 meters in the Swiss Alps. The rock mass is dominantly granite and granodiorite. In the full-scale test two heaters (length: 4.54 m, diameter: 0.90 m) are placed (in a horizontal position) in a TBM-tunnel (diameter: 2.28m). The heaters are embedded in bentonite and the whole test zone is closed with a concrete plug (see Figure 2-6).

In the FEBEX test the duration of the first heating phase was three years. The power supply to the heaters was increased in three steps. During the third step the predestined temperature was reached and the power supply was reduced in order to maintain a constant temperature on the heater surface. The predestined temperature of 100 °C on the heater was reached after barely two months.

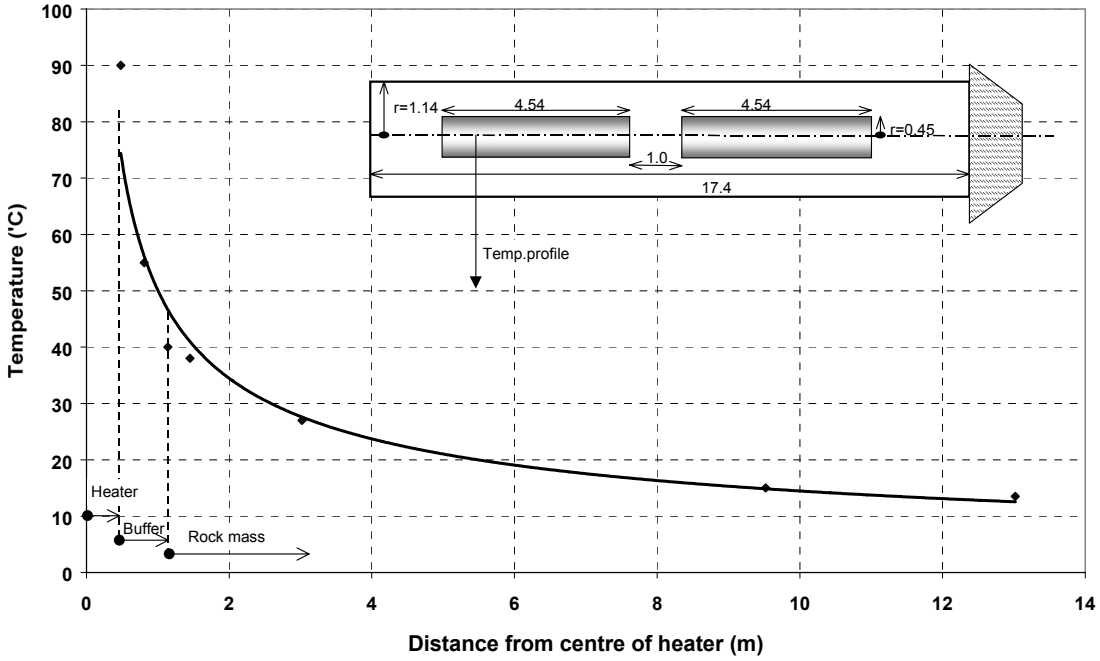

Figure 2-6. *Measured temperature profile from the test site in Grimsel, Switzerland. The temperature on the heater (100 °C) was reached after less than two months. The data are from borehole SF22, 660 days after the heater was started.*

Some of the main conclusions from the FEBEX tests are:

- The thermal field does not appear to be axisymmetric around the drift.
- Displacements in the rock mass were in general overestimated in the prediction work compared to the measured values in the test.

2.3 Fracture deformation/closure

From the literature it is well known that fractures respond to changes in stresses acting on the fracture. It is of great interest to find a reliable method to describe the closure behaviour in order to make it possible to predict the magnitude of the closure as well as the closing process.

Today there are mainly three different approaches to establish a relationship between stress and deformation. The first approach is based on laboratory tests where deformation versus stress is plotted in a diagram. To the data points a curve is fitted and the curve will represent the deformation behaviour of the fracture. In the second approach the relationship includes the condition of the fracture surfaces and laboratory tests results of deformation. In general, the surfaces are described by statistical analyses of the roughness, the aperture variation or the spatial distribution of the contact points (e.g. Swan, 1983; Tsang & Witherspoon, 1981; Pyrak-Nolte & Morris, 2000). These models require detailed analyses of the surfaces. The third approach is based on numerical modelling.

In this section (and report) attention will be paid to the first approach in order to make a rough analytical estimation of the fracture behaviour.

When the relationship between stress and deformation is plotted and a curve is matched to the data points it appears that, for example, a logarithmic or an exponential curve fits very well (e.g. Sun et al., 1985; Zhao & Brown, 1992; Elliott et al., 1985). The relationships can be expressed as (e.g. Sun et al., 1985):

$$\delta = a_0 + a_1 \ln \sigma \qquad \textit{Eq. 2-3}$$

or,

$$\delta = b_0 \sigma^{b_1} \qquad \textit{Eq. 2-4}$$

Where δ = deformation of the fracture
σ = stress
a_0, a_1, b_0, b_1 = constants

The functions above are in general valid if the third or later loading cycle is considered but it has been shown that in some tests the functions are valid even if the first or second cycle is considered. According to Sun et al. (1985) Eq. 2-3 is more applicable to low to medium stress ranges while Eq. 2-4 is more general in its application to various stress level. The authors do not do any attempt to quantify low or medium stress level.

In Figure 2-7 data from two different tests are plotted. The data are picked from figures in Sun et al. 1985 and Raven & Gale, 1985. To each data set both Eq. 2-4 and Eq. 2-5 are matched and extrapolated up to 25 MPa. In this example the logarithmic curve seemed to be more appropriate since the slope decrease quicker for higher stress levels which probably is the behaviour of a fracture, i.e. at some stress level the maximum deformation is reached.

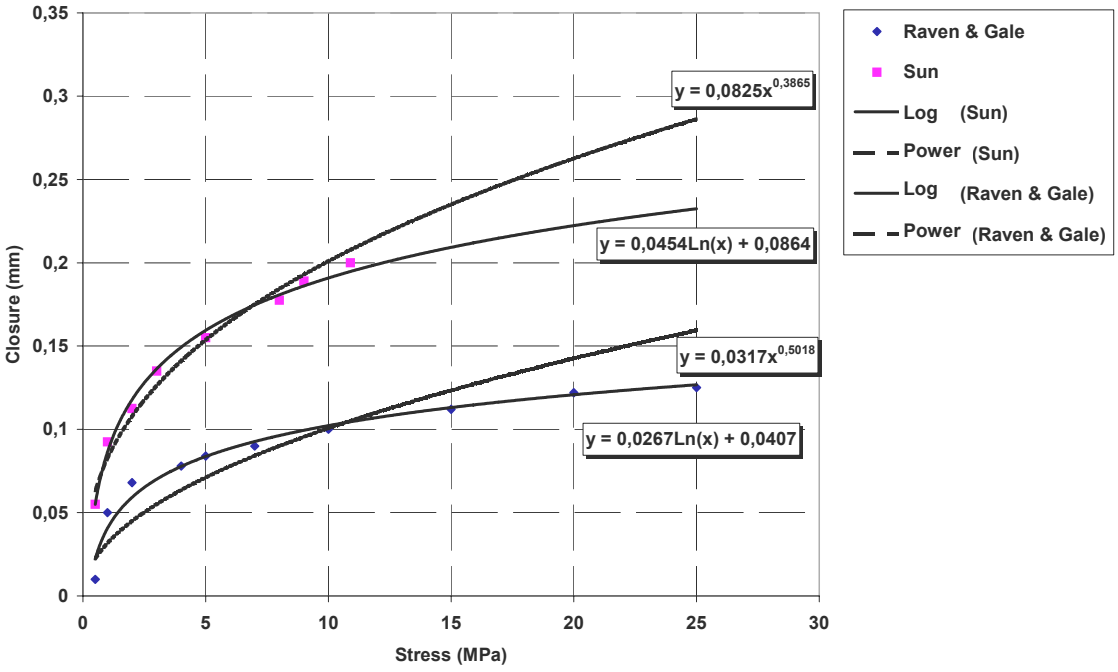

Figure 2-7. *Results from two different tests have been matched to both a logarithmic and an exponential curve respectively. In general, extrapolation of the stress-closure curve to stresses above the highest measured closure must be done by caution.*

It must be emphasised that these tests has been performed within the stress range 0- 25 MPa (Raven & Gale) and 0-12 MPa (Sun) and the matching of a logarithmic or an exponential curve to the data points has its validity within this stress range as well.

A number of laboratory tests (concerning fracture behaviour) have been done during the last decades; some of them are listed in Table 2-1. If the closure versus maximum applied stress is considered it is obvious that the fracture behaviour is irregular. The data of applied stress and fracture closure are plotted in Figure 2-9.

Table 2:1. Summary of some laboratory tests (concerning fracture behaviour) that had been conducted since 1981.

Author	Test or sample	Max σ [MPa]	δ at max σ [mm]	σ at max δ	Load cycle	Curve matching	Sample
Zhao & Brown, 1992	NJ1	7	0.06	Still under comp.	?	Hyperbolic and logarithmic	Natural fracture in Carnmenellis granite oriented along the core axis. 102 mm long and ∅=51mm.
	NJ6	4	0.12	See above	?	See above	See above.
	NJ2	7	0.08	See above	?	See above	At 180°C. See above.
	NJ2	7	0.12	See above	?	See above	At 200°C. See above.
	EF1	8	0.07	See above	?	See above	Artificial fracture in Carnmenellis granite. 102 mm long and ∅=51mm.
	EF3	3	0.04	See above	?	See above	See above.
	EF7	5	0.11	See above	2nd	See above	At 120°C. See above.
Sun et al., 1985	69	10.9	0.2	See above	2nd	Logarithmic	Natural fracture (unmated) in coarse-grained granite. Shape and area: rectangular 731 cm^2
	60	8.2	0.21	See above	2nd	See above	See above.
	63	5.5	0.14	See above	2nd	See above	See above.
	66	2.7	0.13	See above	2nd	See above	See above.
	05	5.9	0.09	See above	2nd		Natural fracture in medium-grained granite. Shape and area: rectangular 1009 cm^2
	03	2.4	0,14	See above	2nd		See above.
	04	2.0	0.04	See above	2nd		See above.
Raven & Gale, 1985	1	30	0.05	See above	2nd	Logarithmic for all three cycles	Granite core (∅=100mm x 700mm). Natural fracture oriented normal to the core axis.
	2	30	0.1	See above	2nd	See above	∅=150 mm
	3	30	0.13	See above	2nd	See above	∅=193 mm
	5	24	0.125	See above	2nd	See above	∅=294 mm

Author	Test or sample	Max σ [MPa]	δ at max σ [mm]	σ at max δ	Load cycle	Curve matching	Sample
Bandis et al., 1983		33	0.08	20	3rd	Logarithmic on third cycle	Natural slate cleavage (*weathered*). The block sizes varies: side lengths 80-100 mm, widths 40-60 mm and heights 50-70 mm.
		50	0.07	Still under comp.	3rd	See above	Natural fracture in limestone (*weathered*).
		30	0.08	Still under comp.	3rd	See above	Natural bedding plane in siltstone (*weathered*).
		50	0.03	22	3rd	See above	Natural slate cleavage (*fresh*).
		50	0.035	20	3rd	See above	Natural fracture in dolerite (*fresh*).
		50	0.015	15	3rd	See above	Natural bedding plane in limestone (*fresh*).
		40	0.13	Still under comp.	2nd	Logarithmic for all three cycles	Natural slate cleavage (*mismatched).*
		42	0.20	See above	2nd	See above	Natural fracture in limestone (*mismatched*).
		30	0.28	See above	2nd	See above	Natural fracture in sandstone (*mismatched*).
		35	0.33	See above	2nd	See above	Natural fracture in siltstone (*mismatched*).
Witherspoon et al., 1980		16	0.12	See above	1st		Artificial fracture in granite. Block size: w= 121mm, l= 207mm and h= 155 mm
Elliott et al., 1985	2	3.7	0.11	See above	?	Logarithmic and hyperbolic	Medium-grained granite. 51mm diameter and 102 mm long. Natural fracture
	3	6	0.08	See above	?	See above	See above.
	4	2.5	0.1	See above	?	See above	See above.
	5	4	0.06	See above	?	See above	See above.
Bart & Shao, 1998		25	0,1	See above	1st	Hyperbolic	Artificial fracture in Tennelles granite. 64mm diameter and 113 mm long.
Dunat et al., 1998		25	0,14	13	?		Artificial fracture in granite. 65mm diameter and 120mm long.

The column "σ at max δ" (in Table 2-1) mean at what values of stress the maximum fracture deformation is reached (see Figure 2-8). The review of the laboratory tests (Table 2-1) indicates that the maximum fracture deformation is seldom reached within the applied stress range.

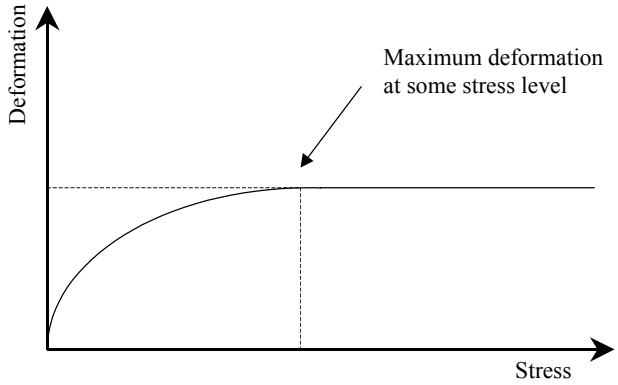

Figure 2-8. *The values in Table 2-1 are taken at that point where the maximum fracture deformation has occurred.*

In Figure 2-9 the results from Table 2-1 are plotted and there are great variations even within the same rock type and it is hard to find any correlation between stress and deformation. However, some vaguely trends can be seen. Such as:

- A mismatched fracture seemed to be softer than a matched one.
- A fresh fracture is stiffer than a weathered fracture.
- A natural fracture is softer than an artificial fracture.

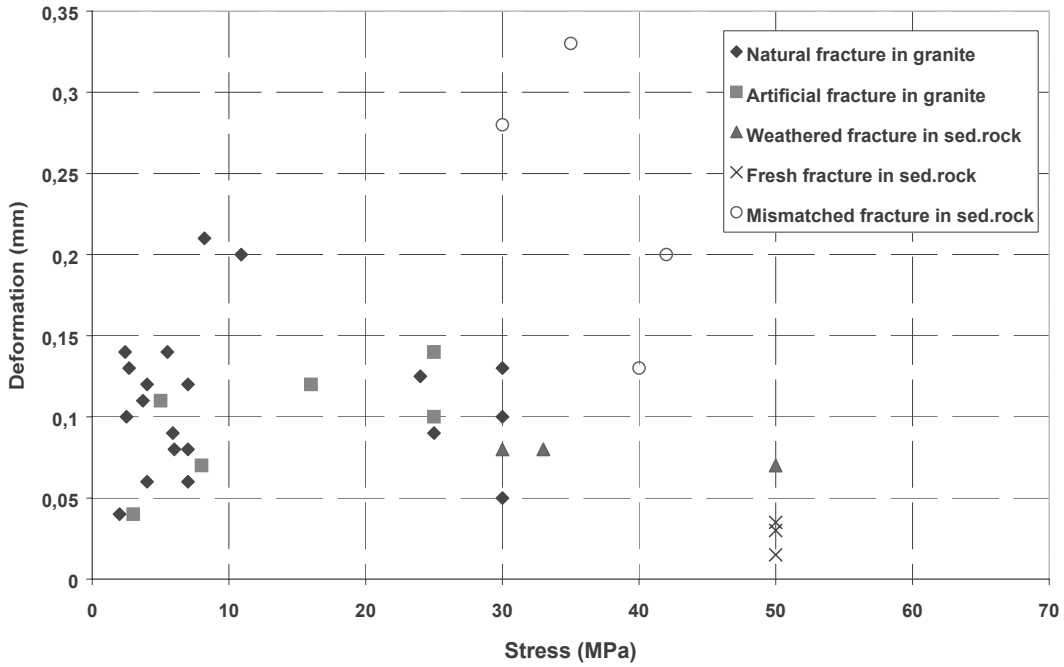

Figure 2-9. *The figures of closure versus maximum applied stress from Table 2-1 are plotted. Note that some of the tests were performed on sedimentary rocks.*

The conclusion is that fracture closure is not only a function of stress and rock type but also the conditions of the fracture surfaces. Many authors (e.g. Cook, 1992; Pyrak-Nolte & Morris, 2000) have pointed out the complexity of the problem and related the closure to some of the following factors:

- Applied stress.
- In-situ stresses before any changes.
- Conditions of the fracture surfaces such as:
  - Contact area.
  - Spatial geometry of the contact area.
  - Roughness.
  - Presence of fracture filling.
  - Mated or unmated surfaces.
- Rock type.

In a situation when no information of the fracture surfaces is available but a rough prediction of the deformation is needed, the Eq. 2-4 can be used together with some information from the literature. The methodology is described hereafter.

If some points of the closure curve are known (Eq.2-3 and Eq.2-4) and if the stress field and the applied stress are known, a rough prediction can be made as follow:

Assume that fracture closure is described by a logarithmic law and the second or later loading cycle is considered. The closure, between an effective initial reference stress (σ'_0) and a final effective stress (σ'), can be described by specifying the slope of the plot of closure, δ, versus *log* σ' (Evans et al., 1992). The logarithmic closure law can thus be written as:

$$\delta = a_0 + a_1 \ln \sigma' \qquad \textbf{\textit{Eq. 2-5}}$$

At the initial reference stress the closure is zero, i.e. $a_0 = -a_1 \ln \sigma'_0$ and Eq. 2-5 becomes,

$$\delta = a_1 \ln \frac{\sigma'}{\sigma'_0} \qquad \textbf{\textit{Eq. 2-6}}$$

The compliance, *C* (defined as the inverse of fracture stiffness), of the fracture is equal to the gradient of he closure curve, i.e. the differential of Eq. 2-6 with respect to σ'

$$C = \delta' = \frac{a_1}{\sigma'} \Rightarrow \frac{1}{C} = K_n = \frac{\sigma'}{a_1} \qquad \textit{Eq. 2-7}$$

Differentiating again gives

$$\frac{dK_n}{d\sigma'} = const. = \frac{1}{a_1} \qquad \textit{Eq. 2-8}$$

The stiffness characteristic of a fracture is defined by evaluate the slope, $dK_n / d\sigma'$ and the closure of a fracture can be written as:

$$\delta = \left(\frac{dK_n}{d\sigma'} \right)^{-1} \ln\left(\frac{\sigma'}{\sigma'_0} \right) \qquad \textit{Eq. 2-9}$$

Furthermore Evans et al. (1992) summarised some laboratory tests and evaluated values of $dK_n / d\sigma'$ (see Table 2:2).

By using Eq. 2-10 and values from the Table 2:2 a good estimation of the change of the aperture width due to the changes in stress can be made.

Table 2:2. Estimations of $dK_n/d\sigma'$, from the literature (modified after Evans et al., 1992)

Author	$dK_n/d\sigma'$ [mm^{-1}]	Interface type	Point estimate of K_n at 1.5 MPa [MPa/mm]	Comments
Laboratory tests				
Bandis et al. (1983)	300	Limestone: mated		bedding plane, log-law slope 0.5-40 MPa
	120	Slate: mated		
	130	Dolorite: mated		tension fracture, log-law sl. 0.5-40 MPa
	54	Slate: unmated		
	38	Slate: unmated		fresh joint, log-law slope 0.5-40 MPa
	26	Limestone: unmated		log-law slope 0.5-40 MPa
	20	Limestone: unmated		"
	16	Sandstone: unmated		"
	18	Siltstone: unmated		"
Raven & Gale (1985)	43-130	Granite: mated	≈ 60	induced frac, log-law slope 0.5-13 MPa
Sun et al. (1985)	11-24	Granite: unmated	≈18.5	natural frac., log-law slope 0.5-10 MPa
In-situ tests				
Walsh & Grosenbaugh (1979)	11	Granite	-	fresh joint, log-law slope 0.5-4 MPa
Evans & Wyatt (1984)	<13	Granite	≈ 20	
Jung (1989)	~ 2	Granite	≈2.5	

2.4 Summary of chapter 2

The rock mass will expand as a result of increased temperature generated by the nuclear waste. The thermal expansion coefficient is approximately $8x10^{-6}$ /°K (for crystalline rock). The expansion will cause increases in stresses acting on the fractures.

The laboratory studies, mentioned here, on single fractures have shown that mechanical deformation is strongly dependent of the effective stress acting on the fracture i.e. the fracture stiffness is a function of effective stress.

The literature also shows that a change in effective stress have a significant influence on the hydraulic properties of the fracture. The empirical relationship established by Dershowitz et al. (1991) is in accordance with that.

The THM-test performed of Terra Tek (Hardin et al., 1982) verified the laboratory tests in a larger scale, field test scale. They also point out the fact that the deformation modulus is dependent of the temperature. The deformation modulus decreases while the temperature increase. During the test the relative transmissivity decrease to approximately 15% of the initial transmissivity.

Furthermore, the literature review showed that the majority of all laboratory tests have been done at stresses up to 10-15 MPa. When results from these tests are plotted together it shows that the results are not unambiguous. According to the literature the deformation is a function of:

- Applied stress
- In-situ stresses before any changes
- Conditions of the fracture surfaces such as:
    - → Contact area
    - → Spatial geometry of the contact area
    - → Roughness
    - → Presence of fracture filling
    - → Mated or unmated surfaces
- Rock type

The magnitude of the fracture deformation can be estimated by using the formula:

$$\delta = \left(\frac{dK_n}{d\sigma'} \right)^{-1} \ln\left(\frac{\sigma'}{\sigma'_0} \right)$$

3 Prototype tunnel at ÄHRL

According to the previous chapter fractures ability to transmit water is strongly affected of the stress field or changes in stress field. The stress field around the prototype repository will be affected during the construction and the operation of the prototype repository. The two main reasons for the change in stress are the actual excavation of (or creation of an open space) and the increase in temperature.

Schematic figures of the prototype tunnel and the surrounding boreholes are shown in Figure 3-1and Figure 3-2.

The aims of this chapter are to analyse the hydro mechanical effects of the change in stresses, quantify the effects and to suggest target areas or fractures to measure on.

The chapter starts with an introduction to Äspö Hard Rock Laboratory (ÄHRL) in terms of stress measurements and fracture mapping at the Prototype Tunnel. Next section presents some results from a numerical modelling of the Prototype Tunnel at different phases during the construction and the operation of the tunnel. The hydraulic and mechanical consequences due to the change in stress are estimated in the following section. The chapter ends up with a section that analyse the most optimum fractures to measure.

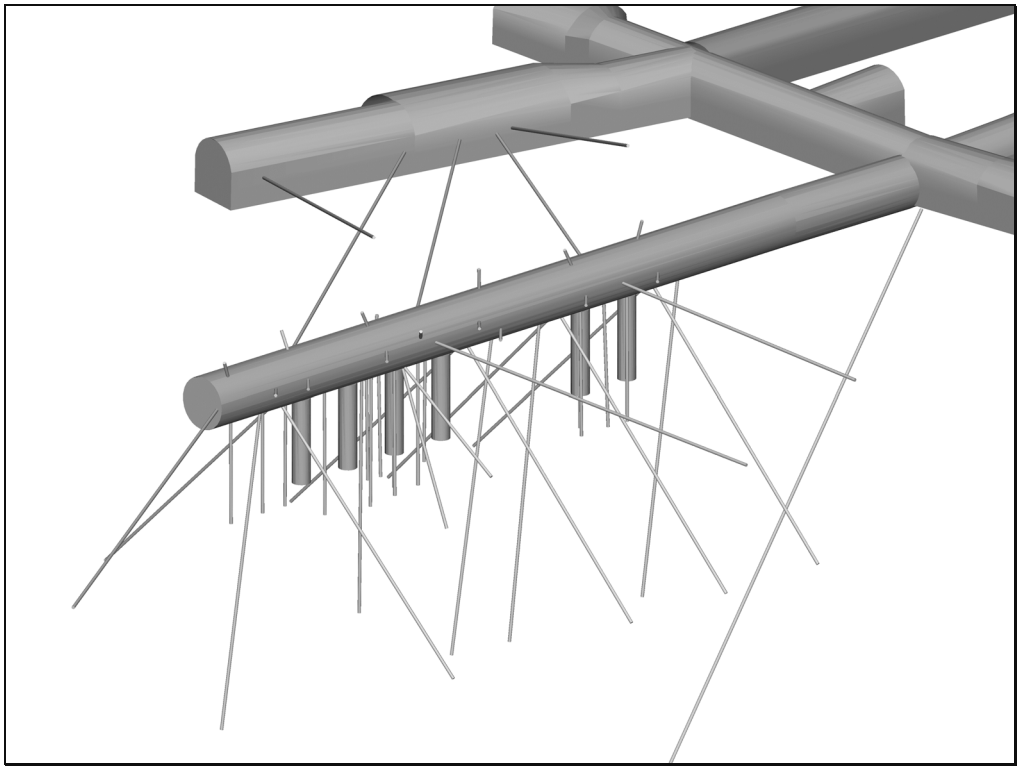

Figure 3-1. *The TBM-bored drift with the six deposition holes and the boreholes used for characterization of the rock mass.*

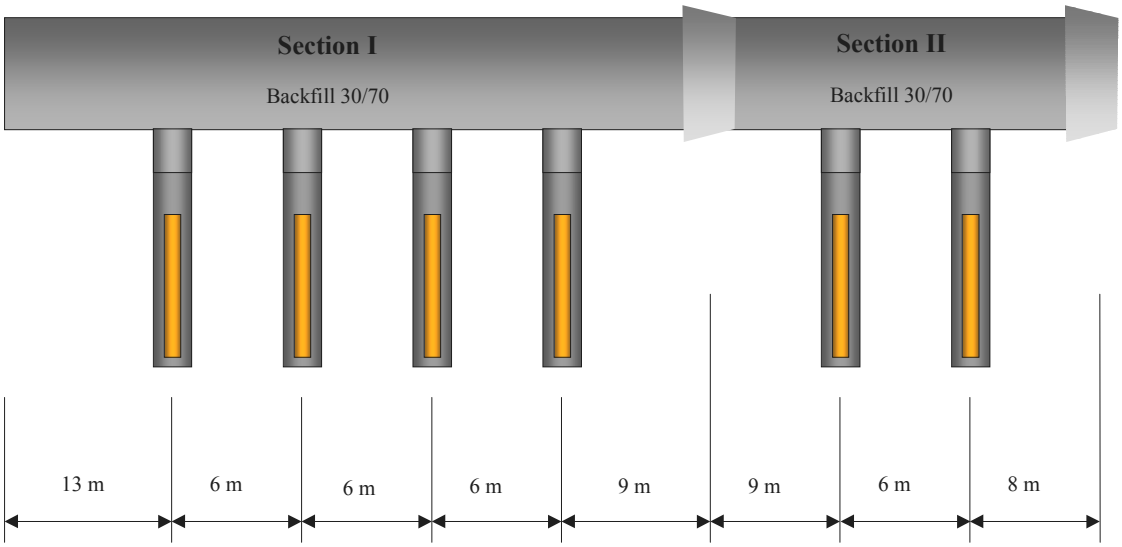

Figure 3-2. *Schematic view of the layout of the Prototype Repository and deposition holes (not in scale).*

3.1 Principal stress field at Äspö and nearby the prototype tunnel

When the changes in the stress field and the hydromechanical effects on fractures should be analysed, it is important to be aware of the in-situ conditions in terms of stresses and fractures.

3.1.1 Rock Stresses

During the excavation of the access ramp to the hard rock laboratory, overcoring measurements were made at 8 locations along the ramp, the deepest at 408 metres. The stress field was also evaluated by using hydraulic fracturing technique (from the surface) in borehole KAS02. The strikes of the maximum principal stress from the overcoring and hydraulic fracturing measurements are presented in Figure 3-3 (Rhén et al. 1997).

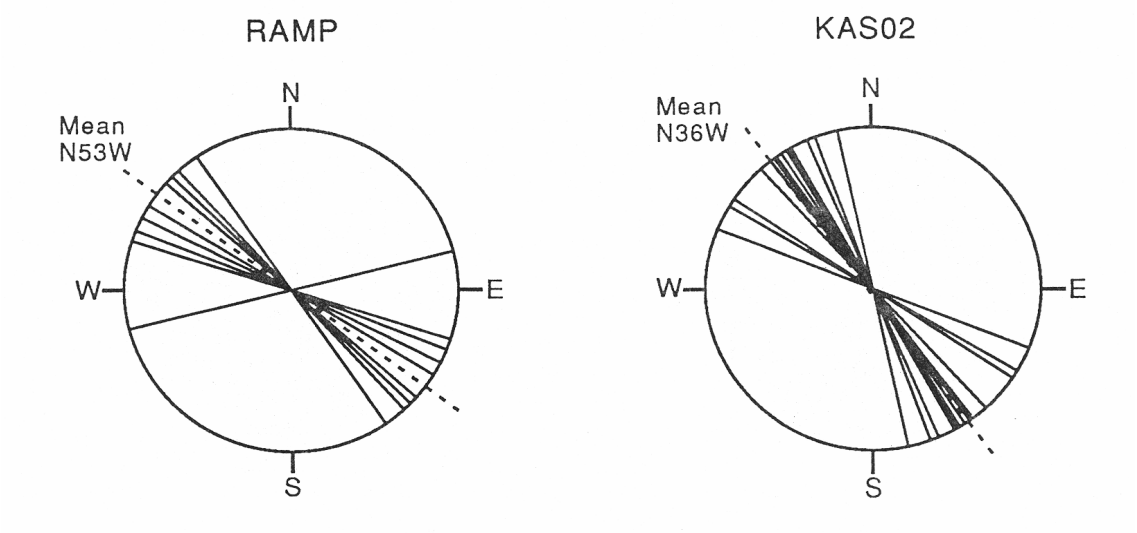

Figure 3-3. *Orientation of maximum horizontal stress, from overcoring holes in the ramp and hydraulic fracturing in KAS02 (from Rhén et al. 1997).*

The ratio between the maximum horizontal stress (σ_H) and the theoretical vertical stress (σ_V) for all boreholes is 2.9. After excavation of the prototype tunnel (at a depth of 450 m), stress measurements were done in a vertical borehole (KA 3579 G, see Figure 3-4 drilled from tunnel floor.

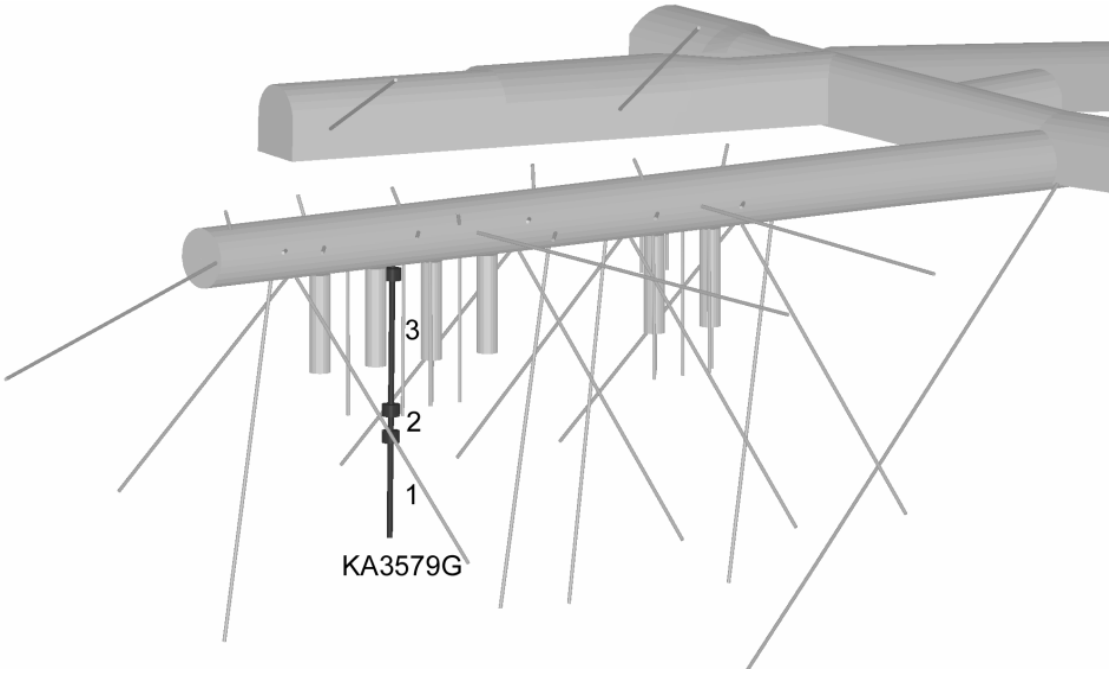

Figure 3-4. *A view of the prototype repository and the boreholes. Stress measurements were made in core hole KA3579G.*

Measurements were done at 11 points along the borehole down to a depth of 22.31 metres (Klasson et al, 2001). The four deepest measurements (from 20.06-22.31) were assumed to be unaffected of disturbance caused by the tunnel itself and therefore the average stresses were evaluated from these four measurements (see Table 3:1 and Figure 3-5).

Table 3:1. The principal stresses at the depth of the prototype repository. The strikes refer to the local north of the Äspö local coordinate system (local north is 12° west of magnetic north) (from. Klasson et al, 2001).

Principal stress	Magnitude [MPa]	Strike [°]	Dip [°]
σ_1	34.2	141	3
σ_2	17.7	245	80
σ_3	13.1	50	10

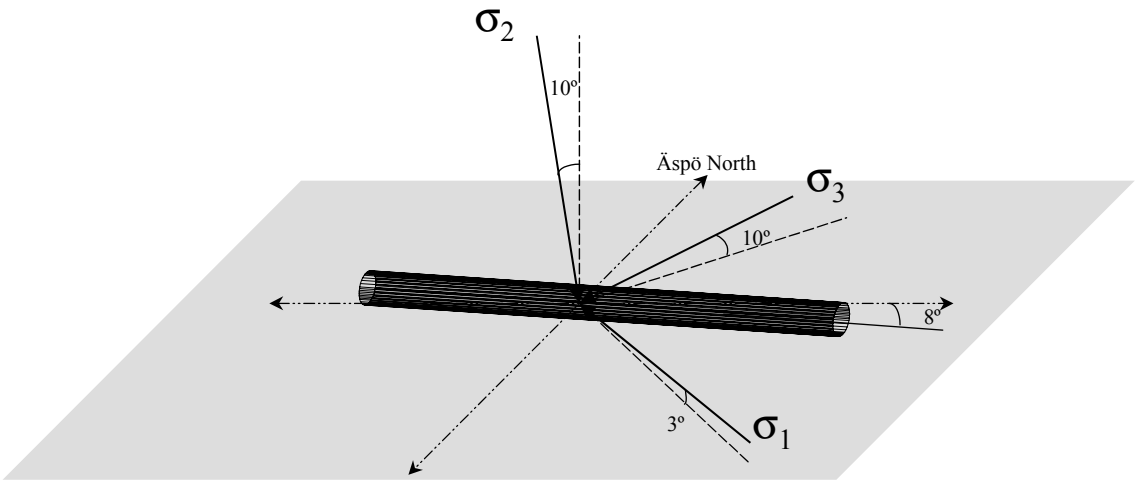

Figure 3-5. *The principal stress directions compared to the tunnel.*

Additional stress measurements (Klee and Rummel, 2002) were done in the rock mass close to the G-tunnel (see Figure 3-4). The technique used in these tests was hydraulic fracturing. The results from the tests are presented in table Table 3:2.

Table 3:2. Results from rock stress measurements done by Klee and Rummel, 2002 close to the F-tunnel at ÄHRL.

Borehole	Depth [m]	σ_v* [MPa]	σ_v [MPa]	σ_h [MPa]	σ_H [MPa]	Strike (σ_H) [°]
KA2599G01	455.7	12.1 ± 0.2	19.5 ± 1.1		21.8 ± 2.9	119 ± 8
KF0093A01	450	11.9	19.5 ± 1.1	11.0 ± 1.2		115 ± 8

Where σ_h and σ_H are the minimum and maximum horizontal principal stresses. σ_v is the measured vertical stress, and σ_v^* is the vertical stress calculated for a mean density of the overburden rock of 2700 kg/m^3.

The results reported in Klee and Rummel (2002) differ slightly from the results obtained from the over coring (Klasson et al, 2001). It is notable that Klee and Rummel (2002) present the maximum horizontal stress while Klasson et al. (2001) present the maximum stress (which not is horizontal). The two different techniques will give to some extent a different result that depends on the assumptions related to the evaluation.

3.1.2 Dominating fracture sets

After fracture mapping and analyses of the prototype tunnel and 36 boreholes three dominating fracture sets have turned out. These are; two sets are striking north-west and are very steep (one on each side of the vertical) and the third is sub-horizontal (see

Figure 3-6).

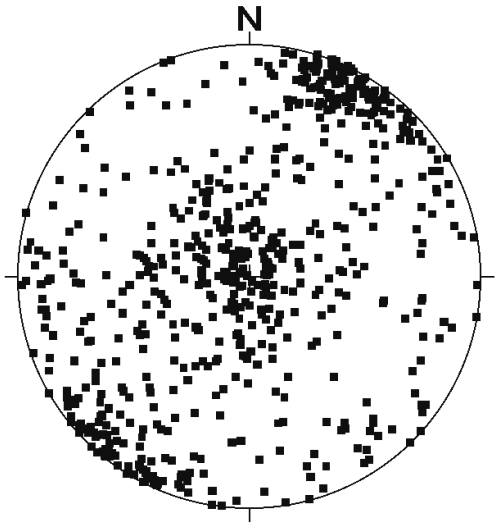

Figure 3-6. *Lower hemisphere projection of poles to fracture planes for open fractures in 36 boreholes (from Stigsson et al.,(2001))*

Hydrogeological tests have shown that the north-west striking fractures are the most conductive fractures when compared to all open fractures (not only the dominating fractures) (Rhén et al., 1997; Forsmark & Rhén, 1999).

3.2 Numerical modelling of rock stresses and temperature increase

Modelling work was carried out during the spring 2001(Claeson et al, 2001) in order to analyse the stress field around the prototype tunnel due to the excavation and the thermal load. Two finite element models were used, a linear elastic model and a Mohr-Coulomb model.

Results from the numerical modelling are used as input in the analyses of the fracture behaviour. In this work results from the Mohr-Coulomb model is used.

The size of the model was 24x35x35 m. The diameter of the tunnel and deposition hole was 5 and 1.75 meter, respectively. The boundary condition was defined in that way that the bottom surface of the model was fixed, i.e. rotation and vertical as well as horizontal movements of the bottom was restrained. The boundary conditions are established so the effect of the neighbouring heater is taken into account (superposition).

The considered load conditions were the initial state of stress (see Table 3:1), stress redistribution due to excavation of the tunnel and deposition holes, and the thermal loading during operation.

In the modelling work the total stress has been considered, i.e. no reduction has been done concerning the water pressure.

As thermal input into the modelling work Claeson et al. (2001) used results from Ageskog & Jansson (1998). In the analyses the temperature (on the rock surface of the deposition hole) is used as a time varying temperature boundary, see Table 3:3.

Table 3:3. The temperature on the rock surface of the deposition hole at different time (from Claeson et al., (2001)).

Year	0	0.5	1.0	2.0	3.0	4.0	5.0	6.0	7.0	8.0	9.0	15
Temp [°C]	14.0	52.0	59.0	64.0	67.0	68.0	69.0	70.0	70.5	71.0	71.5	71.5

Results from the modelling work (Ageskog & Jansson, 1998) concerning the development of the temperature profiles are shown in Figure 3-7. The results show that approximately 80 % of the temperature increase will be reached within 2 years.

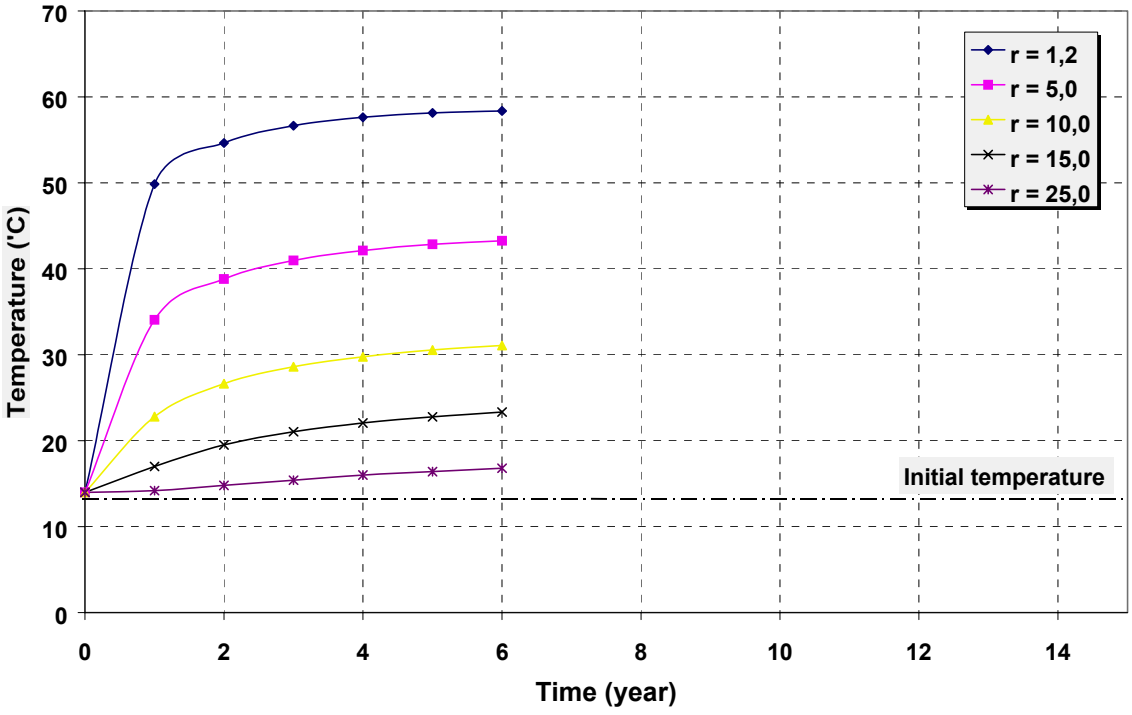

Figure 3-7. *The plot shows the temperature increase during the first six years at different radii (=r (in metres)). The radii are measured (horizontal) from the centre of the canister (heater).*

The increase in temperature will cause an expansion of the rock. This expansion and its distribution depend on the thermal and thermal-mechanical properties of the rock. Following properties have been used of Claeson et al.:

Thermal conductivity:	λ_r= 2.5 W/mK
Specific heat:	C_p= 750 J/kgK
Density:	ρ= 2700 kg/m^3
Thermal expansion coefficient:	α= 8x10^{-6} 1/°K

3.2.1 Changes in stress field due to the different stages during construction and running of the prototype repository

The results from the numerical modelling are presented from different stages during the construction and running of the prototype repository. These stages are:

- After completing the tunnel excavation (phase 1).
- After completing the tunnel excavation and a deposition hole (phase 2).
- After completing the tunnel excavation and a deposition hole and 1 year of heating (phase 3).
- After completing the tunnel excavation and a deposition hole and 10 years of heating (phase 4).

The figures (Figure 3-8 to Figure 3-11) refer to results obtained by the Mohr-Coulomb model.

The figures give a good general picture of the changes of the stress field. Note that only the maximum stress is considered in these figures and a closer analysis of the results is necessary to find the minimum and intermediate stresses at different points. The stresses are analysed in more detail in section 3.3.

After completing the tunnel excavation (phase 1).

In Figure 3-8 the distribution of the stress show the typical pattern obtained from the Kirsch equations. In the tunnel roof and floor the stress is increased while it is decreased in the walls. The vertical section through the tunnel show that the rock mass is affected roughly 4 meters from the tunnel floor and roof. The highest stress is reached close to the tunnel floor and roof and is between 64-67 MPa then the stress decline to the in-situ stress level of 34 MPa at 4 meters from the floor.

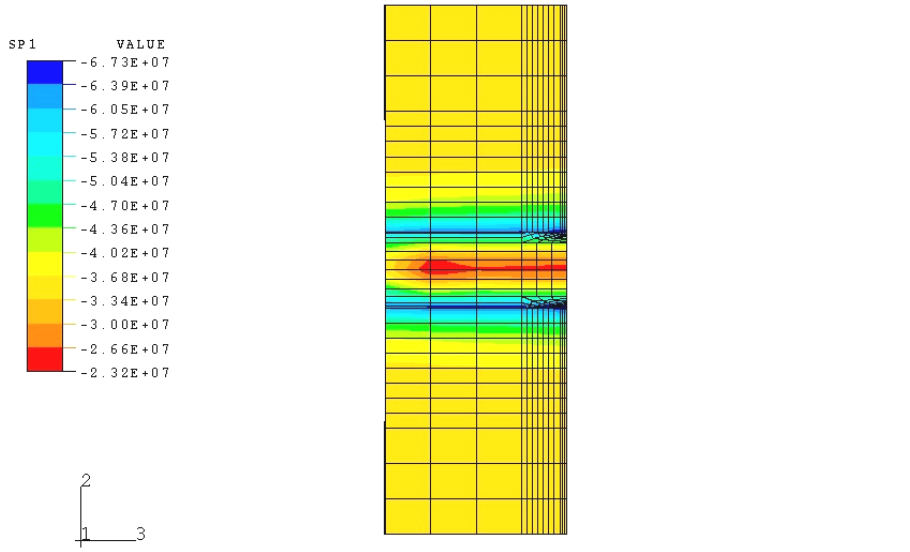

Figure 3-8. *Maximum principal stress after completing the tunnel excavation.*

After completing the tunnel excavation and a deposition hole (phase 2).

The general stress level around the tunnel does not change very much as a result of the drilling of the deposition hole. The drilling affect the stress fields close to the deposition hole. The increase in stress will be find at the part of the wall that lies in the same (more or less) direction (east–west) as the tunnel.

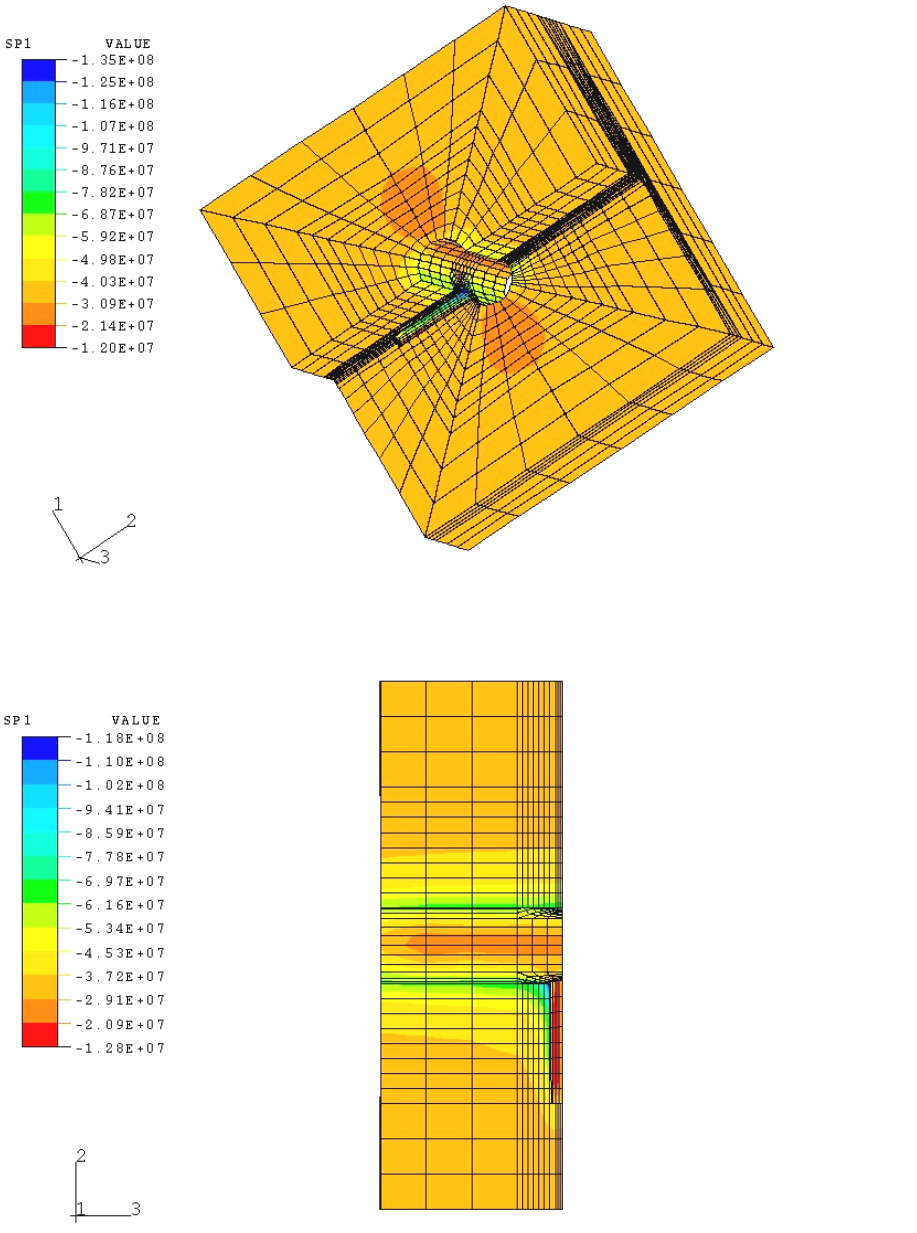

Figure 3-9. *Maximum principal stress after completing the tunnel excavation and drilling of a deposition hole.*

After completing the tunnel excavation and a deposition hole and 1 year of heating (phase 3).

The direction of the stress does not change while the temperature increase. The temperature increase causes an overall increase in stress since the rock mass will expand (more or less) equal in all directions. After 1 year the influences of the heat has reached roughly 8-10 meters below the tunnel floor. The influenced area has an elliptical shape around the heater.

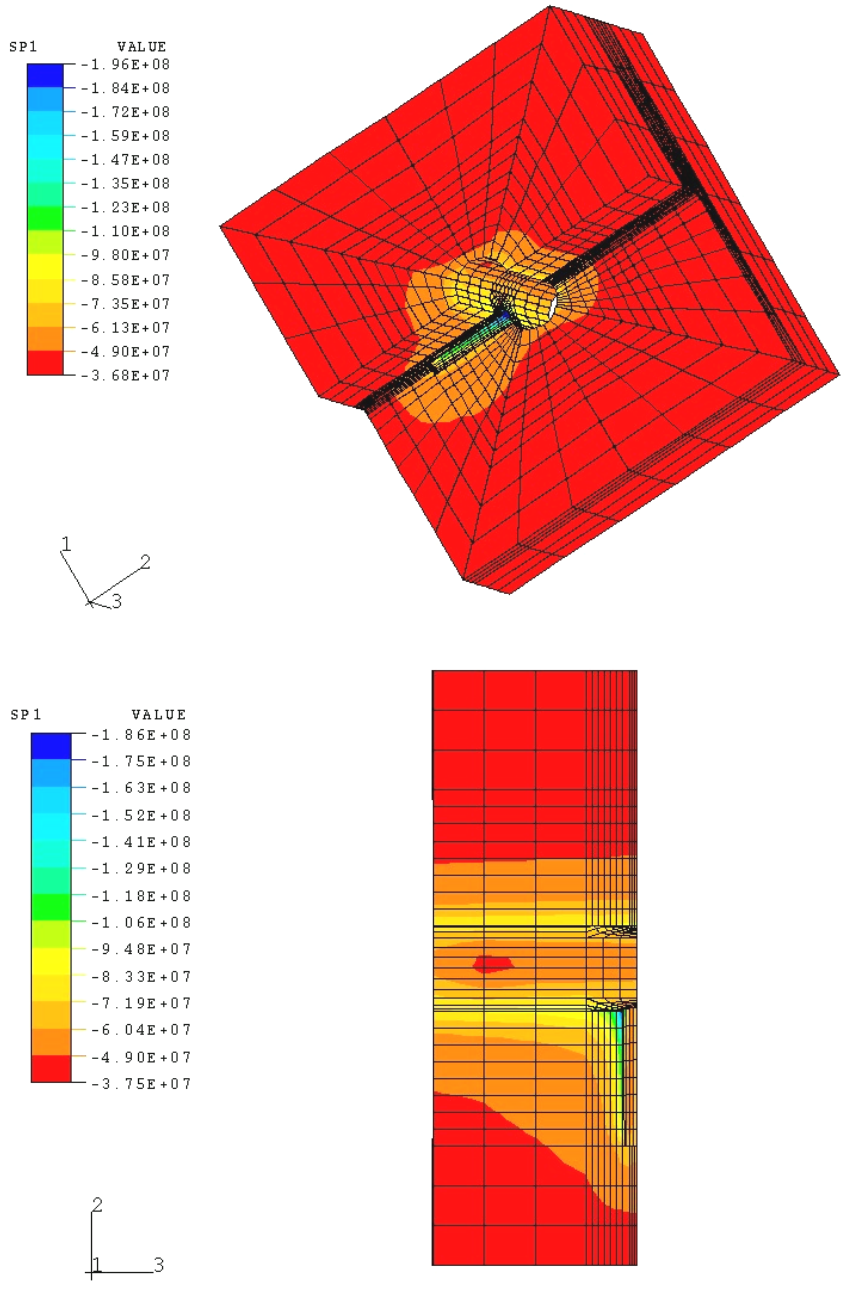

Figure 3-10. *Maximum principal stress after completing the tunnel excavation and drilling of a deposition hole and 1 year of heating.*

After completing the tunnel excavation and a deposition hole and 10 years of heating (phase 4).

After 10 years has the influenced volume increased and has now reached almost 25 meters from the heater.

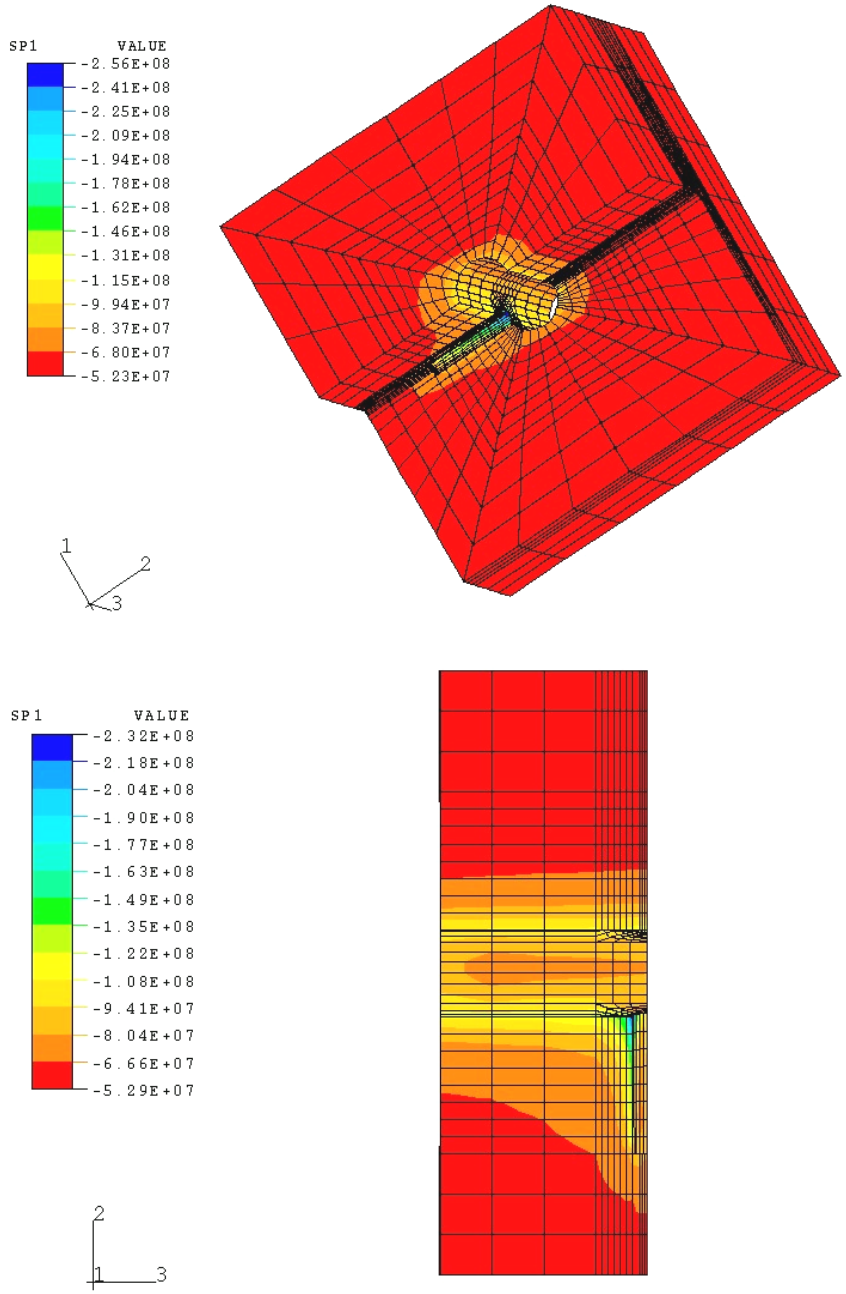

Figure 3-11. *Maximum principal stress after completing the tunnel excavation and drilling of a deposition hole and 10 years of heating.*

3.3 Estimated responses due to the change in stress field

The effect of the excavation and heating decrease the longer out from the tunnel and heater the observation point is. The effect also depends on which principal stress is considered and where the observation point is positioned in space in relation to the tunnel and heater.

In order to estimate the hydromechanical effects the magnitude of the principal stresses are estimated at different locations in the rock mass. For these purpose three fictitious boreholes are placed in different directions in the rock mass (see Figure 3-12). At five points (with increasing distance out from the tunnel wall/floor) the magnitudes of the principal stresses are obtained by analysing the results from Claeson et al. (2001).

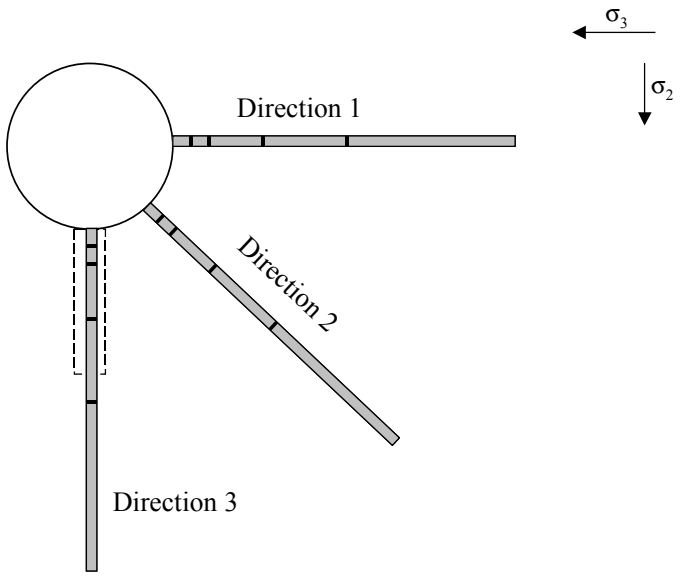

Figure 3-12. *The figure shows the three fictitious boreholes. The dark lines represent the "observation points" at 1, 2, 5, 10 and 20 (bottom of the borehole) metres out from the tunnel wall.*

The different stress levels are presented in Table 3:5, and Table 3:7. At each "observation point", three principal stresses from four phases are interpreted. These phases are:

- Before any activity (*in-situ*).
- After completing the tunnel excavation (phase 1).
- After completing the tunnel excavation and a deposition hole (phase 2).
- After completing the tunnel excavation and a deposition hole and 10 years of heating (phase 4).

As mentioned earlier, the results from the numerical modelling must be adjusted since no attention to the water pressure has been made in the modelling work. The water pressure has been measured (3-4 years after the tunnel was finished) in the rock mass at different distances out from the tunnel (see Figure 3-13). It is obvious that the tunnel work as drainer during the construction phase. However, when the tunnel is sealed off the water pressure will possible increase and reach approximately 4 MPa within 1 year if the drainage is stopped (the drainage of section I and II was ongoing spring 2004 but planned to be stopped autumn 2004).

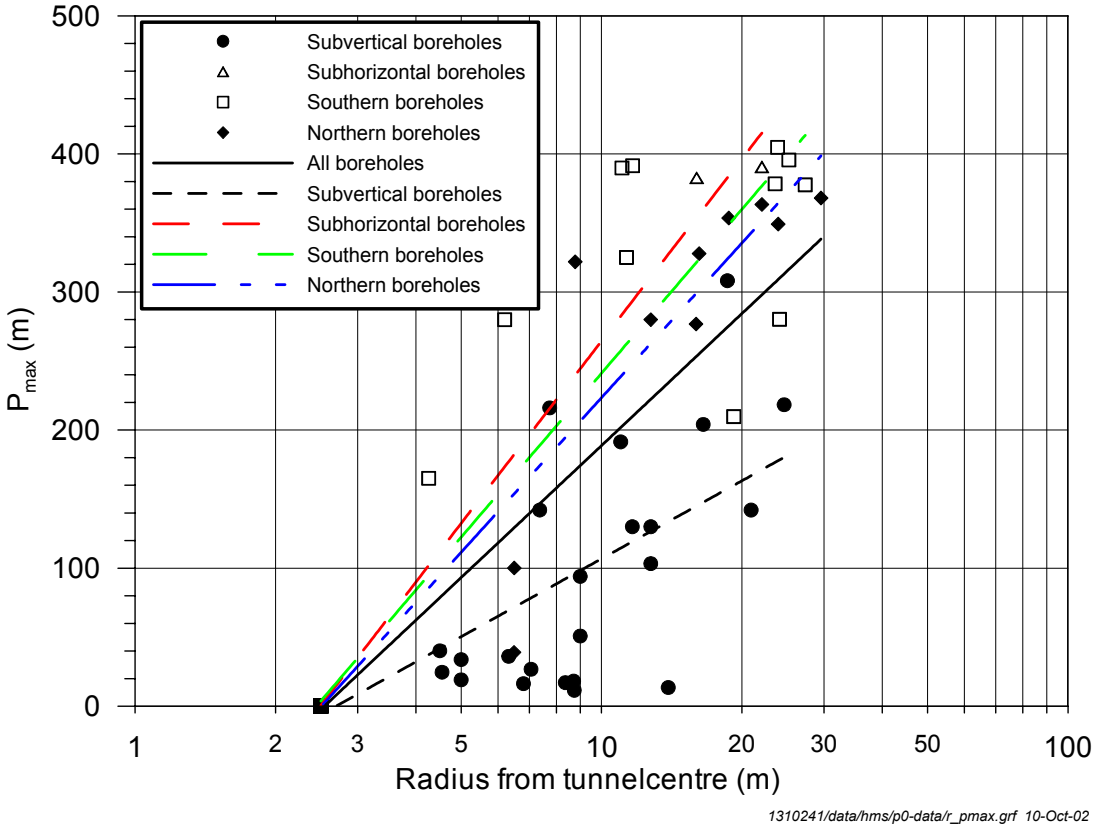

Figure 3-13. *Maximum pressures plotted as function of the distance to the tunnel centre. The pressure was measured 3-4 years after the tunnel is finished (from Rhén & Forsmark, 2001).*

The modelled stresses in 2 of the 4 phases (phase 1 and phase 2) will be reduced according to Figure 3-13 and Table 3:4. In the *in-situ* and 4th phases the stresses will be reduced by 4 MPa.

Table 3:4. The values represent the water pressure at the observation points (seeFigure 3-12). The values of direction 2 correspond to the curve "All boreholes" (see Figure 3-13).

Radius (m)	Direction 1	Direction 2	Direction 3
1	0.6	0.4	0.2
2	1.2	0.8	0.4
5	2.1	1.5	0.8
10	3.15	2.2	1.2
20	4.1	3.0	1.7

Table 3:5. Interpreted effective stresses at different radii from the tunnel wall at three directions (see Figure 3-12). Note that "In-situ", phase 1, phase 2 and phase 4 is explained above.

Distance from tunnel wall [m]	Direction 1											
	σ'_1 [MPa]				σ'_2 [MPa]				σ'_3 [MPa]			
	In-situ	Phase 1	Phase 2	Phase 4	*In-situ*	Phase 1	Phase 2	Phase 4	*In-situ*	Phase 1	Phase 2	Phase 4
1	30	23	19	64	14	16	16	39	9	5	5	14
2	30	24	23	61	14	17	17	44	9	7	7	23
5	30	26	26	59	14	18	18	43	9	10	10	32
10	30	31	31	56	14	15	15	38	9	10	10	32
20	30	30	30	-	14	14	14	-	9	9	9	-

Table 3:6. Interpreted effective stresses at different radii from the tunnel wall at direction 2(see Figure 3-12).

Distance from tunnel wall [m]	Direction 2											
	σ'_1 [MPa]				σ'_2 [MPa]				σ'_3 [MPa]			
	In-situ	Phase 1	Phase 2	Phase 4	*In-situ*	Phase 1	Phase 2	Phase 4	*In-situ*	Phase 1	Phase 2	Phase 4
1	30	32	30	66	14	14	12	42	9	6	6	15
2	30	33	31	64	14	14	12	44	9	7	7	23
5	30	32	32	61	14	16	13	38	9	10	10	33
10	30	32	32	56	14	16	16	36	9	11	11	36
20	30	31	31	-	14	15	15	-	9	10	10	-

Table 3:7. Interpreted effective stresses at different radii from the tunnel wall at direction 3 (see Figure 3-12).

Distance from tunnel wall [m]	Direction 3											
	σ'_1 [MPa]				σ'_2 [MPa]				σ'_3 [MPa]			
	In-situ	Phase 1	Phase 2	Phase 4	*In-situ*	Phase 1	Phase 2	Phase 4	*In-situ*	Phase 1	Phase 2	Phase 4
1	30	47	53	90	14	14	13	45	9	10	6	16
2	30	42	45	81	14	15	15	42	9	14	8	28
5	30	33	36	71	14	17	16	38	9	12	11	34
10	30	33	33	56	14	17	17	36	9	12	12	36
20	30	32	32	-	14	16	16	-	9	11	11	-

If the tables are summarised (see Table 3:8) it is notable that the increase of each principal stress from in-situ stress are in the same range independent of which direction is considered.

Table 3:8. A summary of tables 3:3 to 3:5. The range of the final effective stress level (after 10 years) at the different directions.

	σ'_1 [MPa]	σ'_2 [MPa]	σ'_3 [MPa]
Direction 1	56-64	38-44	14-32
Direction 2	56-66	36-44	15-36
Direction 3	56-90	36-45	16-36

The deformation depends, among other things, on the stress increase and the in-situ stresses, i.e. it is not obvious which principal stress that causes the largest deformation.

3.3.1 Hydraulic and mechanical responses due to the excavation and thermal load

According to section 2.3 a change in stress may cause a change in fracture width. The effect of the change in stress depends (among other things) on the *in-situ* stresses. Since the closure behaviour can be described by a logarithmic or exponential curve, it is clear that the maximum effect of a change in stress (of a specific magnitude) occur at as low stresses as possible (see Figure 3-14).

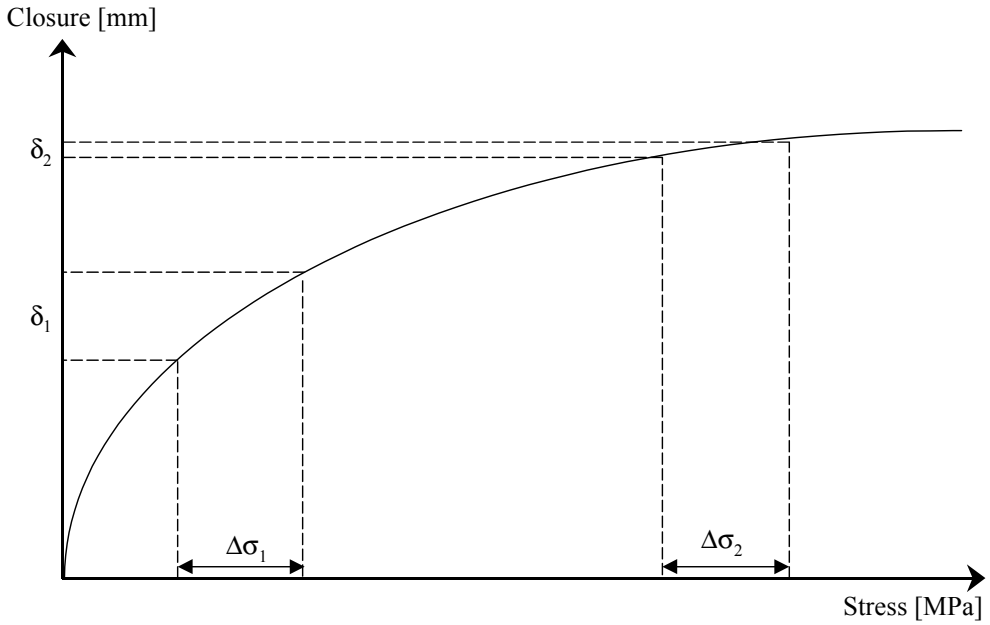

Figure 3-14. *The schematic figure shows the effect of the* in-situ *stress on the response (δ_1 and δ_2) of a change in stress ($\Delta\sigma_1$ and $\Delta\sigma_2$, note that $\Delta\sigma_1 = \Delta\sigma_2$).*

The general strike and dip of the principal stresses is shown in Figure 3-5. According to this figure and the discussion above three cases have been chosen in order to estimate the fracture deformation and the changes in transmissivity. The three fictitious fractures and their relation to the principal stress are:

1. Vertical fractures which strikes perpendicular to the maximum principal stress. The normal stress to these fractures is the maximum principal stress (see Figure 3-15a).
2. Vertical fractures which strikes parallel to the maximum principal stress. The normal stress to these fractures is the minimum principal stress (see Figure 3-15b).
3. Horizontal (or sub-horizontal) fractures where the intermediate principal stress acting as the normal stress to the fracture plane (see Figure 3-15c).

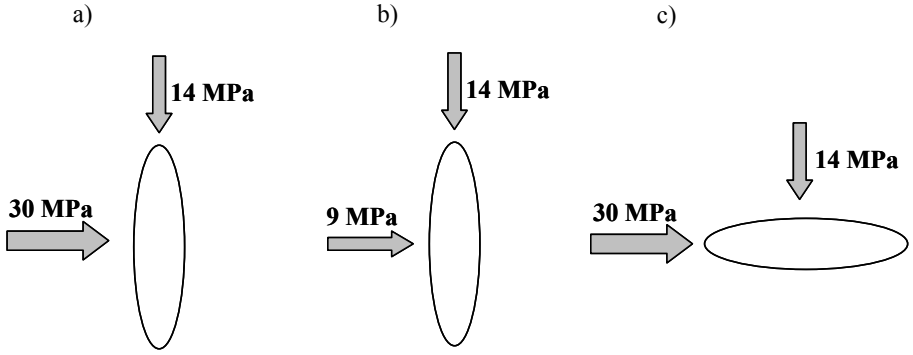

Figure 3-15. *Three cases that are considered when the fracture deformation and hydraulic change are estimated.*

The estimations of the hydraulic and mechanical responses are made by using the relationships that were reported in section 2.1 and 2.3.

In section 2.3 the fracture deformation was described by specifying the slope of a plot of closure, δ, versus *log* σ'. Five different values are picked from the literature (see section 2.3) that represents the stiffness ($dK_n/d\sigma'$). The logarithmic closure law can thus be written as (see Eq. 2-10):

$$-\Delta\delta = \left(\frac{dK_n}{d\sigma'}\right)^{-1} \ln\left(\frac{\sigma'}{\sigma'_0}\right)$$

In section 2.1 the relationship (Eq. 2-2) between changes in fracture transmissivity as a result of change in normal stress was described. The values of β represent the minimum value (0.2), maximum (2.0) and a reasonable value (1.0) according to Dershowitz et al. (1990). In the figures the factor β is denoted with the letter B. The relationship is expressed as:

$$\frac{T}{T_0} = \left(\frac{\sigma'}{\sigma'_0}\right)^{-\beta}$$

In the forthcoming figures (Figure 3-16, Figure 3-17 and Figure 3-18) the fracture deformation and the relative change in transmissivity is plotted for each fracture plane (according to Figure 3-15). The figure shows a wide stress range that incorporates the stress situation close to the tunnel as well as the stress situation far away from the tunnel.

A full set of deformation and transmissivity curves, for each “observation point”, is reported in appendix A.

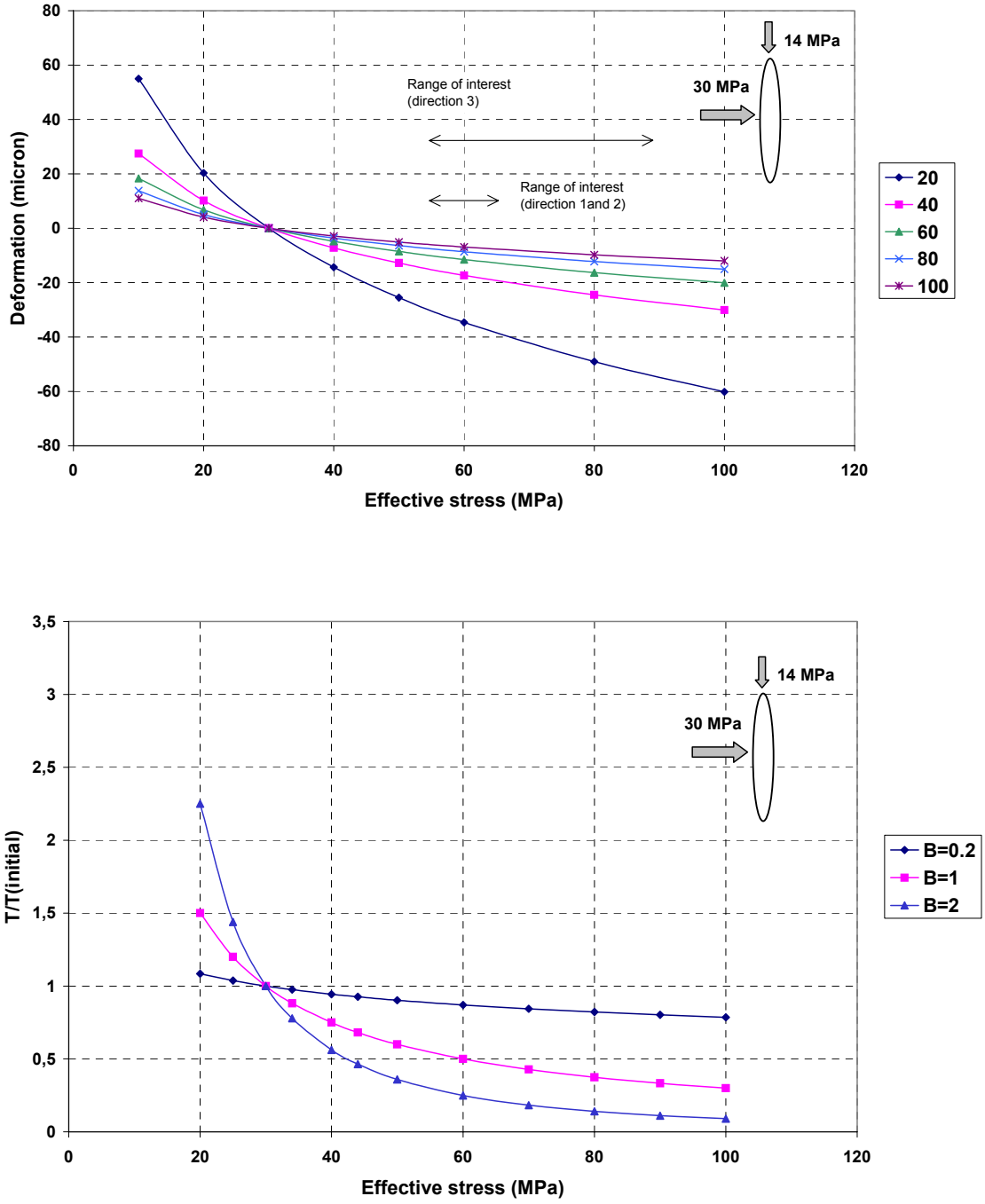

Figure 3-16. *Mechanical and hydraulic response due to a change in stress. The responses refer to a fictious fracture that strikes perpendicular to the maximum stress (30 MPa). Note that the influence of the tunnel is greater in the third direction compared to the other directions. "Range of interest" corresponds to the final stress level (phase 4) at the different observation points.*

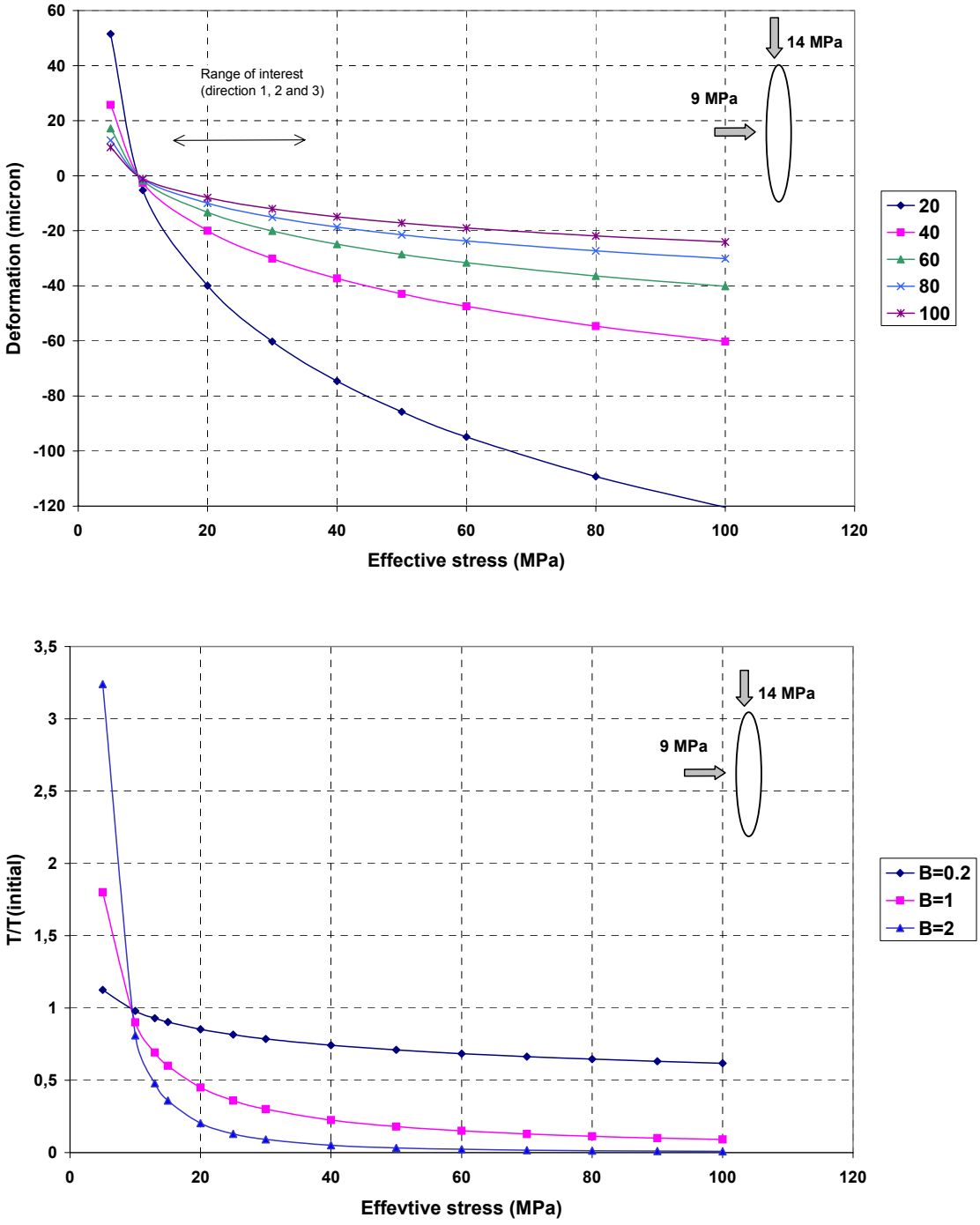

Figure 3-17. *Mechanical and hydraulic response due to a change in stress. The responses refer to a fictious fracture that strikes perpendicular to the minimum principal stress (9 MPa). Note that "range of interest" corresponds to the final stress level (phase 4) at the different observation points.*

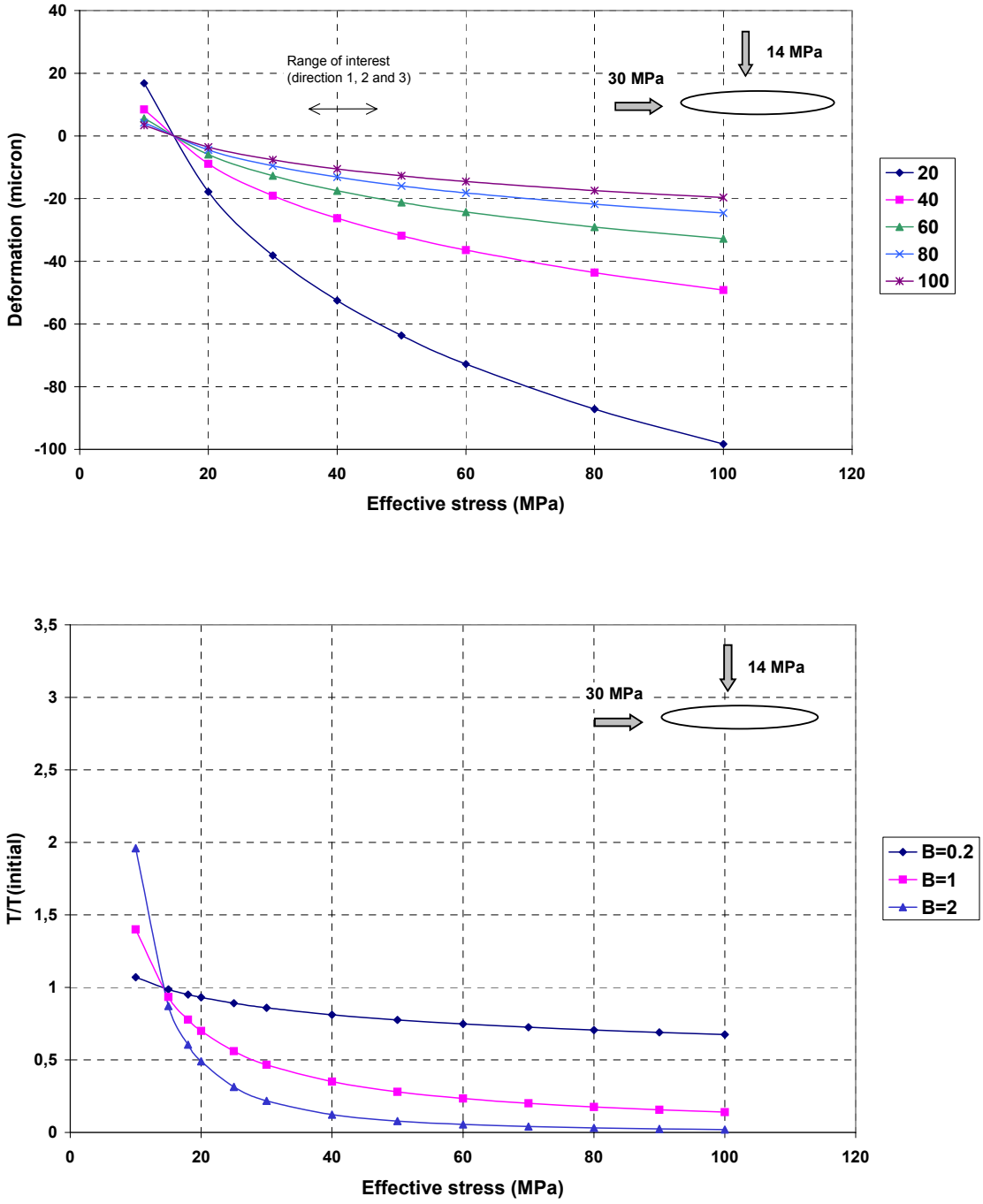

Figure 3-18. *Mechanical and hydraulic response due to a change in stress. The responses refer to a fictious horizontal fracture where the intermediate principal stress (14 MPa) acting as the normal stress to the plane. Note that "range of interest" corresponds to the final stress level (phase 4) at the different observation points.*

In Table 3:9 the predicted fracture deformation and change in transmissivity are summarised. The predicted deformation of fractures that strike perpendicular to σ_2 and σ_3 is in the same range. Slightly bigger are the predictions concerning fractures that strike perpendicular to σ_1.

Table 3:9. Summary of the expected fracture deformation and change in transmissivity that will occur at fracture that strikes perpendicular to each effective principal stress.

	Fracture that strikes perpendicular to: σ'_1	Fracture that strikes perpendicular to: σ'_2	Fracture that strikes perpendicular to: σ'_3
Direction 1 [MPa]	56-64	38-44	14-32
Direction 2 [MPa]	56-66	36-44	15-36
Direction 3 [MPa]	56-90	36-45	16-36
Expected deformation [μm]	20-65	10-50	5-70
Expected change in transmissivity [T/T(initial)]	0.1- 0.9	0.1- 0.8	0.2- 0.9

A detailed analyse of each observation point in each direction is reported in Appendix A.

3.3.2 Areas and fractures of interest

The magnitude of the estimated deformation in a specific point is a function of three factors; position in space, strike and dip of the observed fracture, i.e. which principal stress is considered (magnitude and orientation). The position in space includes both the distance from, and the position in relation to the tunnel. The maximum principal stress is increased in the floor and roof of the tunnel while it decreases at the walls. Same redistribution of the stresses appears during the drilling of the deposition holes. However, the affected volume is smaller since the diameter of the deposition holes is smaller than the diameter of the tunnel. The secondary stress due to the excavation of the tunnel and deposition holes is a bit complex since theirs effects interferes with each other. In Figure 3-19 the affected volumes are visualised.

A)

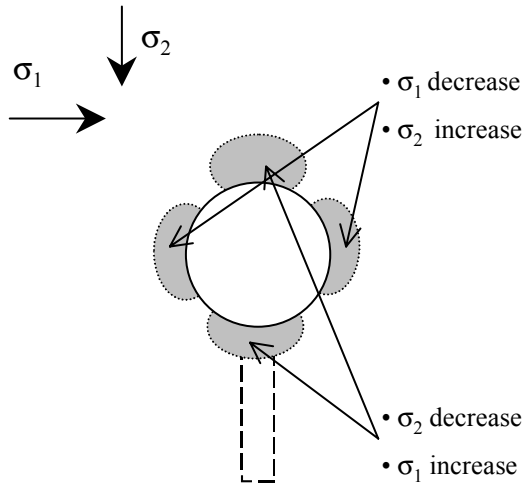

B)

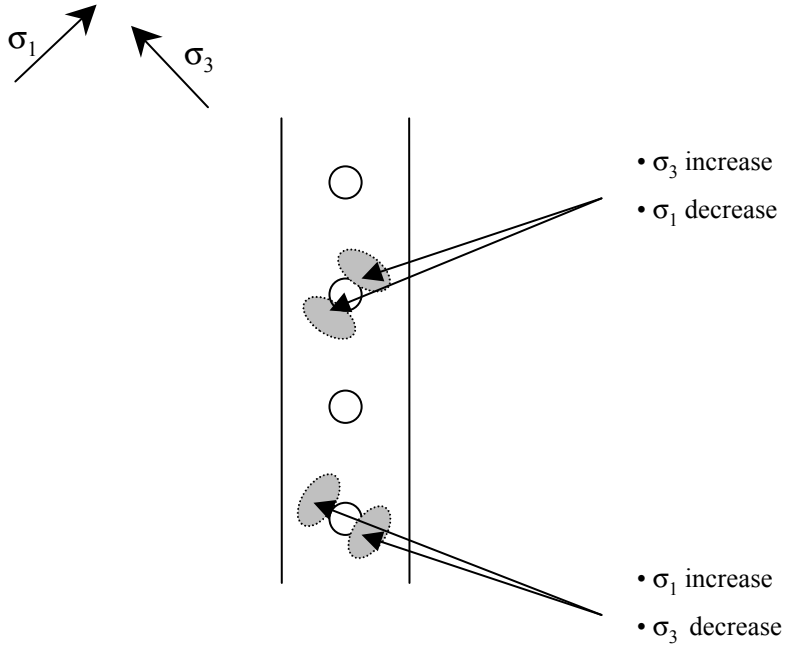

Figure 3-19. *The figure shows where the increase and decrease in stresses occur as a result of the excavation of the tunnel and deposition holes. The upper part (A) shows a vertical section while the lower part (B) shows a horizontal section.*

The affected volume will increase during the heating phase but there will still be differences between the parts of the tunnel.

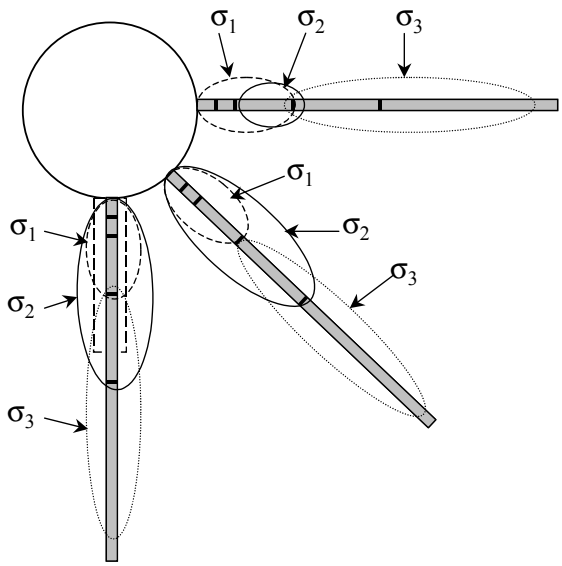

Figure 3-20. *The figure shows in what areas the largest responses of the changes in stress will occur in the different directions. The area depends on which principal stress is considered.*

If fractures at distances more than (or equal) 2 radii from the tunnel wall are observed the stress field is undisturbed. If fractures closer than 2 radii are selected the stress field is started to tighten up around the opening (see Figure 3-21) and the directions of the stresses are more complicated to estimate.

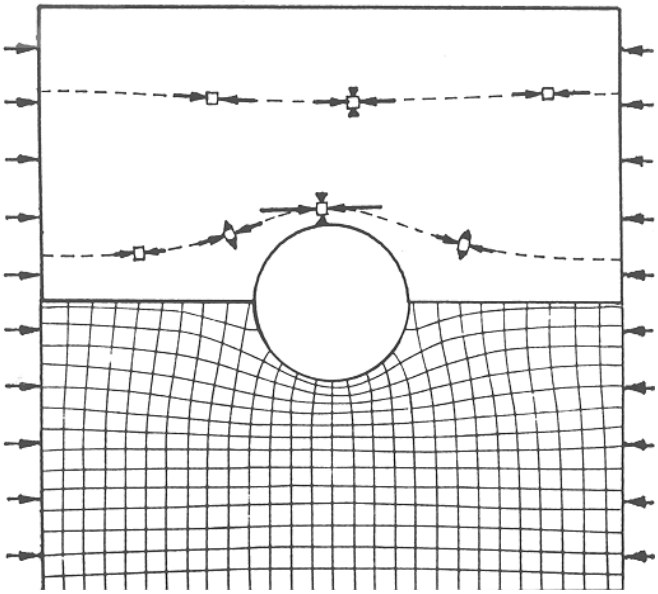

Figure 3-21. *Maximum and minimum principal stress trajectories around a circular hole. From Hoek and Brown, 1982.*

The situation will be even more complicated when the deposition holes and the surrounding tunnels are taken into account.

A numerical modelling of the stresses is necessary in order to analyse the stress directions close to the deposition holes in detail. A numerical modelling is presented in Claeson et al, (2001).

4 Is it possible to measure fracture deformation at high stresses?

As mentioned in chapter 2.1 a number of research projects have been done during the last decades concerning fracture deformation as a result of increased effective stress. In the tests the fracture deformation has been separated from the rock mass deformation and it is clear that the fracture is softer than the rock mass at lower stress. The fracture will deform non-linear in the beginning and after a while react more like intact rock i.e. the rock mass modulus converge to the Young's modulus of the intact rock.

A majority of the laboratory tests have been conducted at stresses up to 10-15 MPa and in few cases up to 30 MPa in crystalline rock. This is important to have in mind in the further discussion.

The questions are:

- At which stress does the fracture behave more or less as the intact rock?
- Is it possible to measure the deformation and separate the fracture deformation from the rock mass deformation at high stresses?

The proposed measurement technique consists of two anchors placed in a borehole with a sensor between them. The sensor registers if one anchor move relative the other one. The borehole intersects a fracture plane and the anchors are placed on each side of the fracture.

4.1 Conceptual model

To analyse the problem a conceptual model was formulated and an analytical approach was used. The model is 1.0x1.0x0.3 m^3 and a horizontal fracture divided the block in two pieces and the borehole intersects the fracture. A schematic overview of the model including the anchors is shown in Figure 4-1 and the actual conceptual model is shown in Figure-4-2.

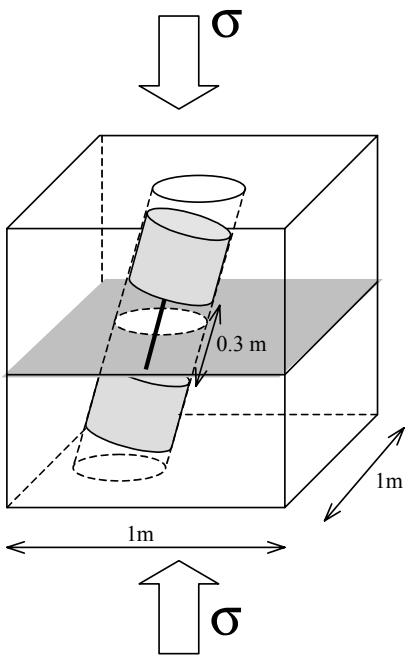

Figure 4-1. *A schematic figure that describes a rock block including one borehole, which intersects the fracture. The distance between the anchors is 0.3 m.*

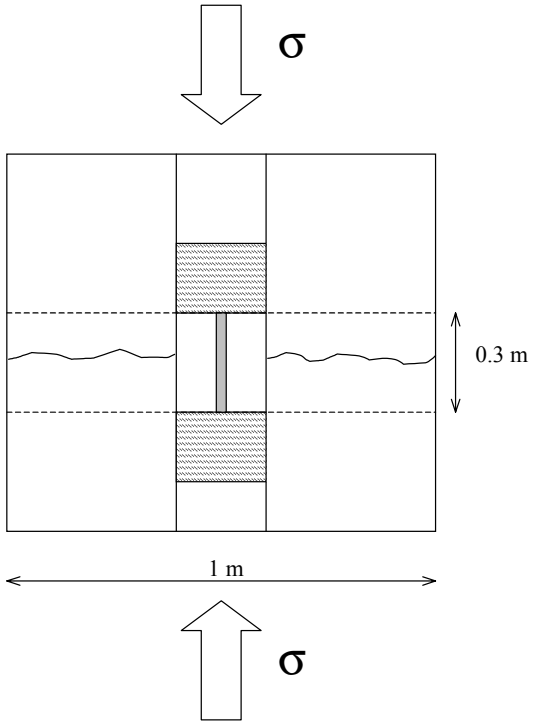

Figure 4-2. *The conceptual model that is used to estimate the rock and fracture deformation.*

4.2 Analyses

In this analysis the deformation of the fracture is assumed to follow the relationship (Swan, 1983). Accordnig to Swan (1983) this relationship is applicable to various stress levels (see section 2.3):

$$\delta = b_0 \sigma^{b_1} \qquad \textit{Eq. 4-1}$$

Values for the constants are taken from the literature. Sun et. al (1985) did a number of tests in three different types of rock, two granites and one slate. The constant b_1 varies between 0.41 and 0.56. In this analysis b_1 varies between 0.40 and 0.55.

Equation 4-1 is based on tests that were performed at stresses lower than the expected final stress at prototype area at Äspö Hard Rock Laboratory. Nevertheless, in this analysis the relationship has been used to extrapolate the fracture behaviour up to the expected final stress level in order to give a scope estimation of the behaviour.

The deformation of the intact rock, δ_{rock}, as a result of increased stress is estimated by using the expression:

$$\delta_{rock} = \frac{L\sigma}{E_i} \qquad \textit{Eq. 4-2}$$

Where	L = the length of the sample	[m]
	σ = stress	[MPa]
	E_i = Young's modulus	[GPa]

The Young's modulus used is in the same range as the modulus evaluated at Äspö Hard Rock Laboratory (75 GPa). At some stress level the rate of fracture deformation will be the same as the deformation rate of the intact rock. In Figure 4-3 the endpoint of the different curves indicates at which stress level the deformation rate is the same. As can be seen, the stress level (or endpoints) varies and that depends on the fracture stiffness. Note that the deformation curve for intact rock is strongly dependent of the length of the observed specimen.

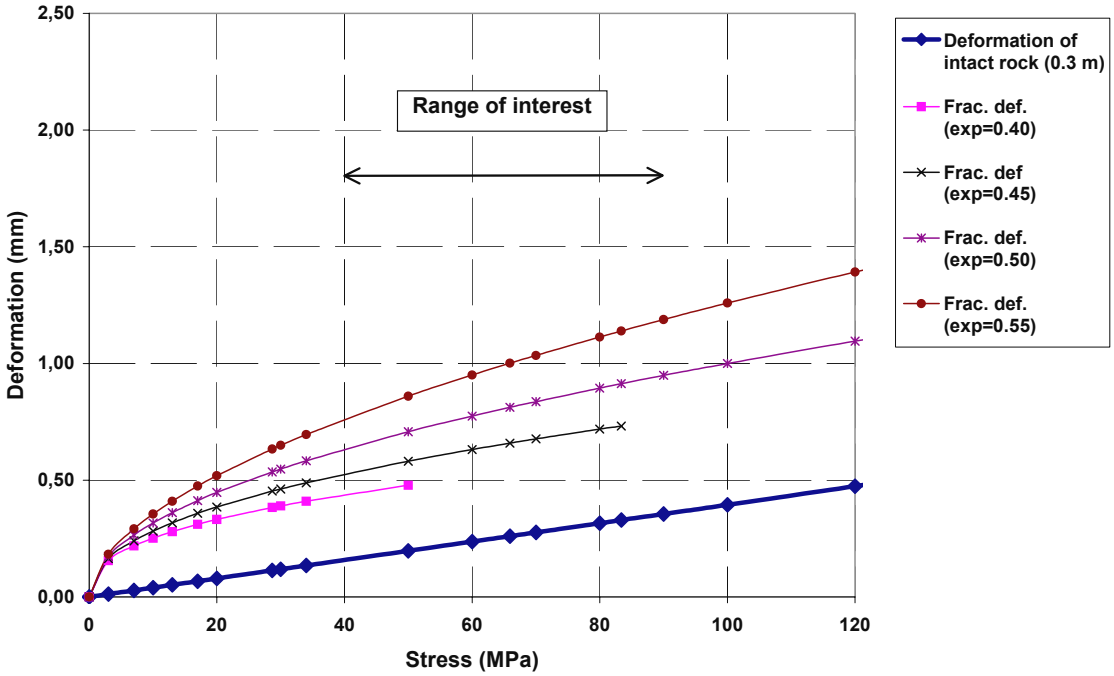

Figure 4-3. *The figure shows the deformation curves of a fictive fracture with different values on b_1 as well as the deformation curve for intact rock (with L= 0.3 m). The endpoints show at which stress the deformation rate is equal for both fracture and intact rock (L= 0.3m). Range of interest shows the estimated stress level at prototype area at ÄHRL (see Table 3:8).*

If a measurement concept as shown in Figure 4-2 is used the measured deformation consist of both fracture deformation and intact rock deformation. The estimated behaviour of rock and fracture deformation is shown in Figure 4-4.

At stresses close to the endpoint the fracture deformation rate decrease and the rate will be less than the deformation rate of the intact rock. Above this stress level the fracture deformation can be hard to separate from the deformation of intact rock.

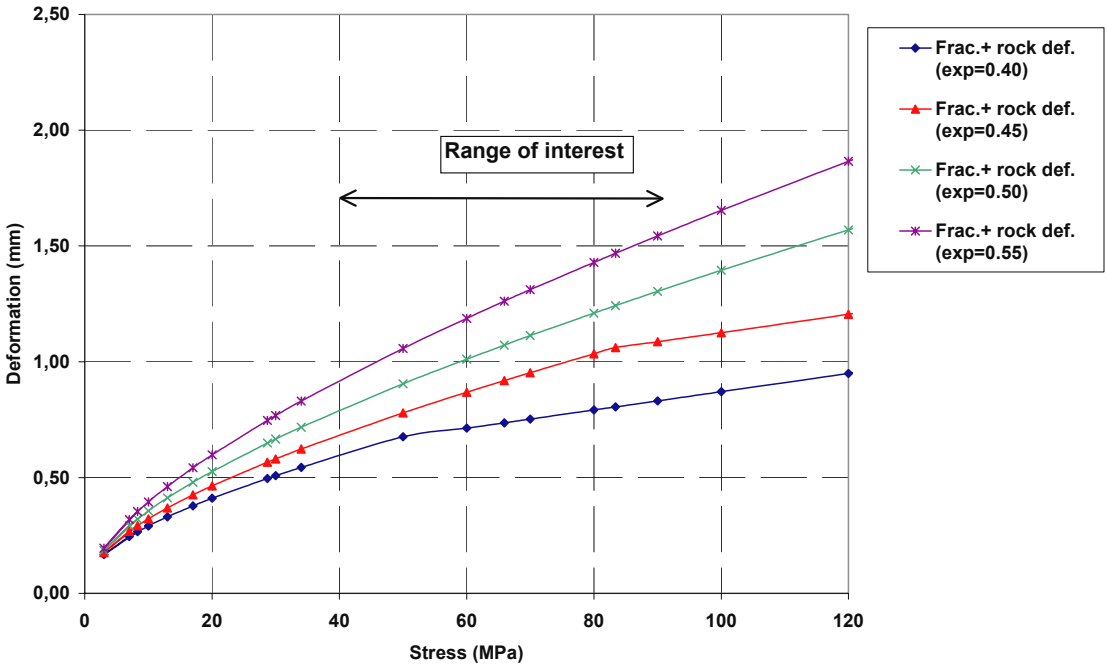

Figure 4-4. *The estimated total deformation, fracture and intact rock. Range of interest shows the estimated stress level at prototype area at ÄHRL (see Table 3:8).*

The maximum expected stress level at prototype repository after three to five years was shown in Table 3:8. According to the estimated stress levels the maximum stress will be roughly 90 MPa but the major part will be in an order of 40-60 MPa.

4.3 Analytical results

The analytical model indicates that it may be difficult to separate the fracture deformation from the deformation of the intact rock if the in-situ stresses before heating are too high. The total deformation is strongly dependent of the ratio between rock and fracture stiffness.

In order to separate the two deformations from each other it is essential to know the behaviour of the intact rock. The proposed measurement equipment should therefore be made with three anchors and two sensors. The test sections will be chosen so that two of the anchors will be placed on each side of a fracture in order to measure both fracture deformation and deformation of the rock mass. The third anchor will then be placed so the measured section only will be of intact rock (see Figure 4-5).

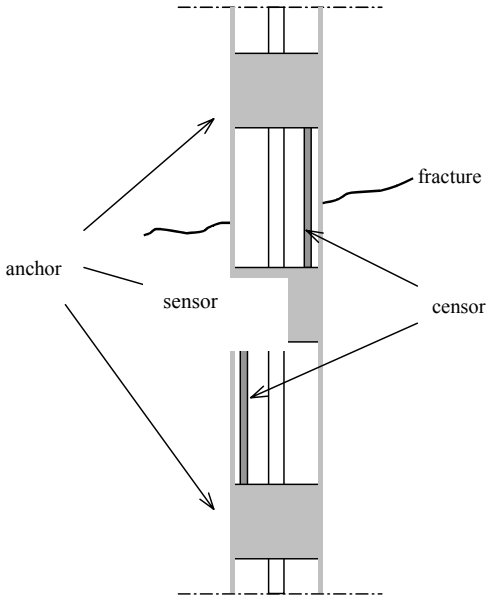

Figure 4-5. *Schematic figure of the proposed measurement equipment*

The fracture deformation ($\delta_{fracture}$) will then be calculated as follows (if the test section lengths between the anchors are equal):

$$\delta_{fracture} = \delta_{fracture + intact\ rock} - \delta_{intact\ rock}$$

The answers of the two questions in the beginning of this chapter are

- It is possible to measure the deformation and separate the fracture deformation from the over all rock mass deformation. This is done by measuring the deformation of the intact rock at the same position (more or less) as the fracture deformation is measured.
- However, it is hard to say at which stress the fracture deformation rate is equal or less than the deformation rate of intact rock.

5 Conclusions

The conclusions are:

- The hydraulic response will in general be decreased transmissivity. The decrease will be larger the closer the fractures are to the canisters.
- The transmissivity is expected to be reduced to something between 10 and 80 percent of the in-situ values.
- The fracture closure is expected to be reduced to be in the range of 5-70 micrometer.
- The hydraulic and mechanical responses on the fracture depend on the orientation of the fracture relative the principal stress field.
- Major part (~80%) of the increase in stress and temperature is reached within two years.

References

Ageskog L., and Jansson P., 1998: Finite element analyses of heat transfer and temperature distribution in buffer and rock, general part & case No 1. Äspö Hard Rock Laboratory. Prototype Repository. SKB Progress Report HRL-98-20, Stockholm.

Ahola M. P., Mohanty S. and Makurat A., 1996: Coupled mechanical shear and hydraulic flow behaviour of natural rock joints. In: Stephansson O., Jing L. and Tsang C.-F. (eds.), Coupled thermo-hydromechanical processes of fractured media, Developments in Geotechnical Engineering, vol. 79, Elsevier Science B.V., Amsterdam, pp. 393-423.

Alm P., 1999: Hydromechanical Behaviour of a Pressurised Single Fracture: An *in-situ* Experiment. PhD-thesis, Department of Geology, Chalmers University of Technology

Amadei B. and Stephansson O., 1997: Rock Stress and its Measurement, Chapman & Hall.

Bandis S. C., Lumsden A. C. and Barton N. R., 1983: Fundamentals of rock joint deformation. International Journal of Rock Mechanics and Mining Sciences & Geomechanics Abstracts, Vol. 20, No. 6, pp. 249-268.

Bart M. and Shao J. F., 1998: Damage mechanics approach for hydromechanical coupling in rock joints under normal stress. In: Rossmnith (ed.), Mechanics of jointed and faulted rock, Balkema, Rotterdam, pp. 613-619.

Chijimatsu M., Sugita Y., Fujita T., and Amemiya K., 1999: Experimental results. Coupled Thermo- Hydro- Mechanical Experiment at Kamaishi Mine. Technical Note 15-99-02. Japan.

Claeson C., Dahlström L.-O., and Sandén M., 2001: Finite element analyses of mechanical consequences due to the rock excavation and thermal load. SKB International Progress Report, IPR, In press, Stockholm.

Cook N. G. W., 1992: Natural joints in rock: mechanical, hydraulic and seismic behaviour and properties under normal stress. International Journal of Rock Mechanics and Mining Sciences & Geomechanics Abstracts, Vol. 29, No. 3, pp. 198-223.

Dershowitz W., Wallman P. and Kindred S., 1991: Discrete fracture modelling for the Stripa site characterization and validation drift inflow predictions. SKB Stripa project report TR 91-16, SKB, Stockholm

Dunat X., Vinches M., Henry J.-P. and Sibai M., 1998: Modelling of hydromechanical coupling in rock joints. In: Rossmnith (ed.), Mechanics of jointed and faulted rock, Balkema, Rotterdam, pp. 441-446.

Esaki T., Hojo H., Kimura T., and Kamedam N., 1991: Shear-flow coupling test on rock joints. Seventh International Congress on Rock Mechanics, Aachen, Germany, Vol. 1, Ed. Wittke, Rotterdam, Netherlands: A.A Balkema, pp. 389-392.

Elliott G. M., Brown E. T., Boodt P. I. and Hudson J. A., 1985: Hydromechanical behaviour of joints in the Carnmenellis granite, S. W. England. In: Stephansson, O. (ed.), Fundamentals of rock joints, Centek Publ., Luleå, Sweden, pp. 249-258.

Evans K. F., Kohl T., Hopkirk R. J. and Rybach L., 1992: Modelling of energy production from Hot Dry Rock systems. Project Report, Eidgenössische Technische Hochschule / Polydynamics, Zürich, Switzerland.

FEBEX, 2000: Full-Scale Engineered Barriers Experiment for a Deep Geological Repository for High Level Radioactive Waste in Chrystalline Host Rock. Final Report. Madrid, Spain.

Forsmark T. and Rhén I.,1999: Hydrogeology interference test campaign 1 after drill campaign 3. SKB International Progress Report, IPR-00-07, Stockholm.

Goodman R. E., 1976: Methods of geological engineering in discontinuous rocks. West New York.

Hardin E., Barton N., and Lingle D., 1982: Heated flatjack test series to measure the thermomechanical and transport properties of in-situ rock masses. ONWI-260. Office of Nuclear Waste Isolation, Columbus.

Hoek E. and Brown E., T., 1982: Underground excavation in rock. The institution of mining and metallurgy, London.

Jung R., 1989: Hydraulic In-situ investigation of an artificial fracture in the Falkenberg granite. International Journal of Rock Mechanics and Mining Sciences & Geomechanics Abstracts, Vol. 26, pp. 301-308.

Klasson H., Persson M. and Ljunggren C., 2001: Rock stress measurements by overcoring at the Äspö HRL, Prototype Repository: borehole KA3579G (revised data) and K-tunnel: borehole KK0045G01. SKB International Progress Report, IPR-01-67, Stockholm

Klee G., and Rummel F., 2002: Rock stress measurements at the Äspö HRL. Hydraulic fracturing in boreholes KA2599G01 and KF0093A01. SKB International Progress Report, IPR-02-02, Stockholm

Makurat A., Barton N., Vik G., Chryssanthakis P., and Monsen K., 1990: Jointed rock mass modelling, Proceedings of the International Conference on Rock Joint, Eds. Barton N and Stephansson O., Loen, Norway, pp. 647-656.

Pyrak-Nolte L. J., Morris J. P., 2000: Single fractures under normal stress: The relation between fracture specific stiffness and fluid flow. International Journal of Rock Mechanics and Mining Sciences, Vol. 37, pp. 245-262.

Raven K. G. and Gale J. E., 1985: Water flow in a natural rock fracture as a function of stress and sample size. International Journal of Rock Mechanics and Mining Sciences & Geomechanics Abstracts, Vol. 22, No. 4, pp. 251-261.

Rhén I (ed)., Gustafson G., Stanfors R., and Wikberg P., 1997: Äspö HRL – Geoscientific evaluation 1997/5. Model based on site characterization 1986-1995. SKB Technical Report TR 97-06, Stockholm.

Rhén I. and Forsmark T:, 2001: Äspö HRL Prototype Repository. Hydrogeology. Summary report of investigations before the operation phase. SKB International Progress Report, IPR-01-65, Stockholm

Stephansson O., Jing L. and Tsang C.-F., (eds), 1996: Coupled thermo-hydromechanical processes of fractured media, Developments in Geotechnical Engineering, vol. 79, Elsevier Science B.V., Amsterdam,

Stigsson M., Outters N. and Hermansson J., 2001: Äspö HRL Prototype Repository. Hydraulic DFN model no:2. SKB International Progress Report, IPR-01-39, Stockholm

Sun Z., Gerrard C. and Stephansson O., 1985: Rock joint compliance tests for compression and shear loads. International Journal of Rock Mechanics and Mining Sciences & Geomechanics Abstracts, Vol. 22, No. 4, pp. 197-213.

Swan G., 1983: Determination of stiffness and other joint properties from roughness measurements. Rock Mechanics and Rock Engineering, Vol. 16, pp. 19-38.

Tsang Y. W. and Witherspoon P. A., 1981: Hydromechanical behaviour of a deformable rock fracture subject to normal stress. Journal of Geophysical Research, Vol. 86, No. B10, pp. 9287-9298.

Witherspoon P. A., Wang J. S. Y., Iwai K. and Gale J. E., 1980: Validity of cubiclaw for fluid flow in a deformable rock fracture. Water Resources Research, Vol. 16, No. 6, pp. 1016-1024.

Yeo I. W., de Freitas M. H. and Zimmerman R. W., 1998: Effect of Shear Displacement on the Aperture and Permeability of a Rock. International Journal of Rock Mechanics and Mining Sciences. Vol. 35, No. 8, pp. 1051- 1070.

Zhao J. and Brown E. T., 1992: Hydro-thermo-mechanical properties of joints in Carnmenellis granite. Quartely Journal of Engineering Geology, Vol. 25, pp. 279-290.

Zhao J., 1993: Effects of normal stress and temperature on hydraulic properties of rock fractures. Memories of the XXIVth Congress of the International Association of Hydrogeologists. Eds. Banks and Banks, Geol. Survey of Norway, Trondheim, Vol. 1, pp. 115-122

Appendix A. Deformation plots

Introduction

In appendix A the hydraulic and mechanical effects of changes in stress in the rock mass will be estimated.

The effects are estimated at different observation points. These observation points have been chosen with increased radii out from the tunnel wall at three different directions (see Figure A1) in order to incorporate different stress situations.

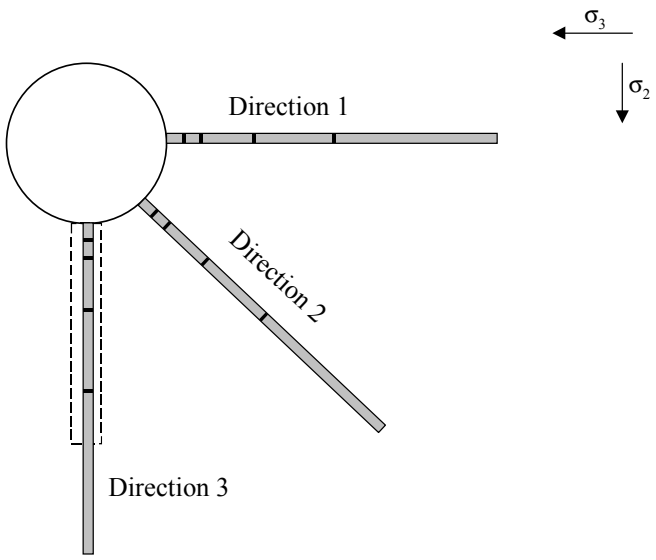

Figure A1. *The figure shows the three fictitious boreholes. The dark lines represent the observation points at 1, 2, 5,10 and 20 metres out from the tunnel wall.*

At each observation point, the magnitudes of the principal stresses are obtained by analysing results from Claeson et al. (2001). In order to see the development of the stress field, stresses from four phases are interpreted. These phases are:

1. Before any activity (*in-situ*).
2. After completing the tunnel excavation (phase 1).
3. After completing the tunnel excavation and a deposition hole (phase 2).
4. After completing the tunnel excavation and a deposition hole and 10 years of heating (phase 4).

The stress levels from the three different directions and four phases are presented in Table A1, Table A2 and Table A3.

Table A1. Interpreted effective stresses at different radii from the tunnel wall at three directions (see Figure A1). Note that "In-situ", "phase 1", "phase 2" and "phase 4" are explained above.

Distance from tunnel wall [m]	Direction 1											
	σ'_1 [MPa]				σ'_2 [MPa]				σ'_3 [MPa]			
	In-situ	Phase 1	Phase 2	Phase 4	*In-situ*	Phase 1	Phase 2	Phase 4	*In-situ*	Phase 1	Phase 2	Phase 4
1	30	23	19	64	14	16	16	39	9	5	5	14
2	30	24	23	61	14	17	17	44	9	7	7	23
5	30	26	26	59	14	18	18	43	9	10	10	32
10	30	31	31	56	14	15	15	38	9	10	10	32
20	30	30	30	-	14	14	14	-	9	9	9	-

Table A2. Interpreted effective stresses at different radii from the tunnel wall at direction 2 (see Figure A1).

Distance from tunnel wall [m]	Direction 2											
	σ'_1 [MPa]				σ'_2 [MPa]				σ'_3 [MPa]			
	In-situ	Phase 1	Phase 2	Phase 4	*In-situ*	Phase 1	Phase 2	Phase 4	*In-situ*	Phase 1	Phase 2	Phase 4
1	30	32	30	66	14	14	12	42	9	6	6	15
2	30	33	31	64	14	14	12	44	9	7	7	23
5	3	32	32	61	14	16	13	38	9	10	10	33
10	30	32	32	56	14	16	16	36	9	11	11	36
20	30	31	31	-	14	15	15	-	9	10	10	-

Table A3. Interpreted effective stresses at different radii from the tunnel wall at direction 3(see Figure A1).

Distance from tunnel wall [m]	Direction 3											
	σ'_1 [MPa]				σ'_2 [MPa]				σ'_3 [MPa]			
	In-situ	Phase 1	Phase 2	Phase 4	*In-situ*	Phase 1	Phase 2	Phase 4	*In-situ*	Phase 1	Phase 2	Phase 4
1	30	47	53	90	14	14	13	45	9	10	6	16
2	30	42	45	81	14	15	15	42	9	14	8	28
5	30	33	36	71	14	17	16	38	9	12	11	34
10	30	33	33	56	14	17	17	36	9	12	12	36
20	30	32	32	-	14	16	16	-	9	11	11	-

At each observation point three fictitious fracture planes has been analysed in terms of hydraulic and mechanical responses. The three fictitious fractures and their relation to the principal stress are:

1. Vertical fractures which strikes perpendicular to the maximum principal stress. The normal stress to these fractures is the maximum principal stress (see Figure A2a).
2. Vertical fractures which strikes parallel to the maximum principal stress. The normal stress to these fractures is the minimum principal stress (see Figure A2b).
3. Horizontal (or sub-horizontal) fractures where the intermediate principal stress acting as the normal stress to the fracture plane (see Figure A2c).

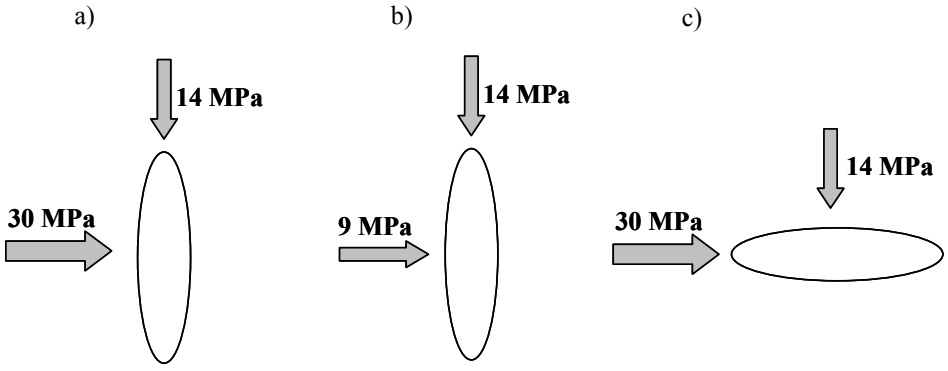

Figure A2. *Three fracture planes that are considered when fracture deformation and hydraulic change are estimated.*

Interpretation of the figures

How to interpret the following figures is described in figure A3.

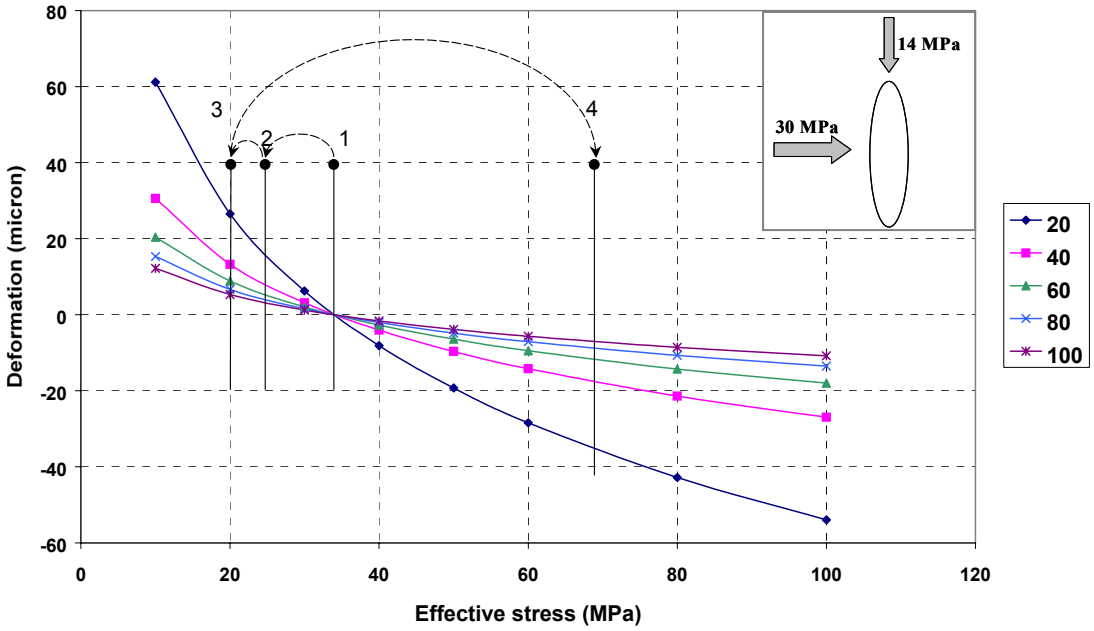

Figure A3. *An example how to interpret the stress-deformation figures. The example shows the stress and deformation history of a position 1 meter into the tunnel wall (direction 1, see Figure A1) and consider a fracture that strikes perpendicular to the maximum principal stress. Line 1 is the in-situ stress (30 MPa) at this depth before the tunnel is excavated. When the tunnel is excavated the stresses around the opening are redistributed (phase 1) and at this point the stress is unloaded (24 MPa), line 2. Further redistribution and unloading occur when the deposition holes are drilled (phase 2) (20 MPa), line 3. During the heating the stresses increases due to expansion of the rock mass and end up at 68 MPa (phase 4, line 4). The curves represent different values of the fracture stiffness (the higher value the stiffer fracture).*

Change in fracture width due to changes in effective stress.

Direction 1. Vertical fracture which strikes perpendicular to the maximum principal stress.

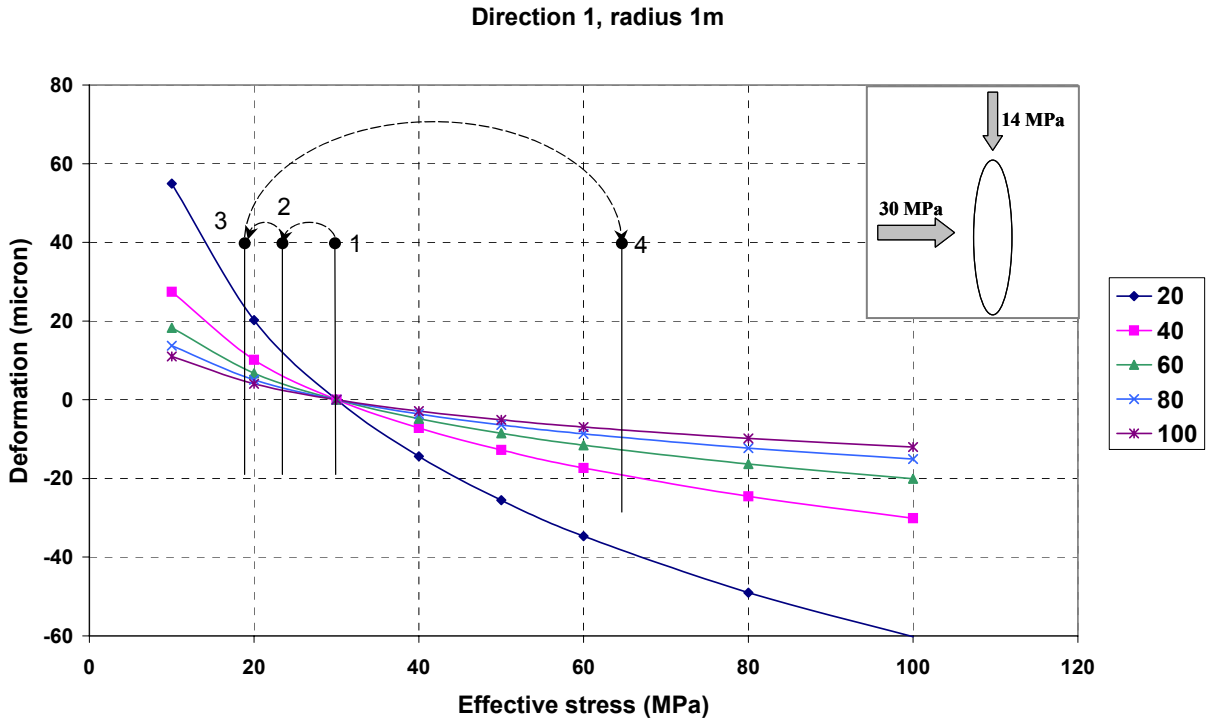

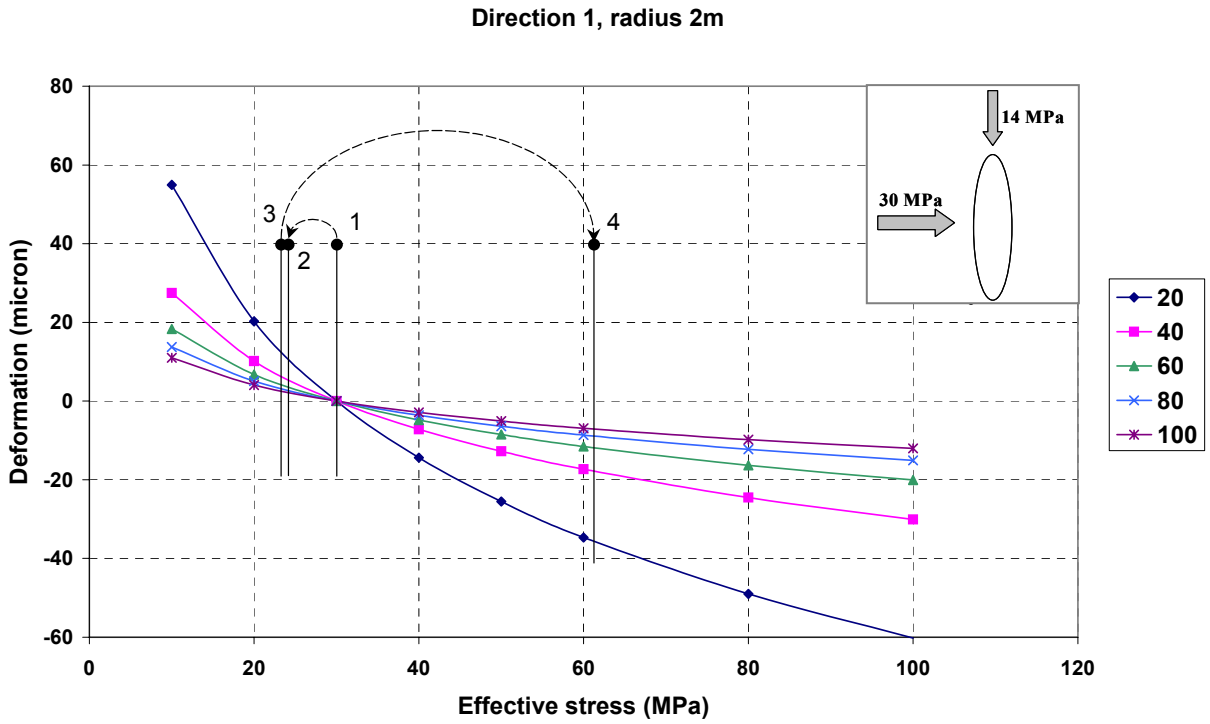

Direction 1, radius 5m

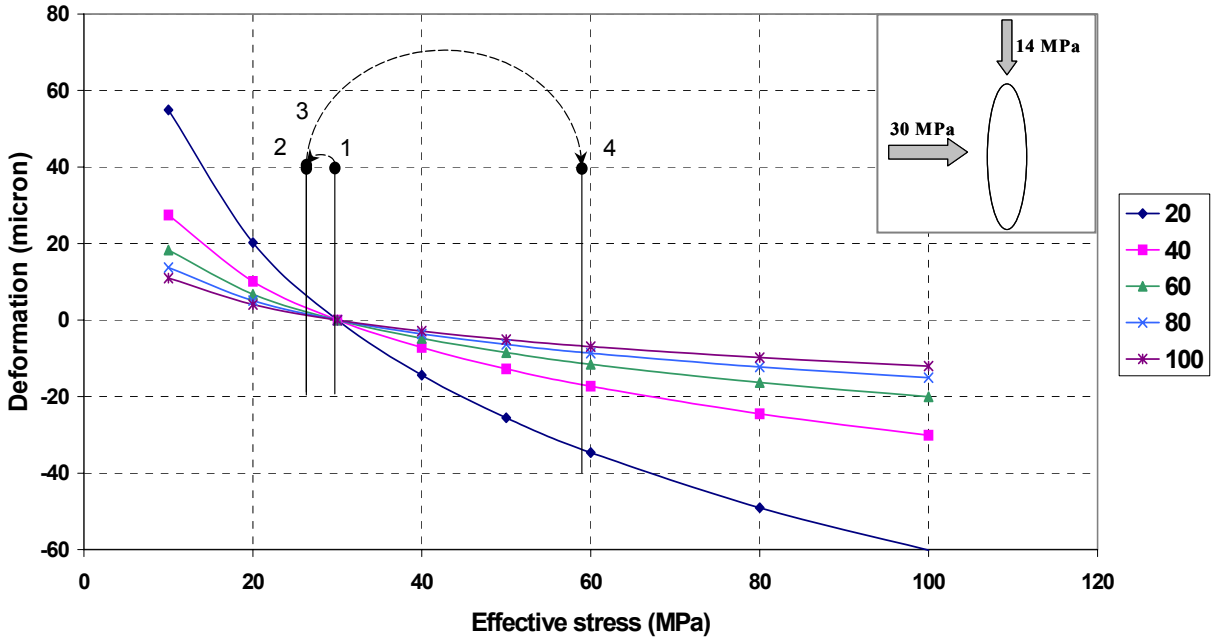

Direction 1, radius 10m

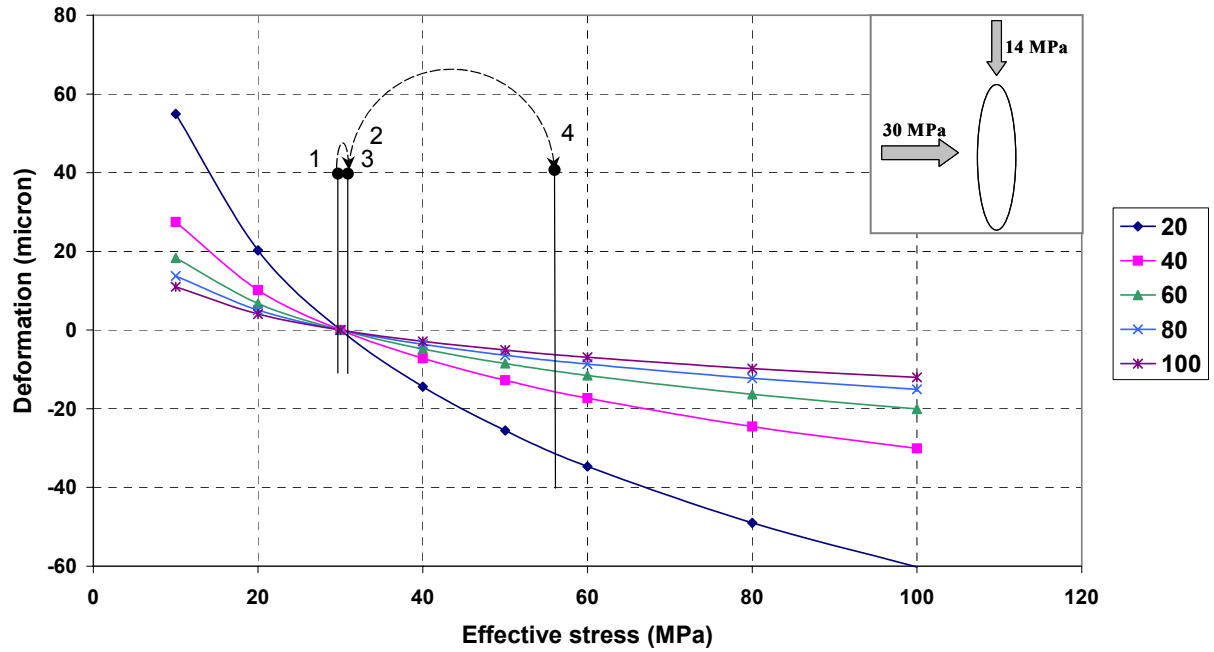

Direction 1. Horizontal fracture where the intermediate principal stress acts as the normal stress to the fracture plane.

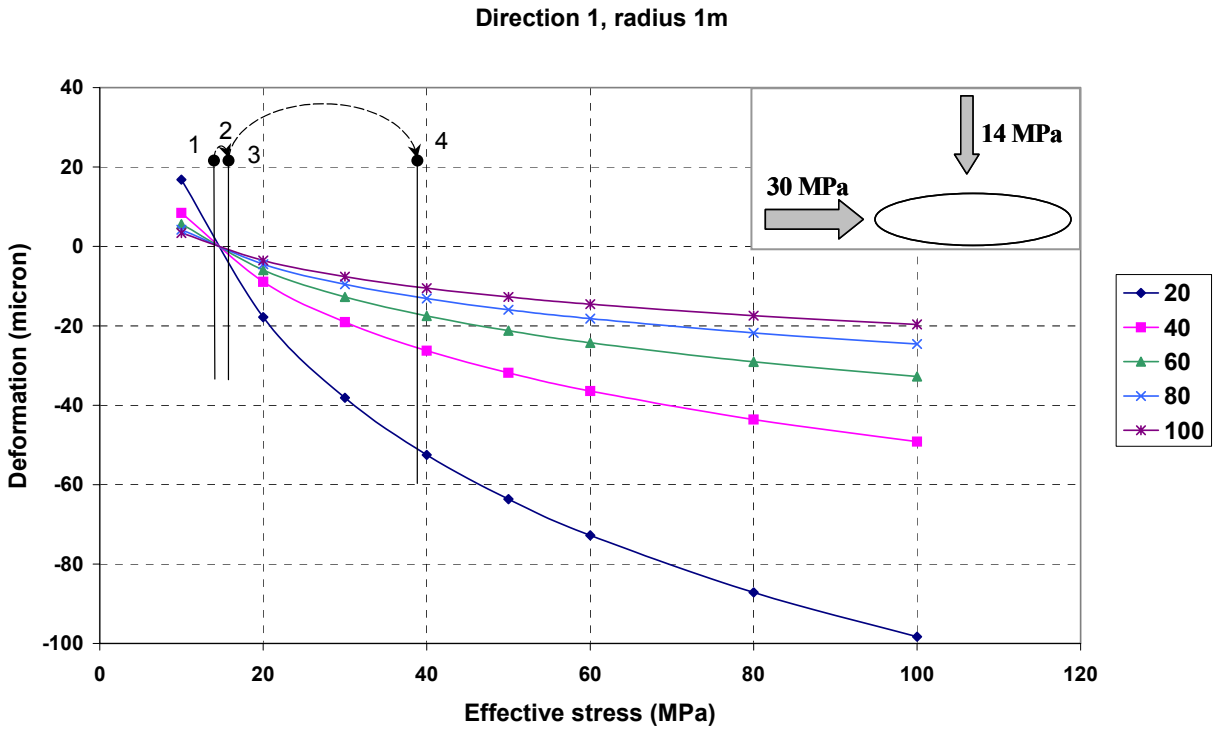

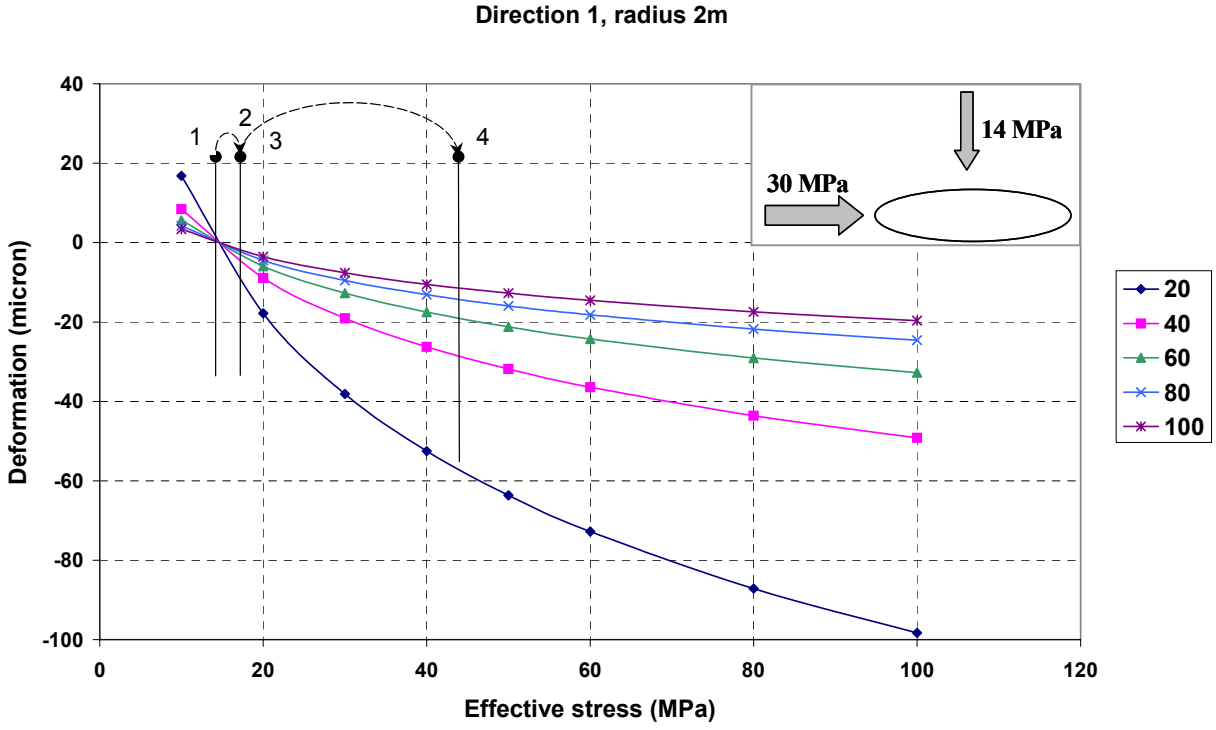

Direction 1, radius 5m

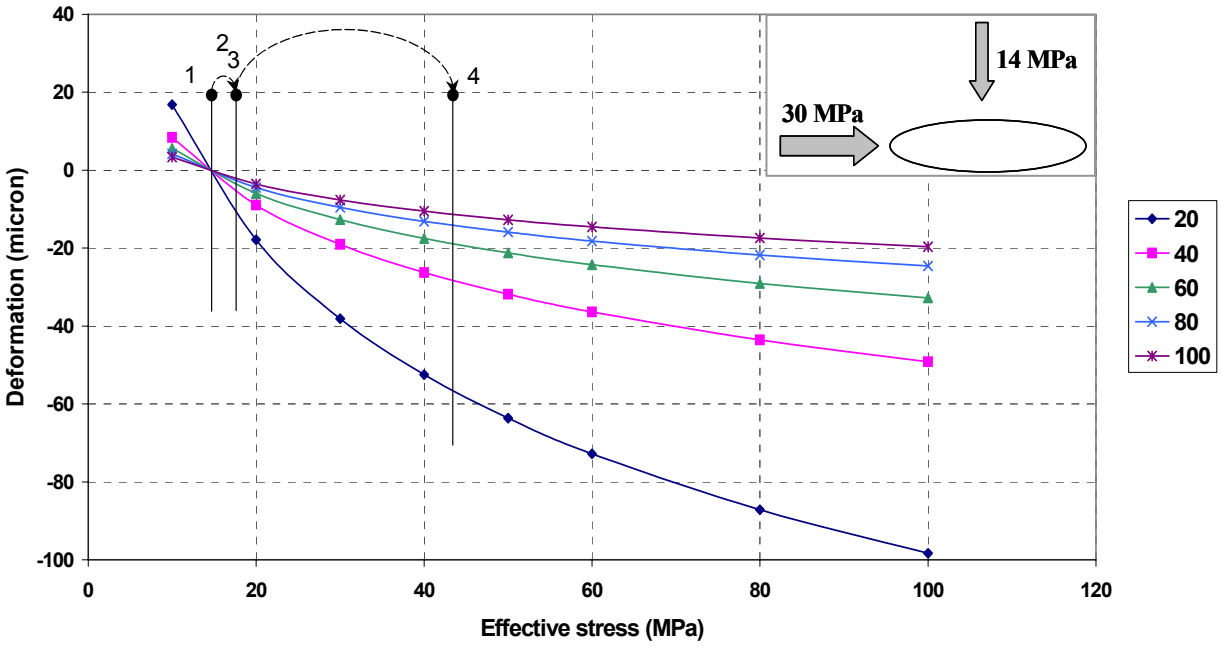

Direction 1, radius 10m

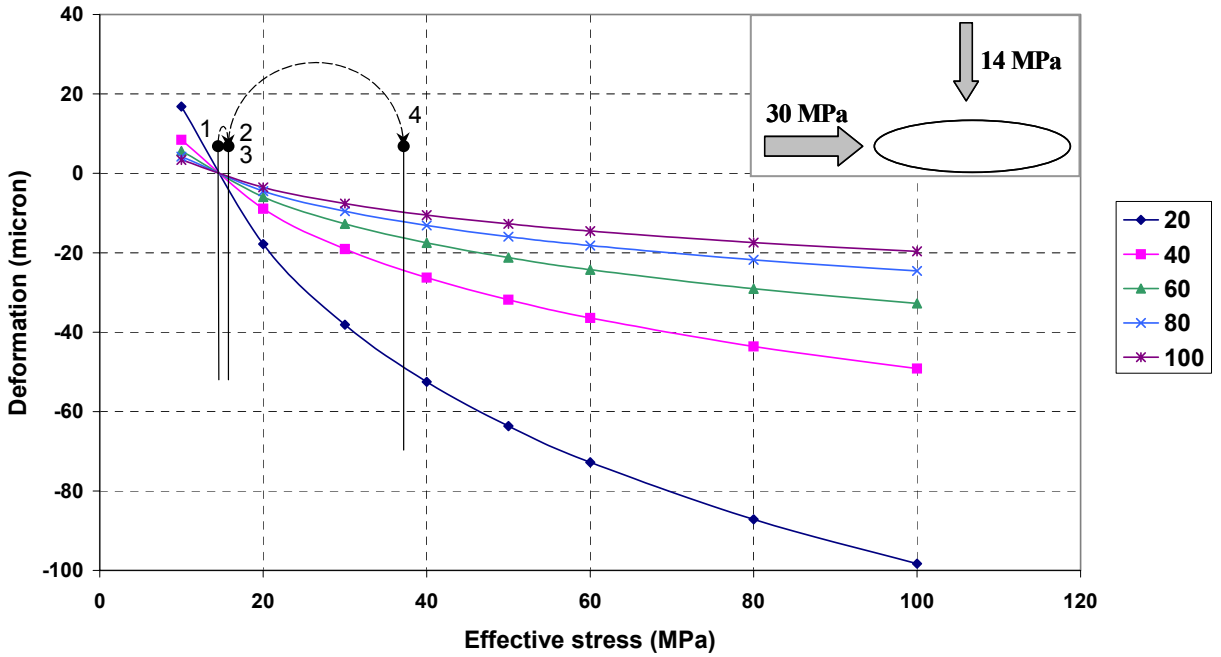

Direction 1. Vertical fracture that strikes parallel to the maximum principal stress.

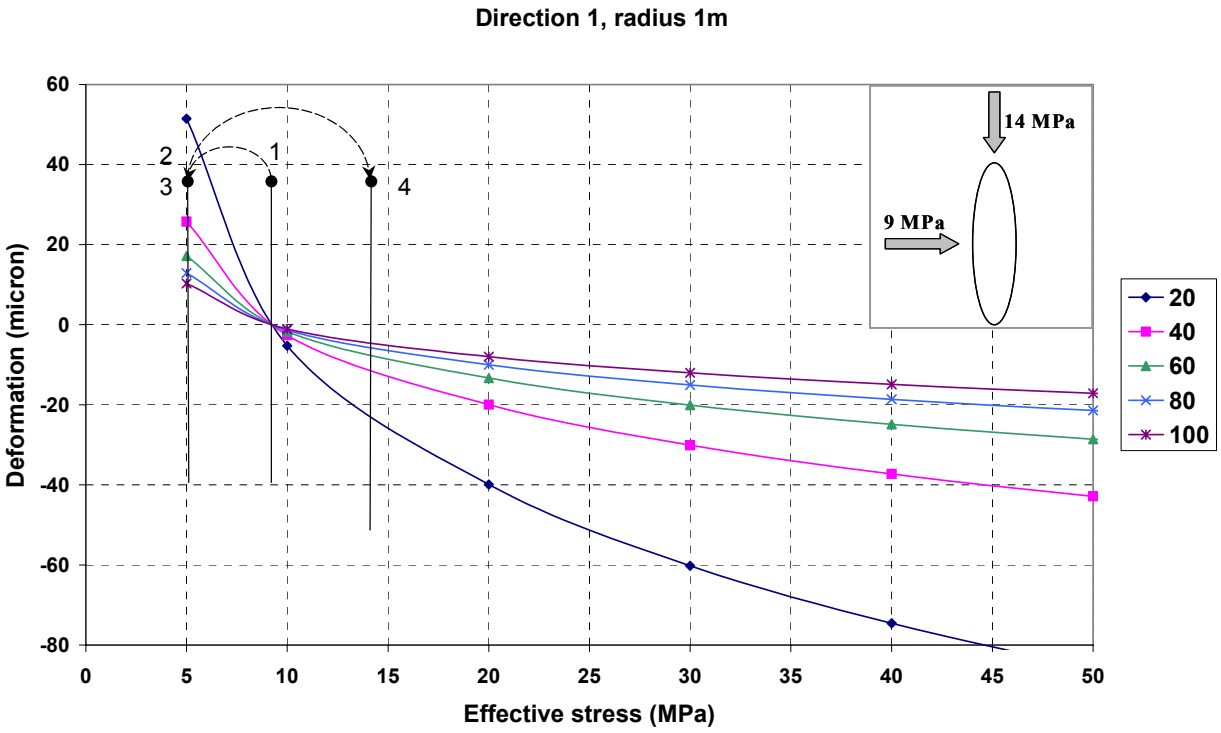

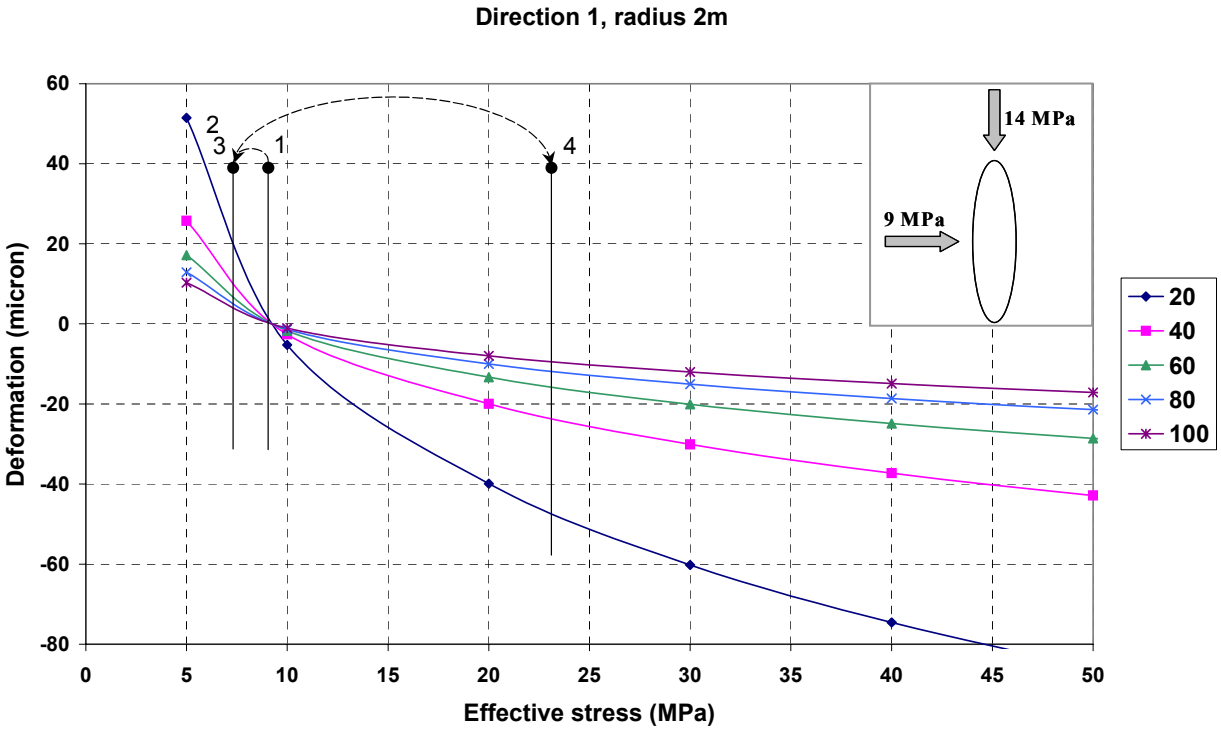

Direction 1, radius 5m

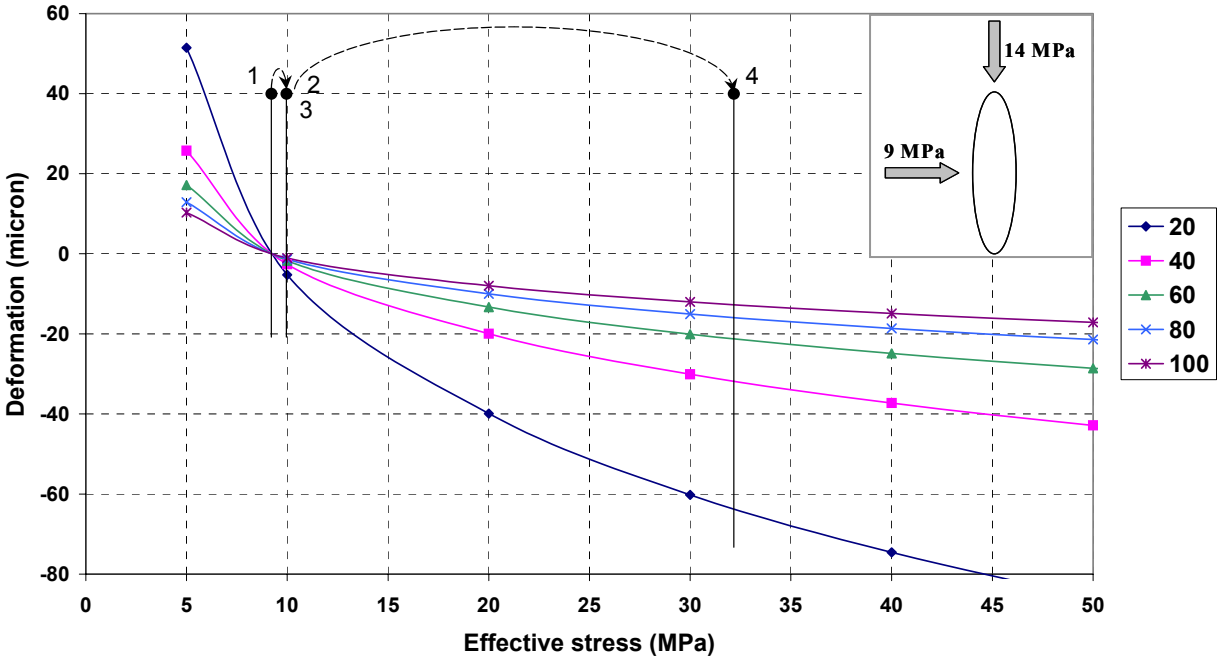

Direction 1, radius 10m

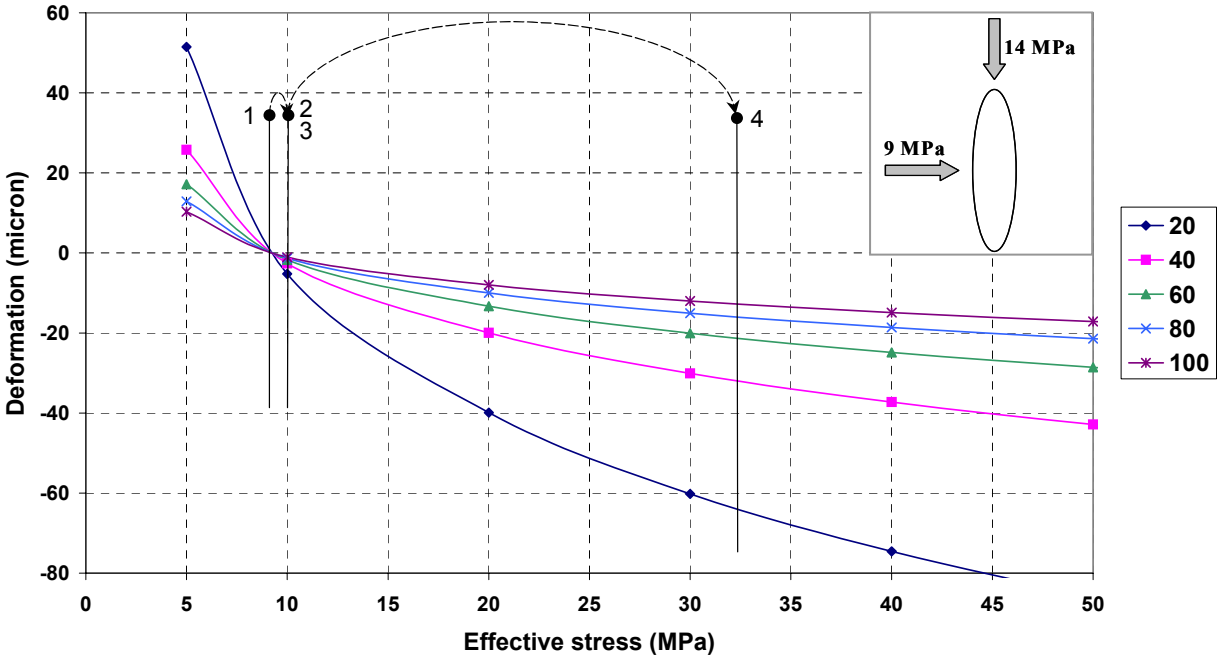

Direction 2. Vertical fracture which strikes perpendicular to the maximum principal stress.

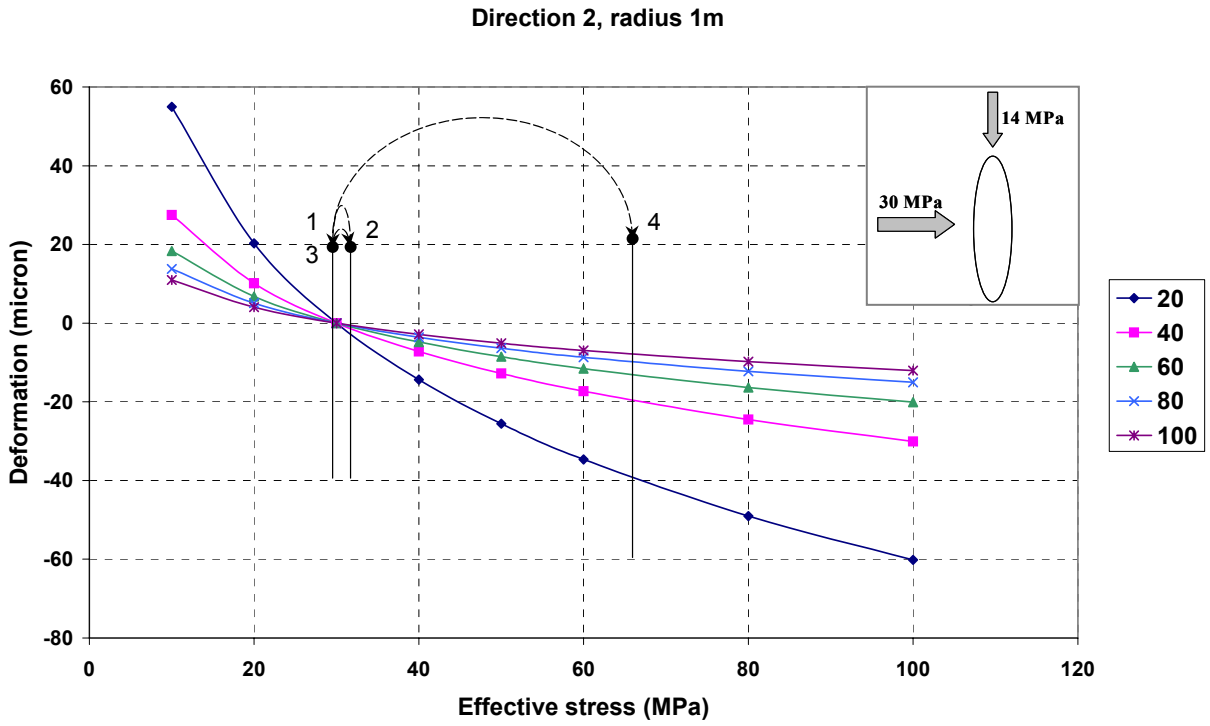

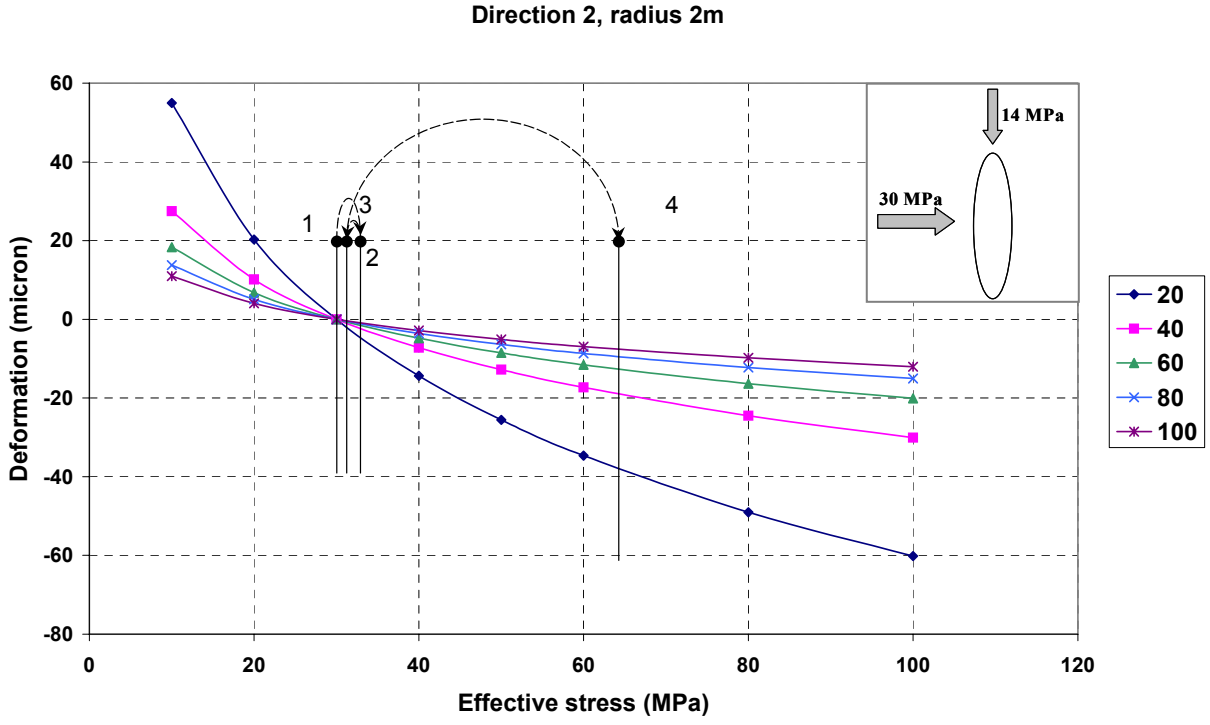

Direction 2, effective in-situ stress = 30 MPa

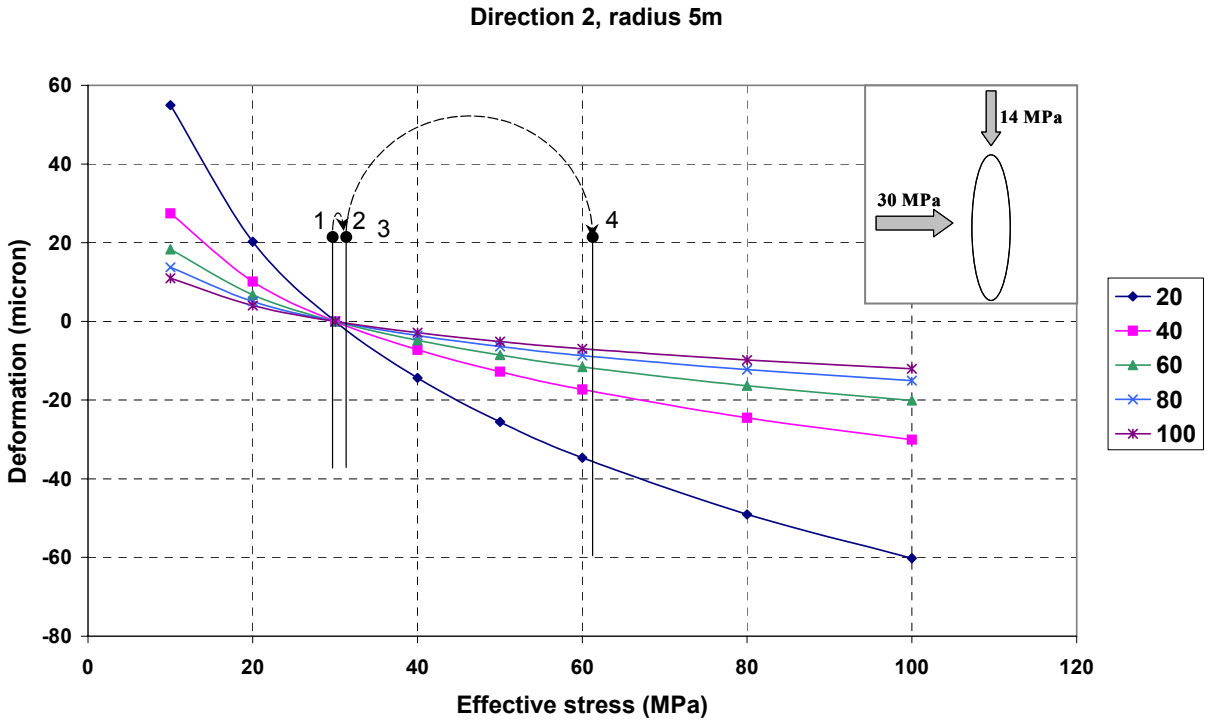

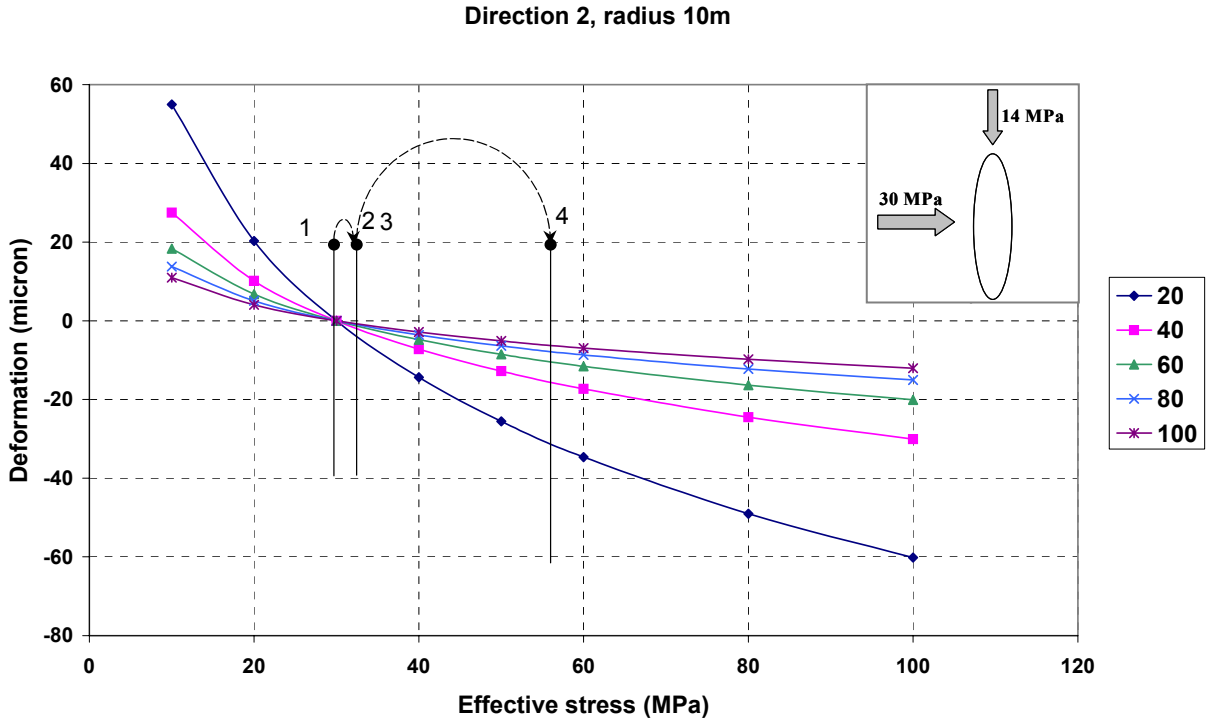

Direction 2. Horizontal fracture where the intermediate principal stress acts as the normal stress to the fracture plane.

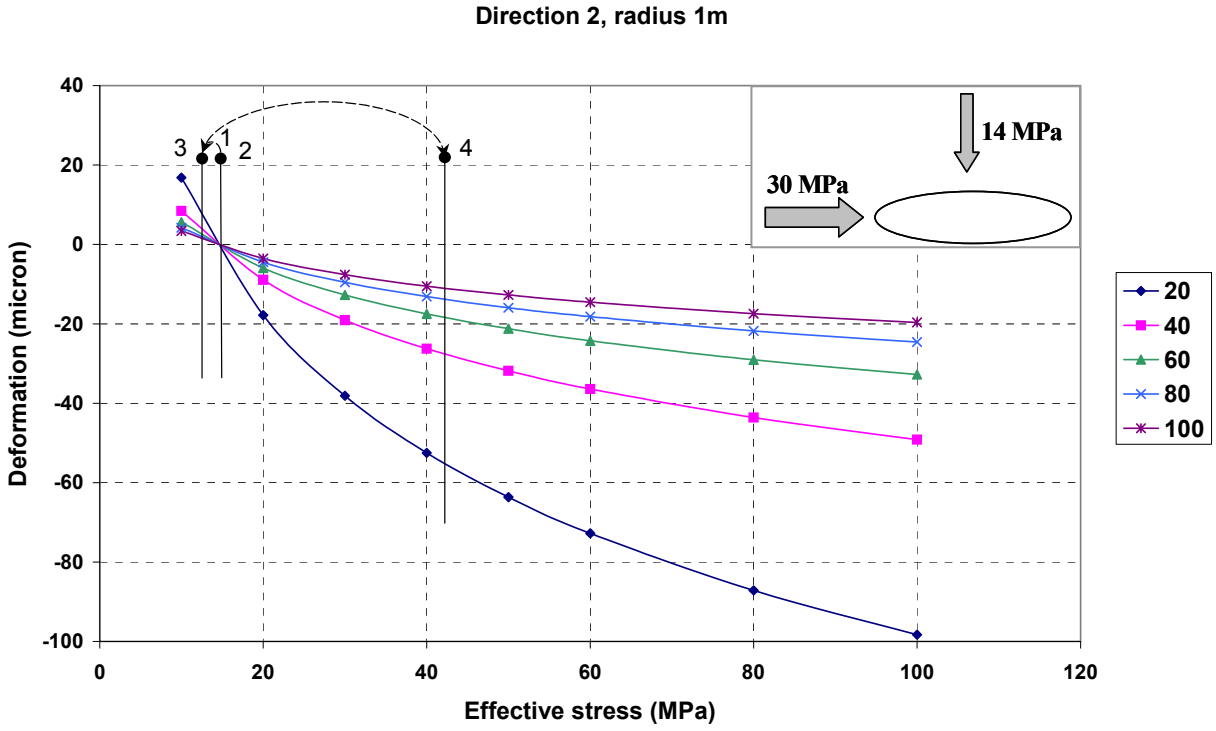

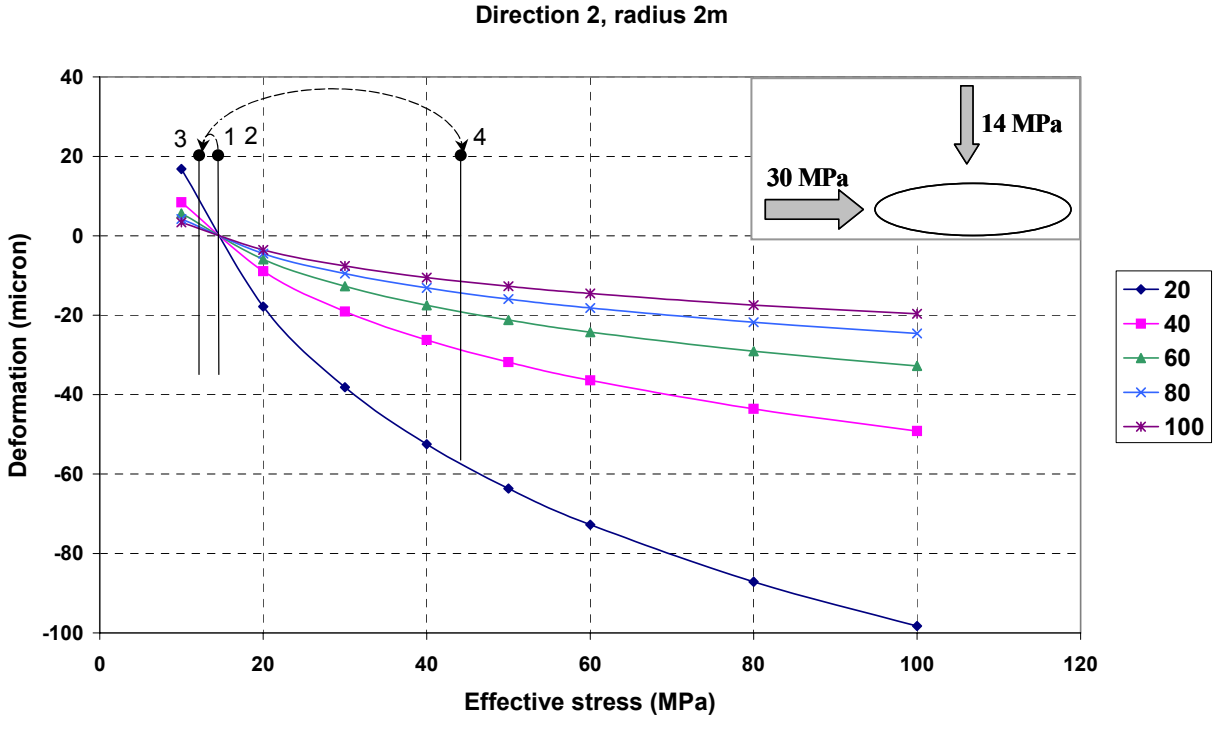

Direction 2, radius 5m

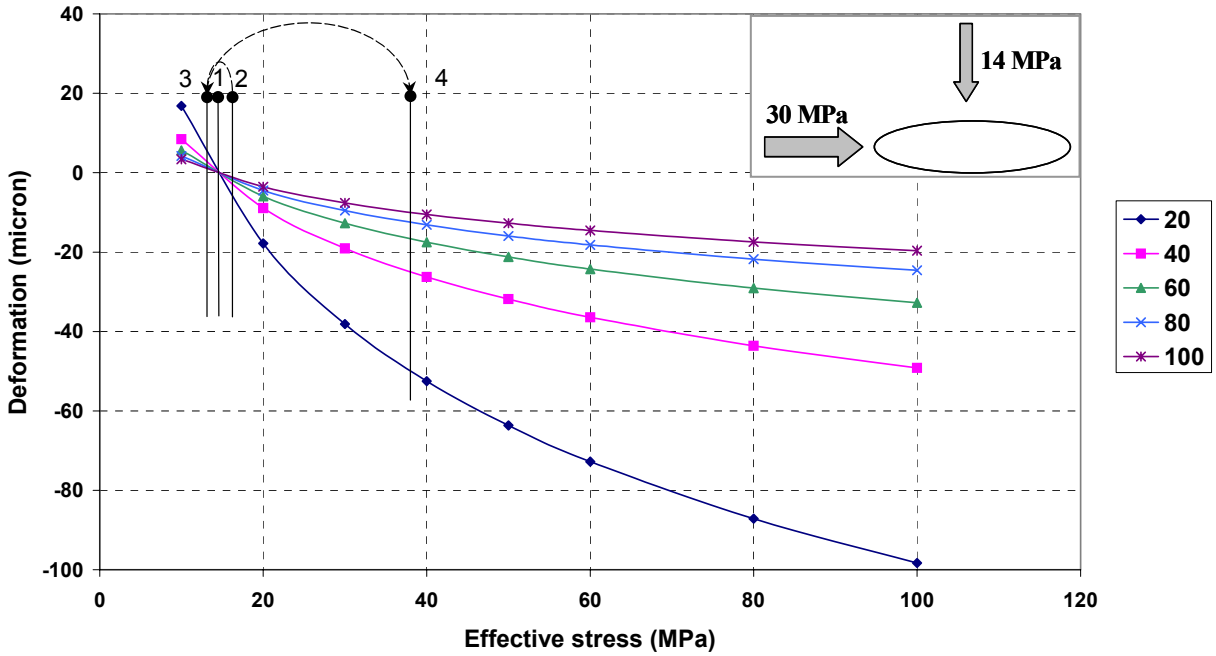

Direction 2, radius 10m

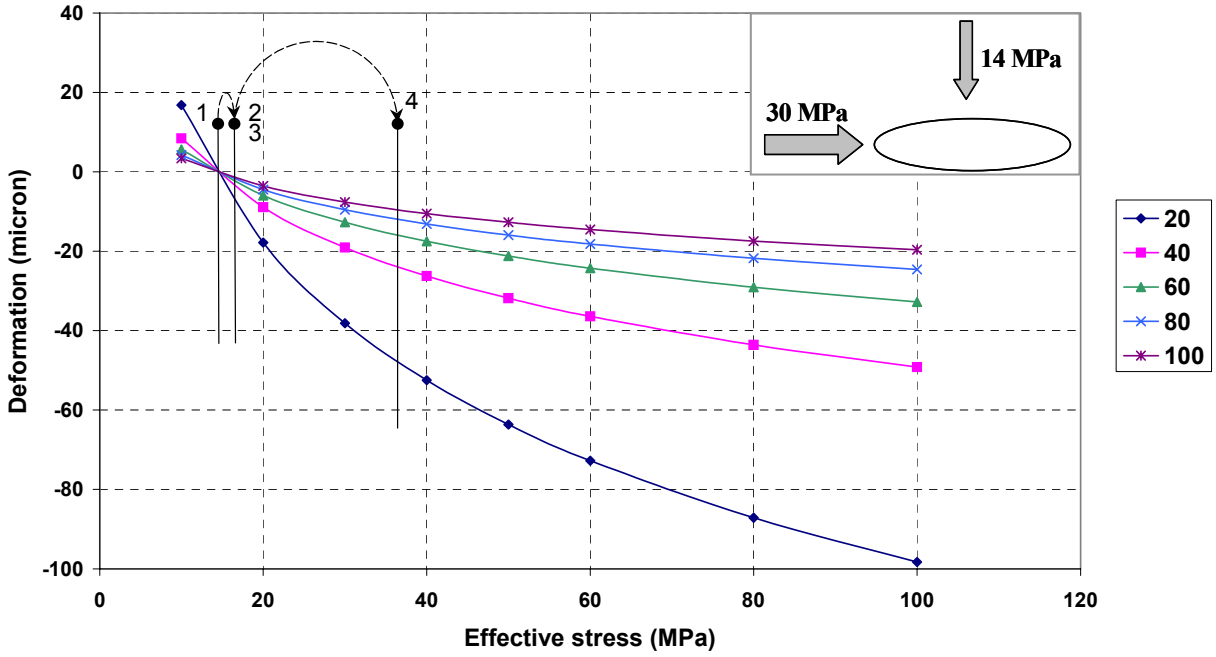

Direction 2. Vertical fracture that strikes parallel to the maximum principal stress.

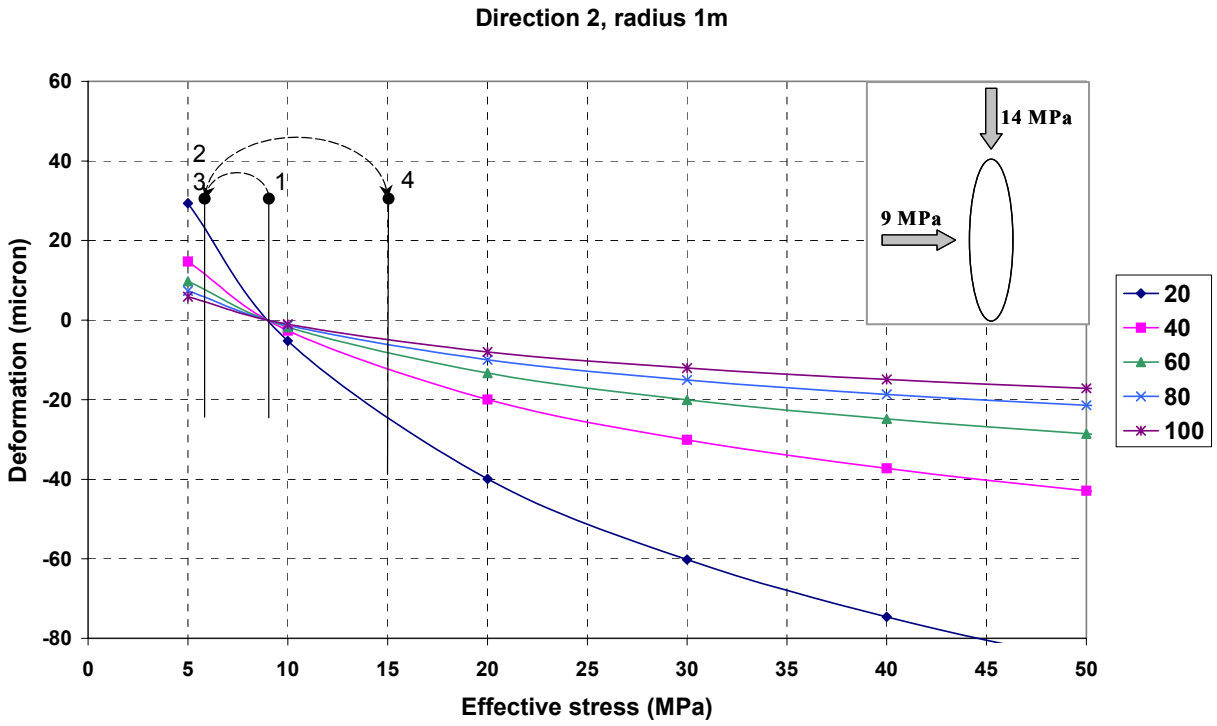

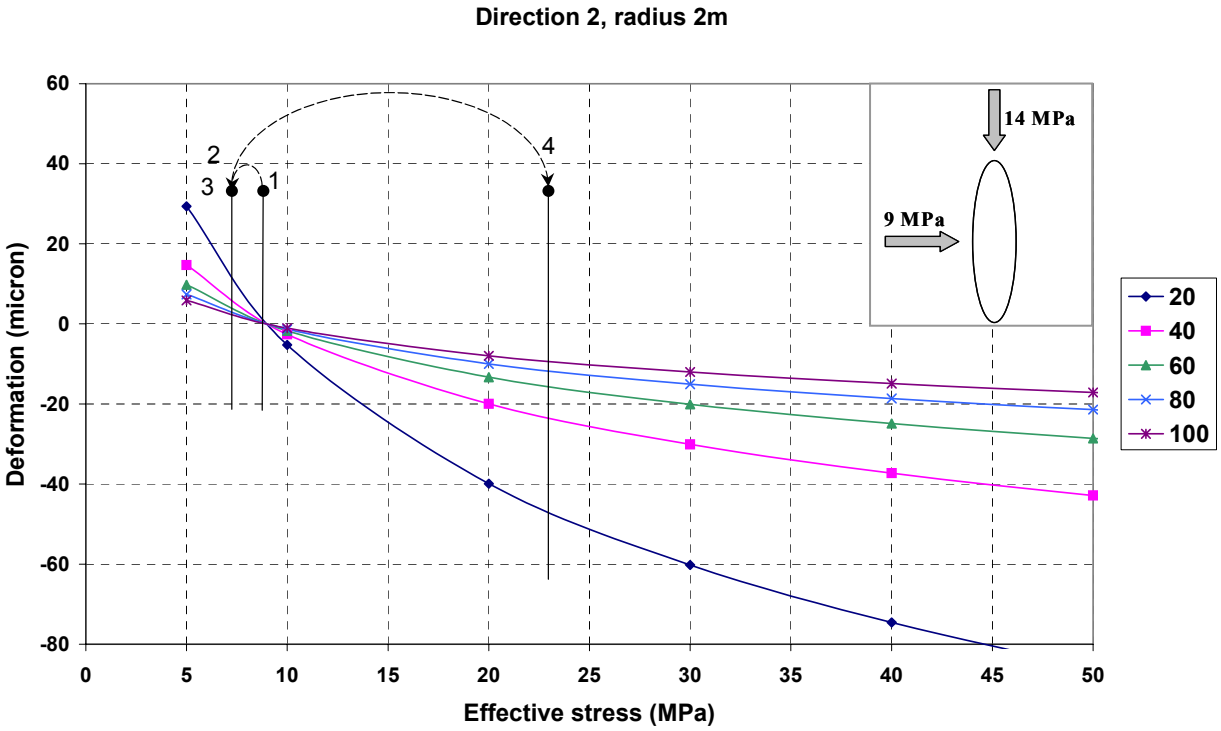

Direction 2, radius 5m

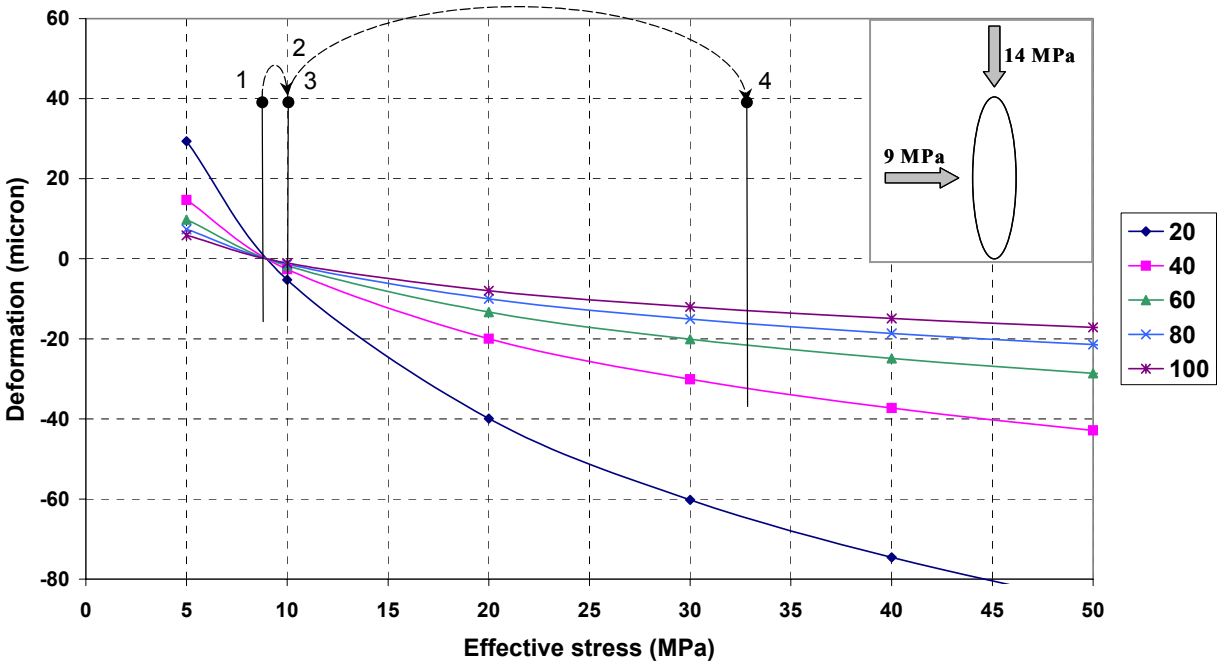

Direction 2, radius 10m

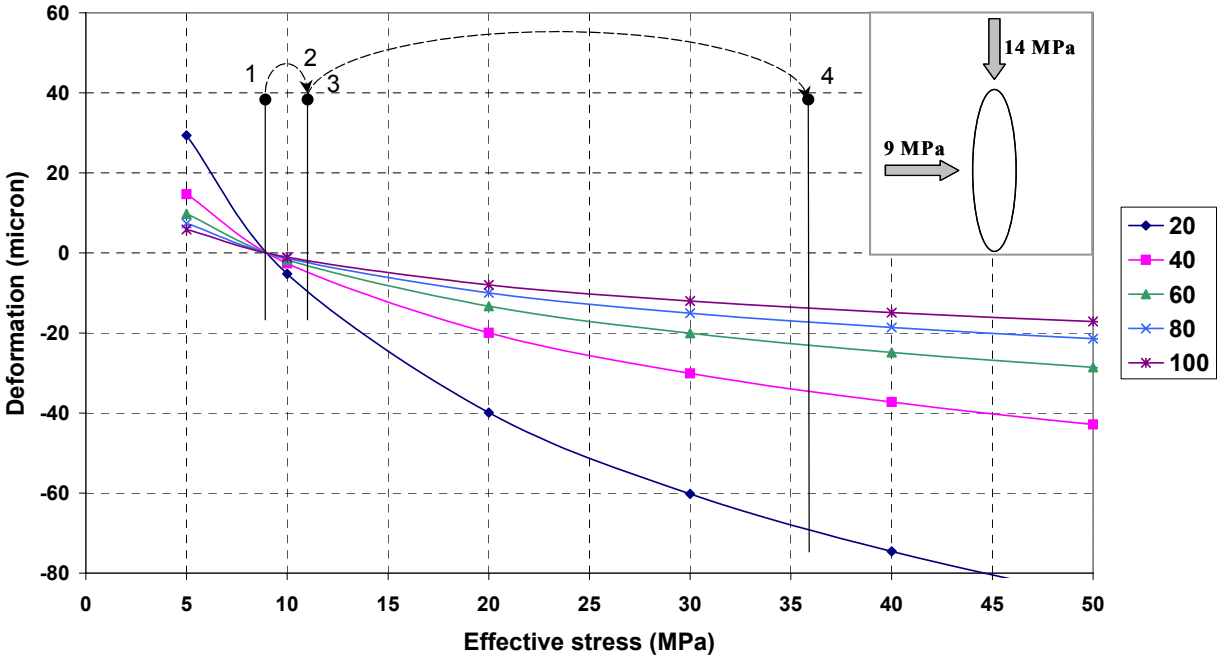

Direction 3. Vertical fracture which strikes perpendicular to the maximum principal stress.

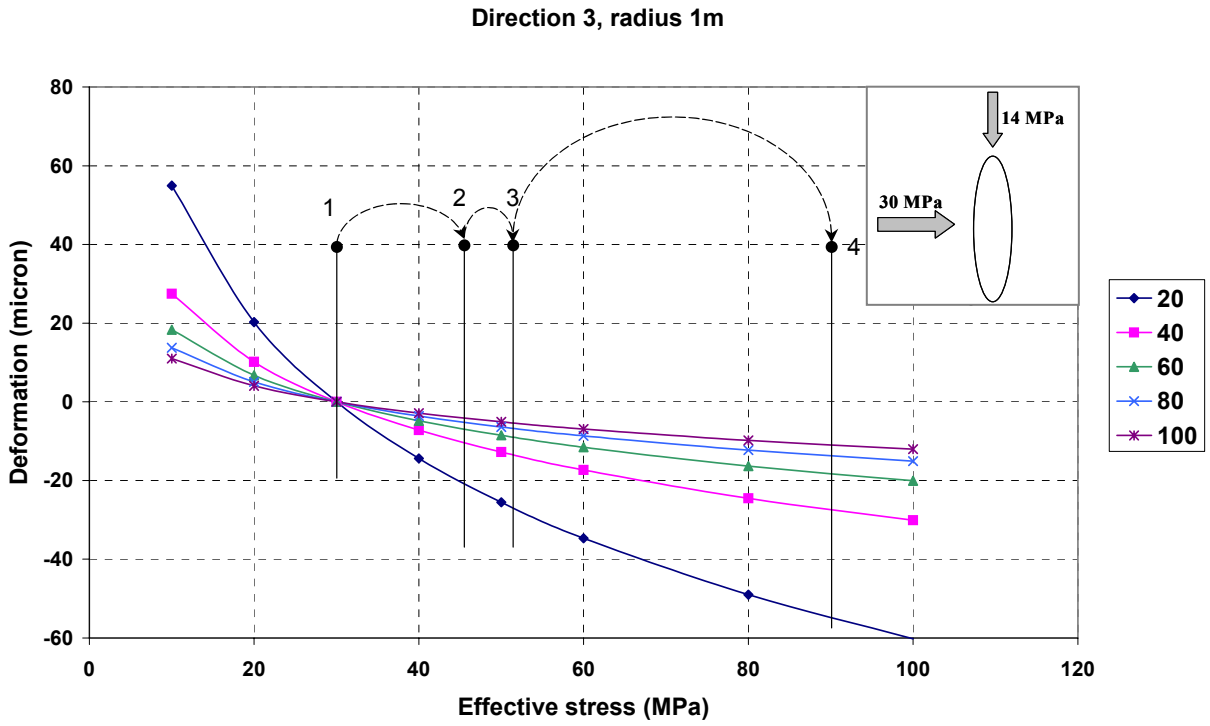

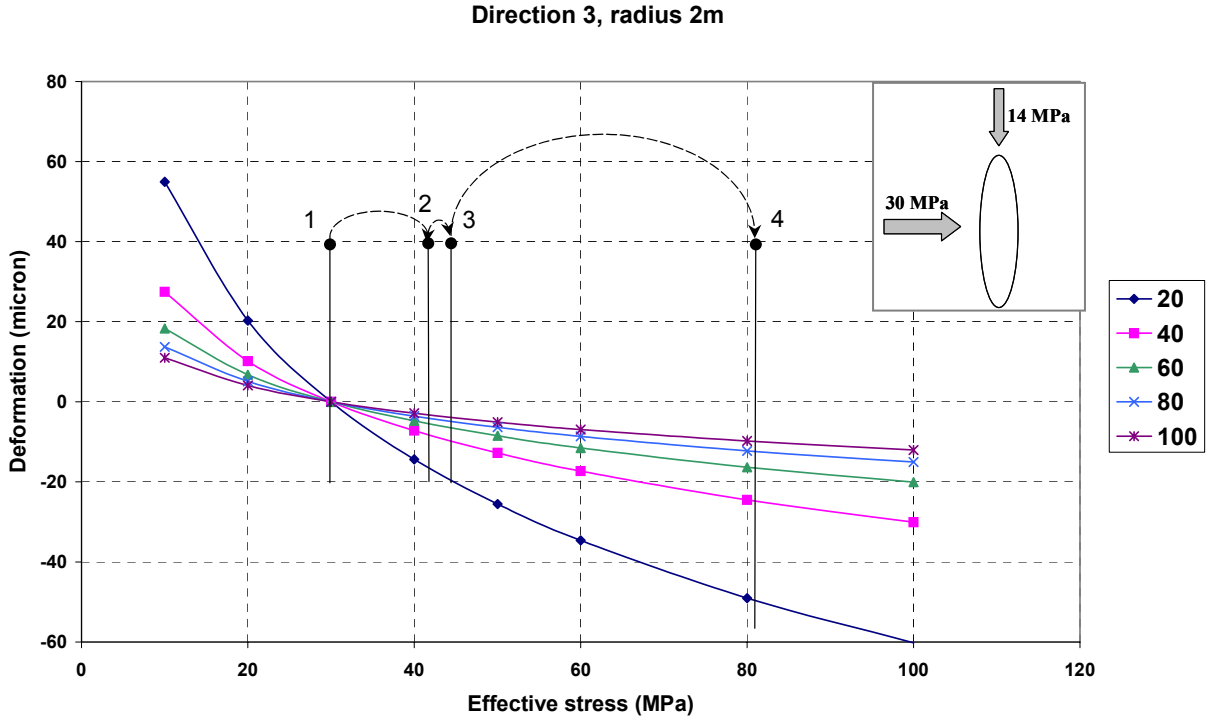

Direction 3, radius 5m

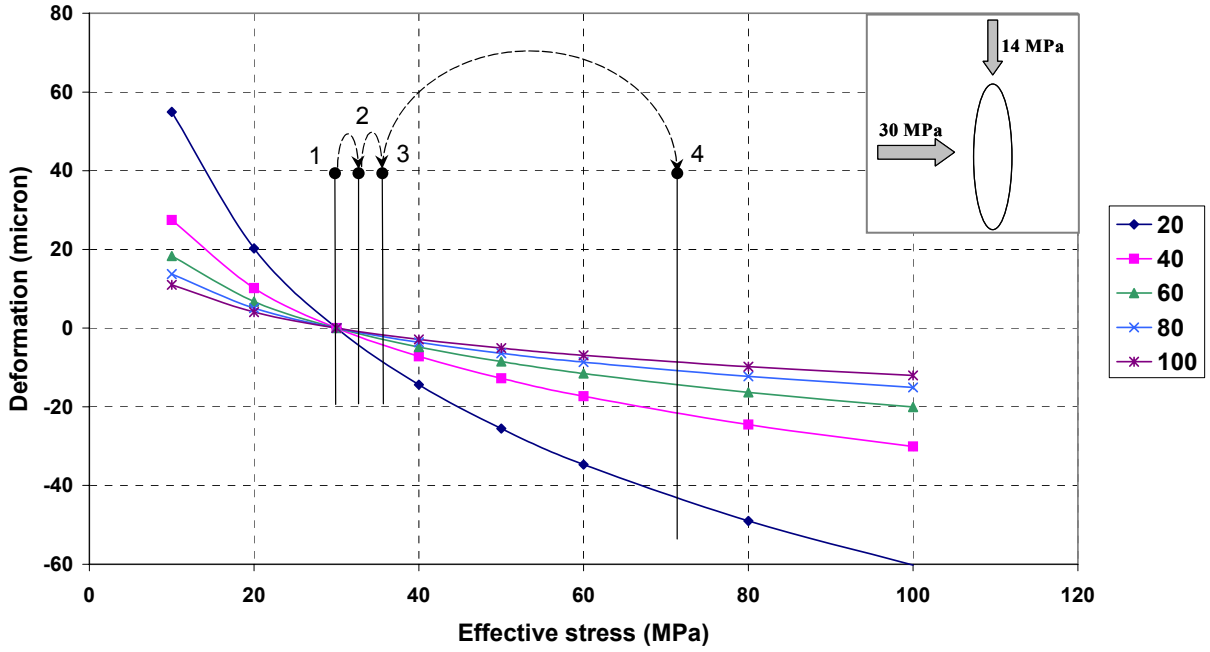

Direction 3, radius 10m

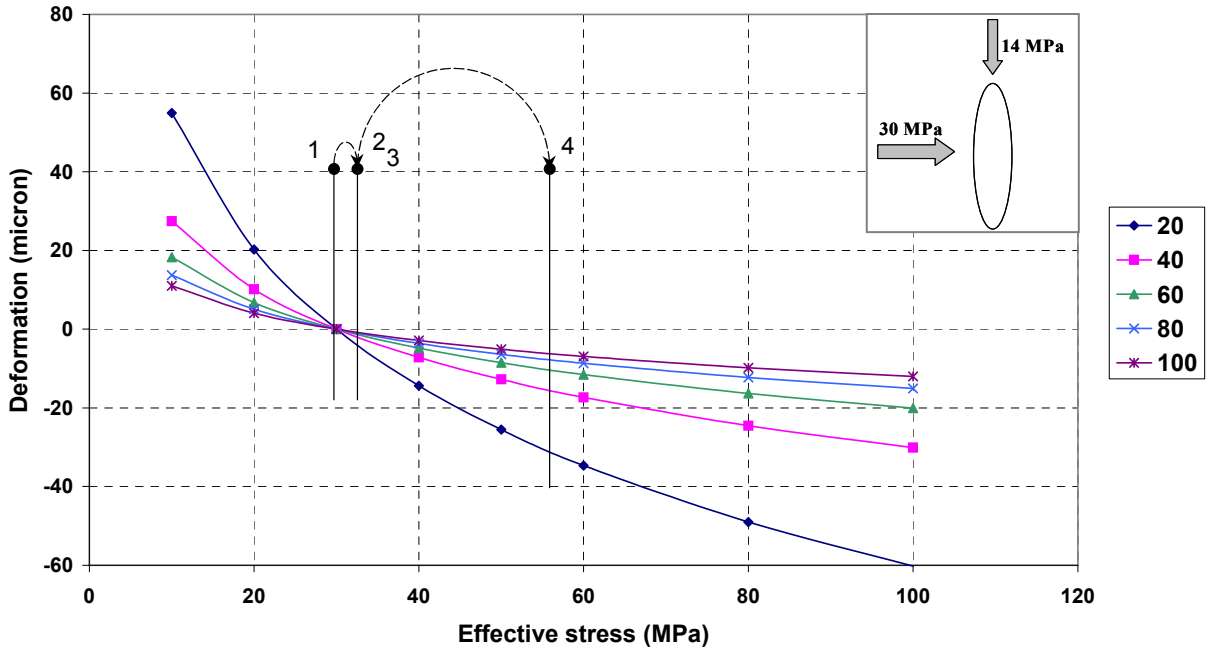

Direction 3. Horizontal fracture where the intermediate principal stress acts as the normal stress to the fracture plane.

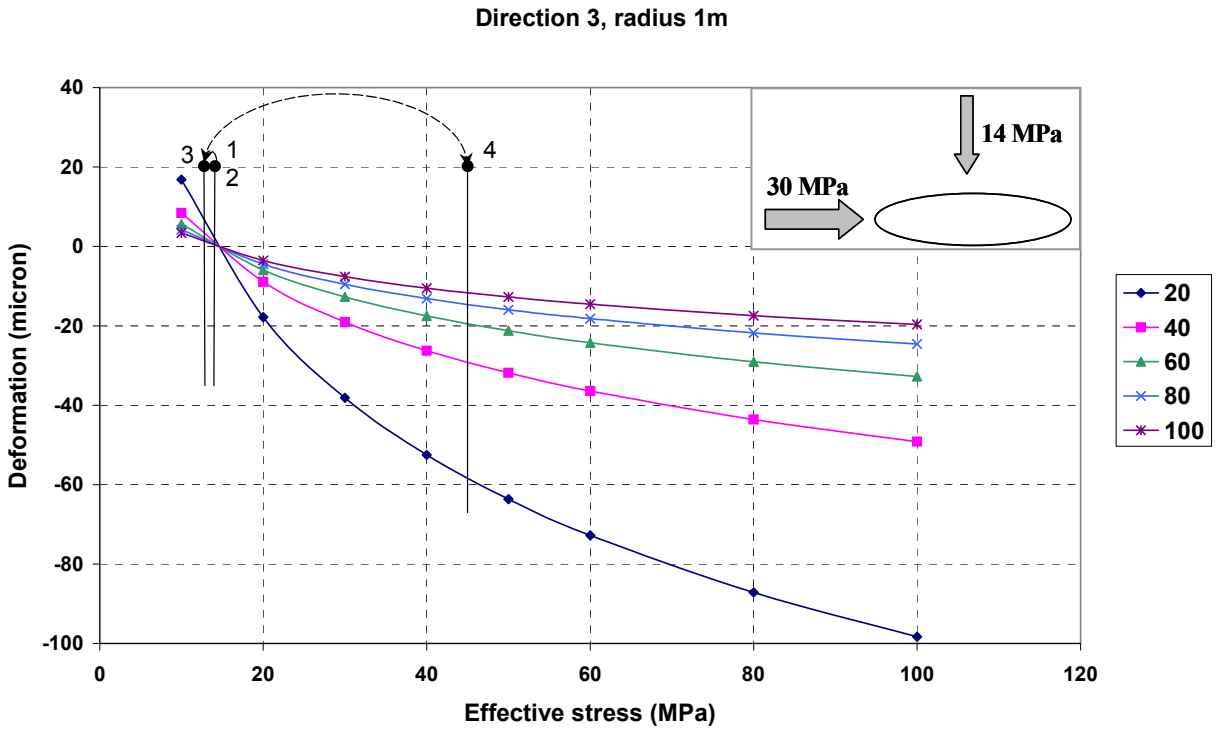

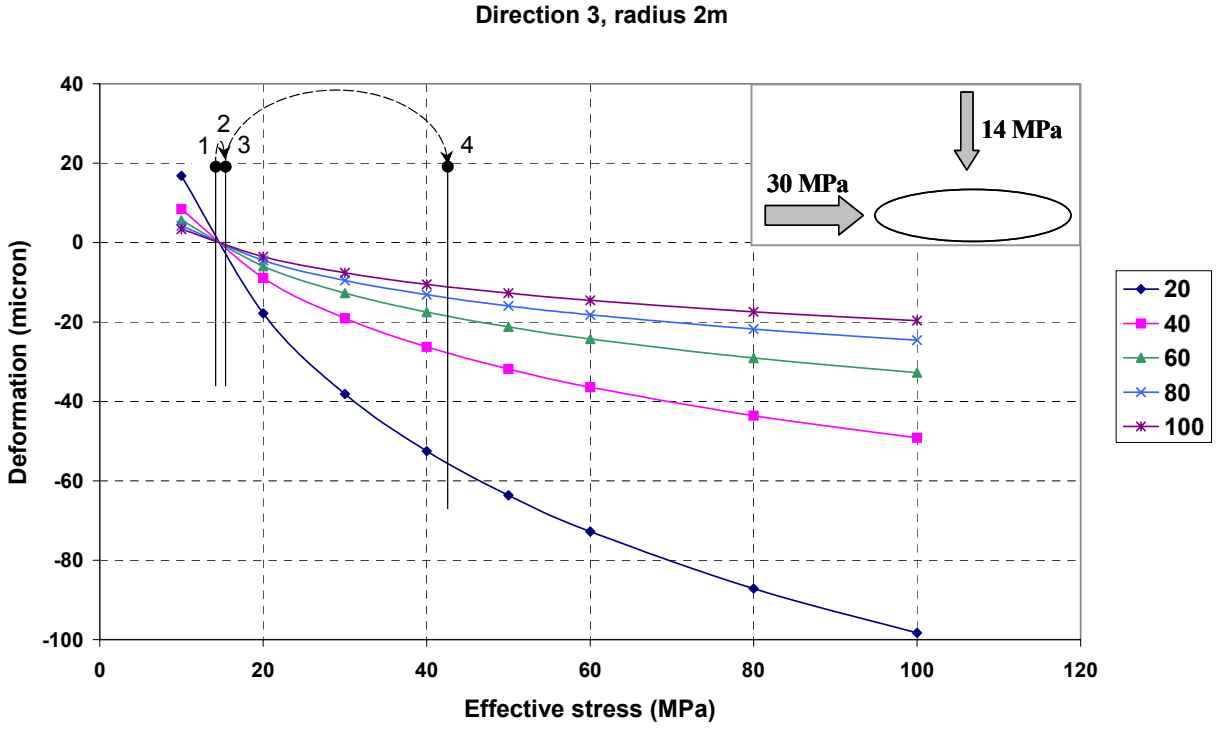

Direction 3, radius 10m

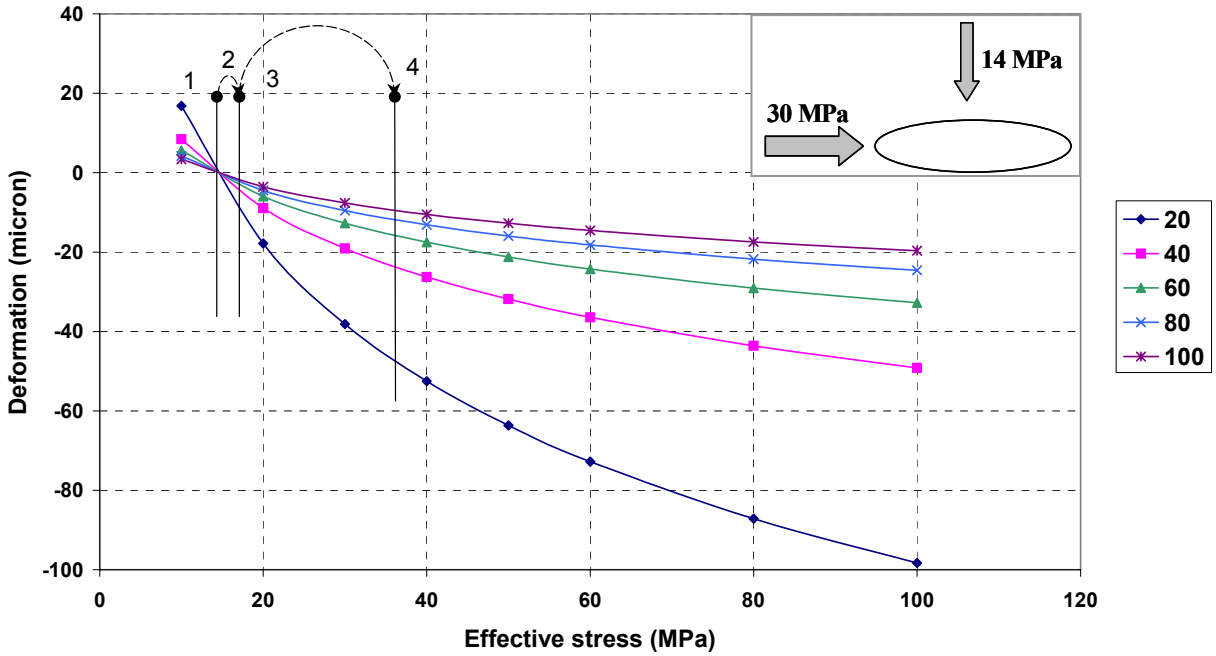

Direction 3, radius 5m

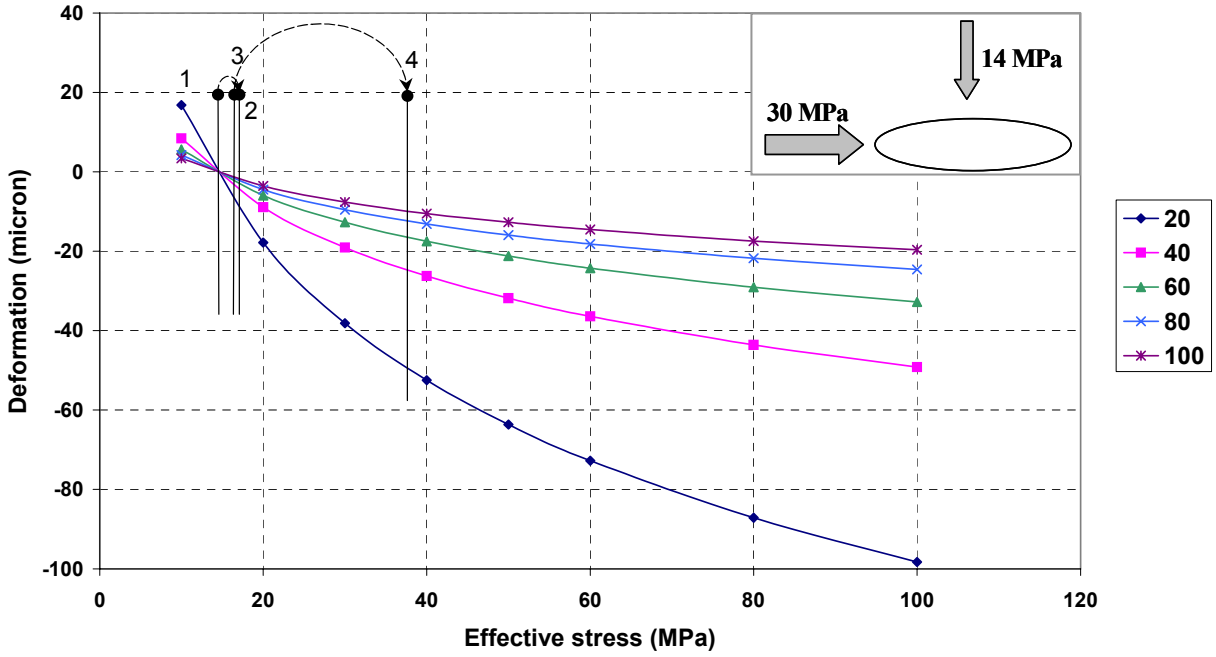

Direction 3. Vertical fracture that strikes parallel to the maximum principal stress.

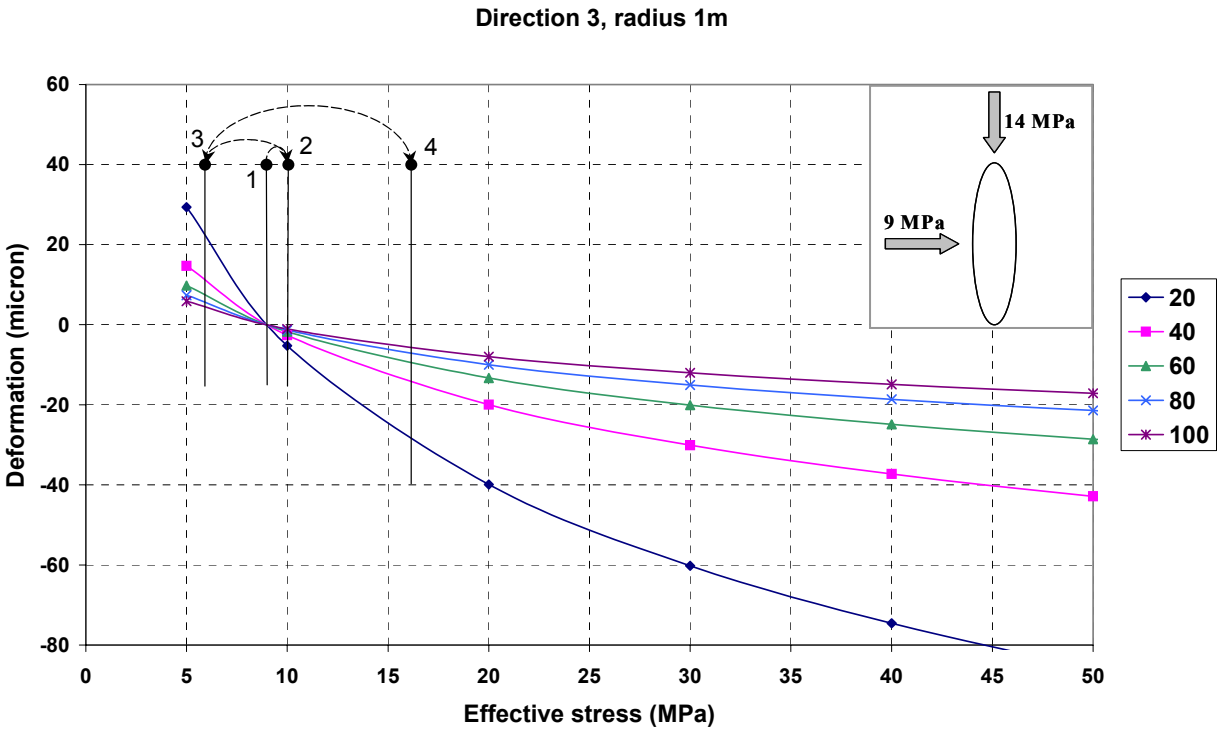

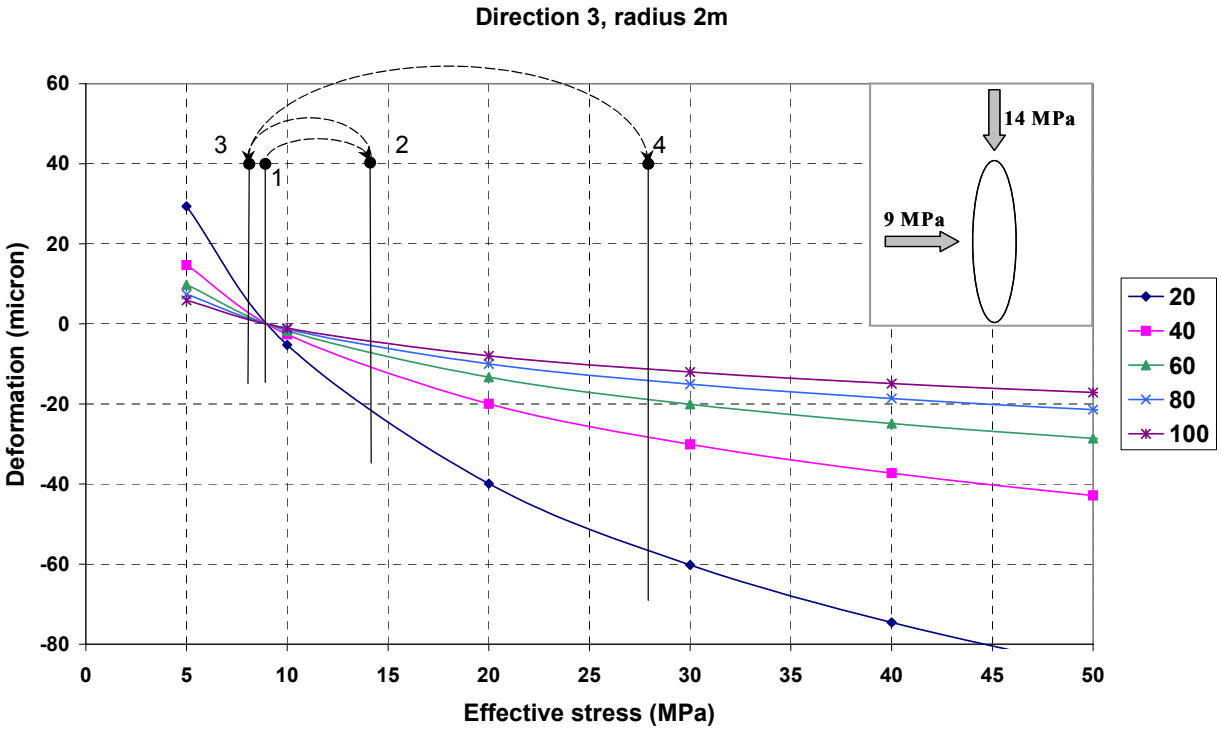

Direction 3, radius 5m

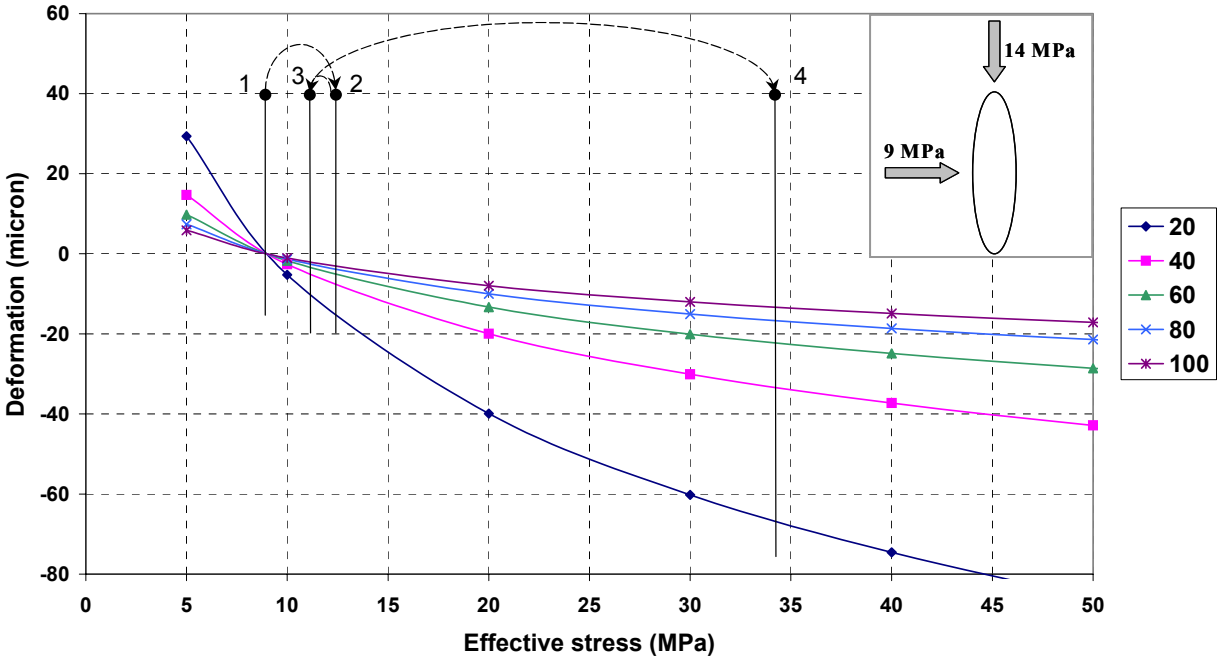

Direction 3, radius 10m

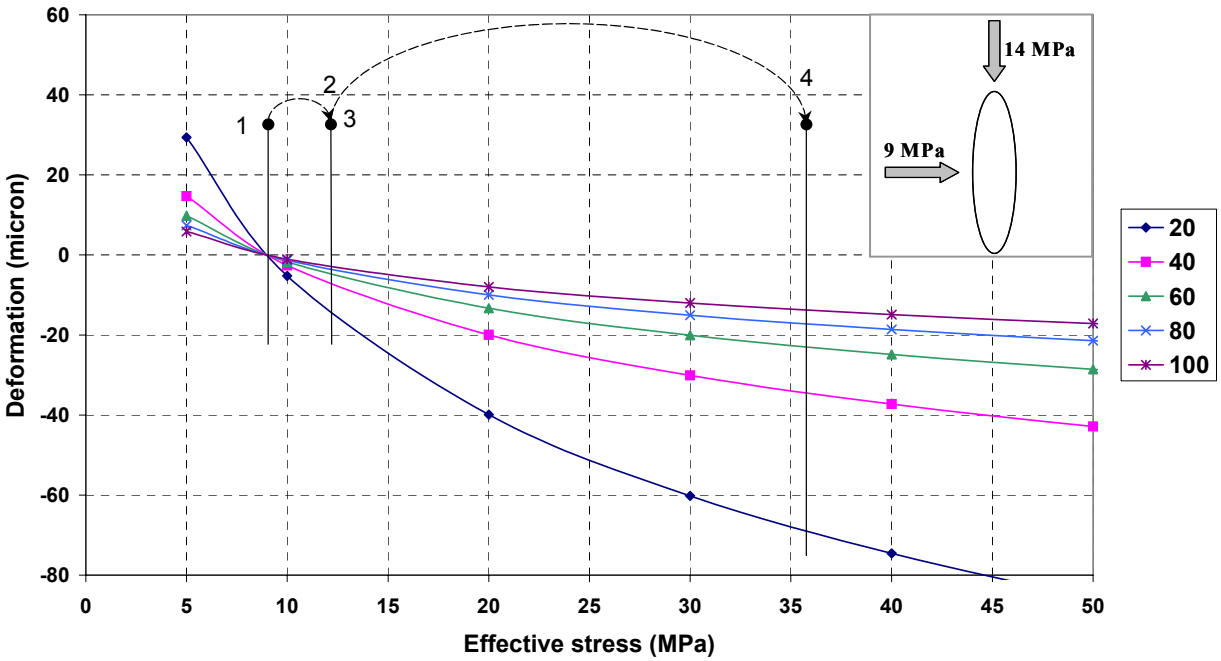

Relative transmissivity variation due to changes in effective stress.

Direction 1. Vertical fracture which strikes perpendicular to the maximum principal stress.

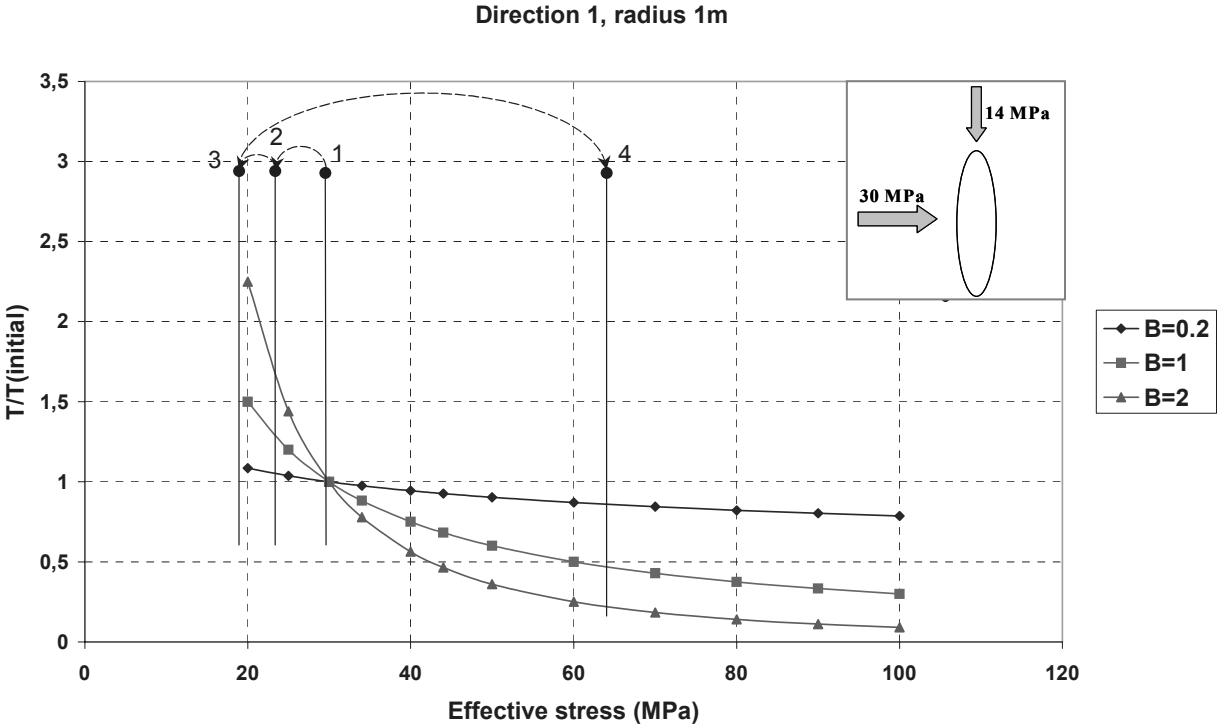

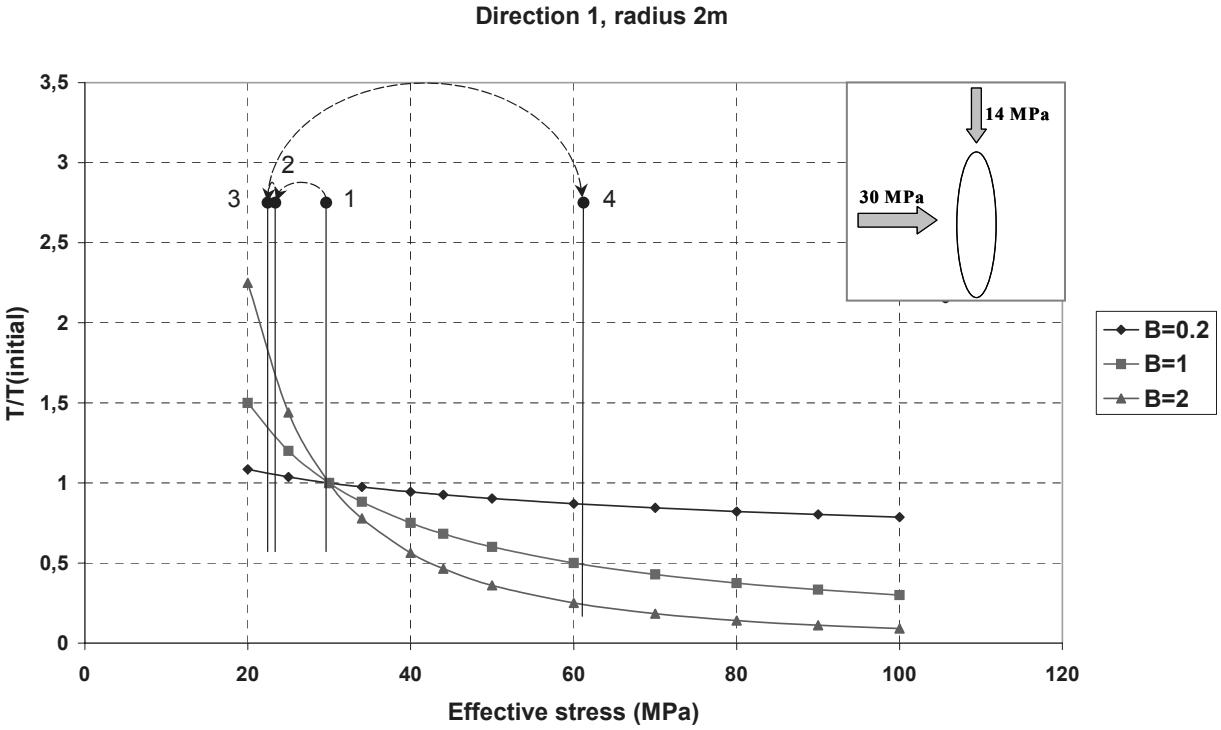

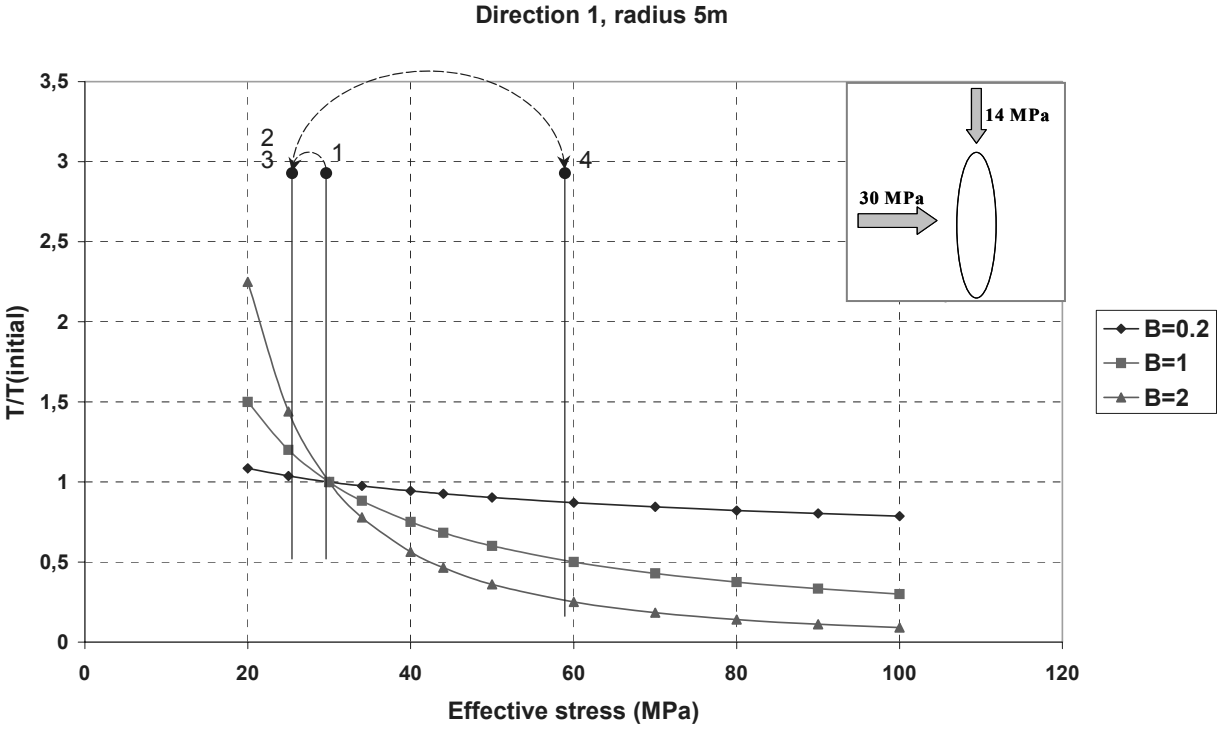
Direction 1, radius 5m
T/T(initial)
Effective stress (MPa)
14 MPa
30 MPa
1
2
3
4
B=0.2
B=1
B=2

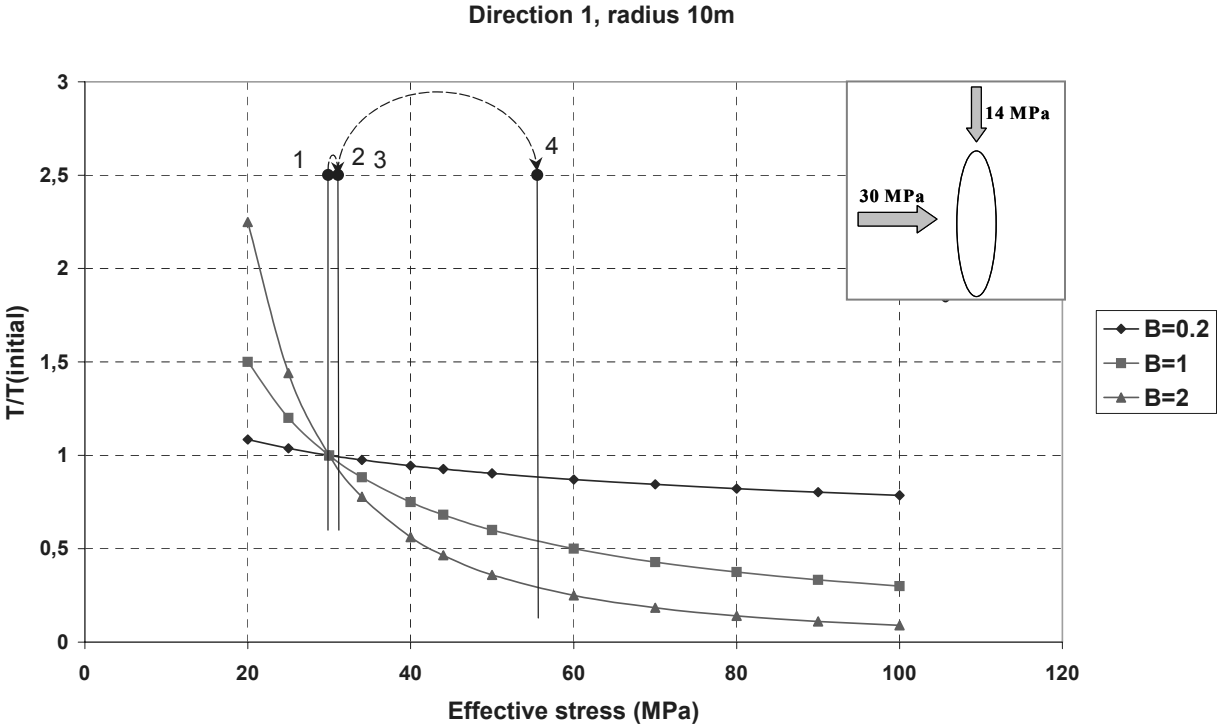
Direction 1, radius 10m
T/T(initial)
Effective stress (MPa)
14 MPa
30 MPa
1
2 3
4
B=0.2
B=1
B=2

Direction 2. Vertical fracture which strikes perpendicular to the maximum principal stress.

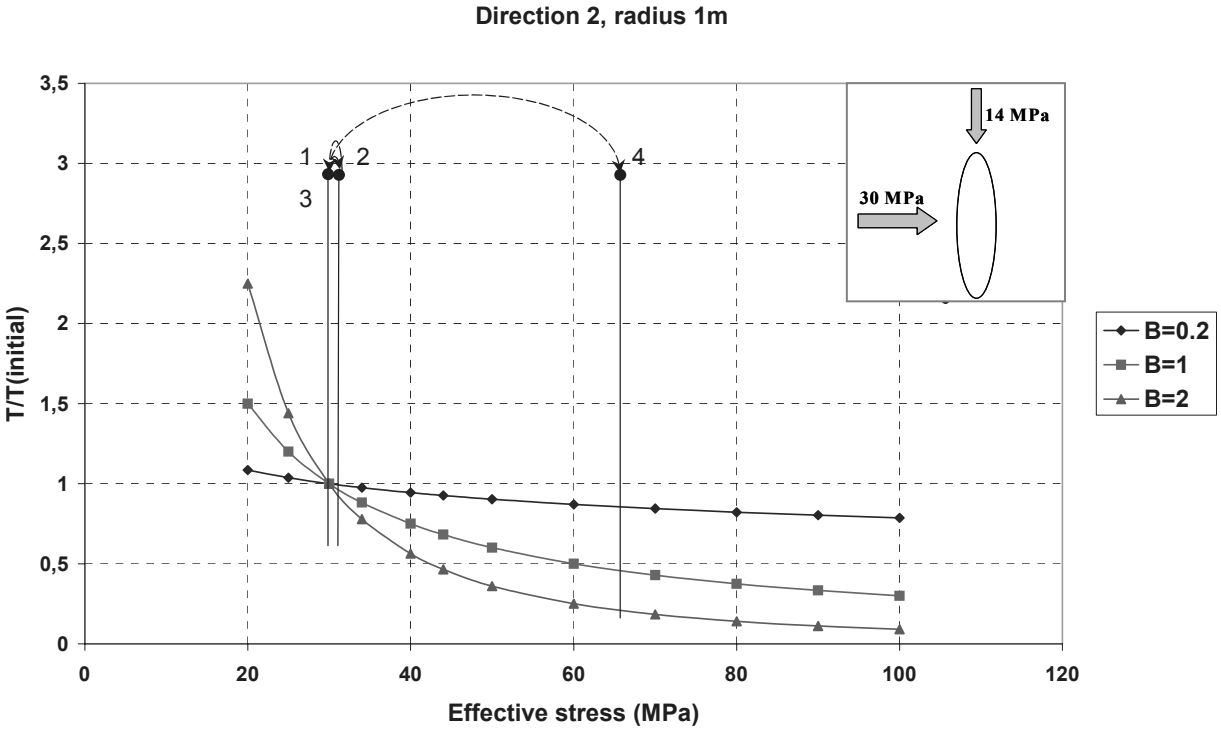

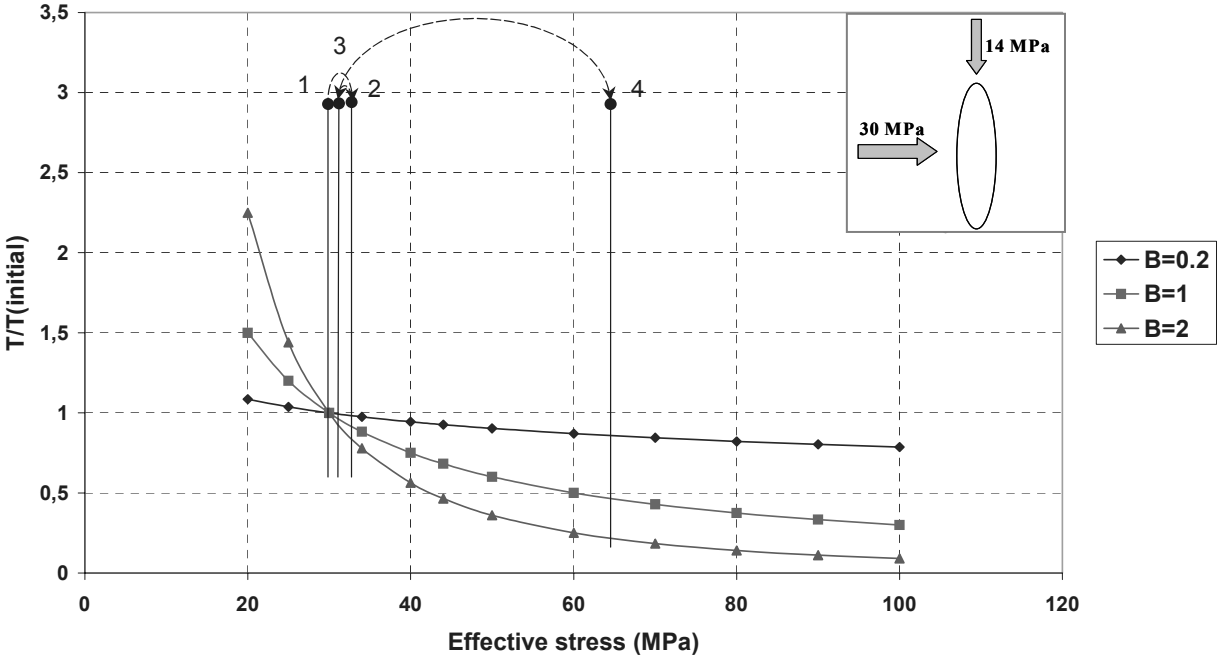

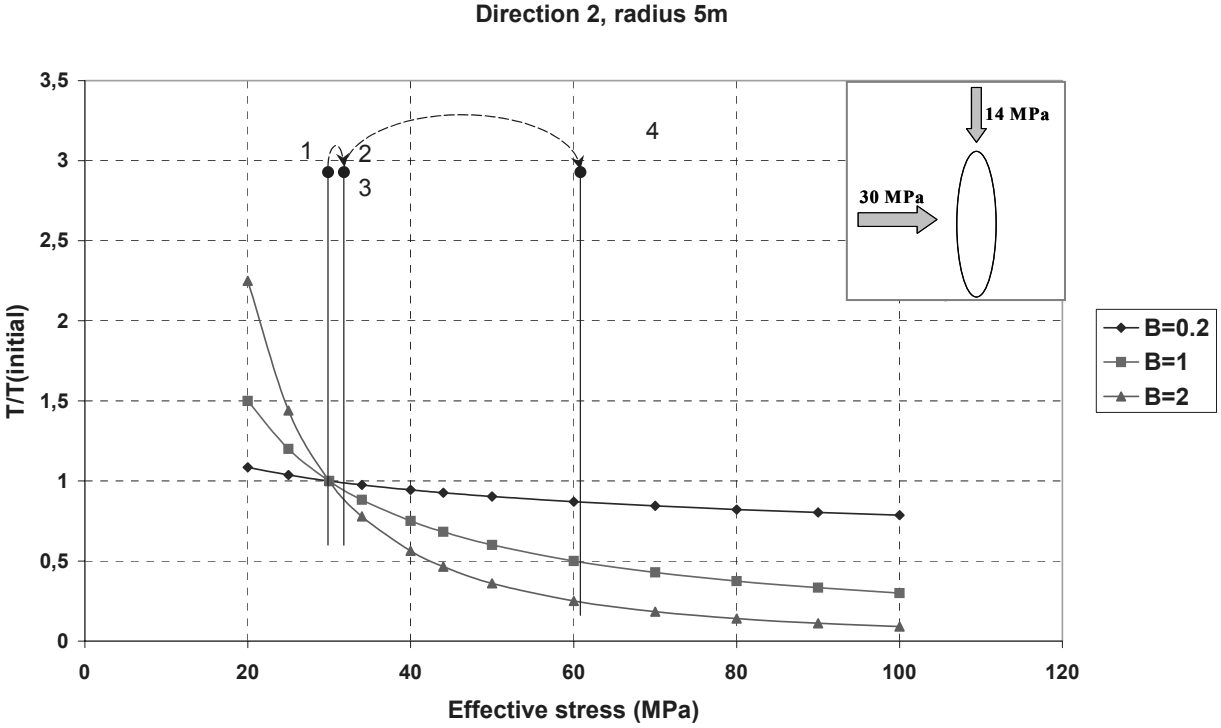
Direction 2, radius 5m
T/T(initial)
Effective stress (MPa)
1
2
3
4
14 MPa
30 MPa
B=0.2
B=1
B=2

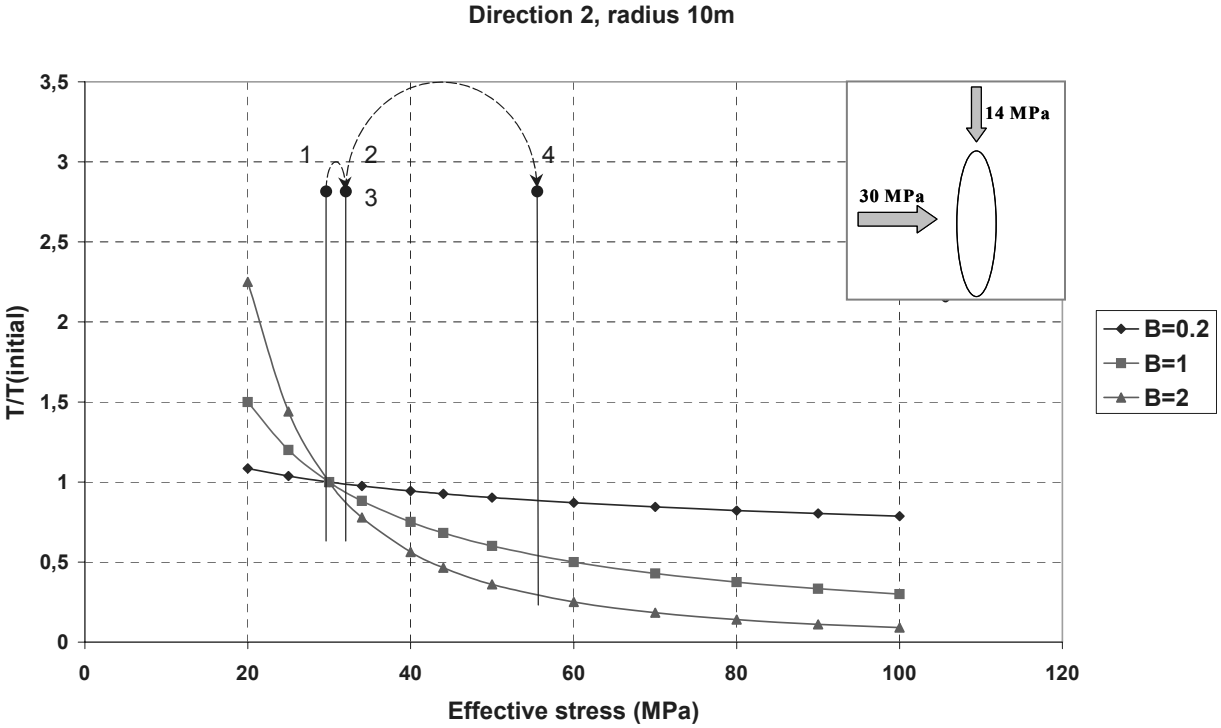
Direction 2, radius 10m
T/T(initial)
Effective stress (MPa)
1
2
3
4
14 MPa
30 MPa
B=0.2
B=1
B=2

Direction 3. Vertical fracture which strikes perpendicular to the maximum principal stress.

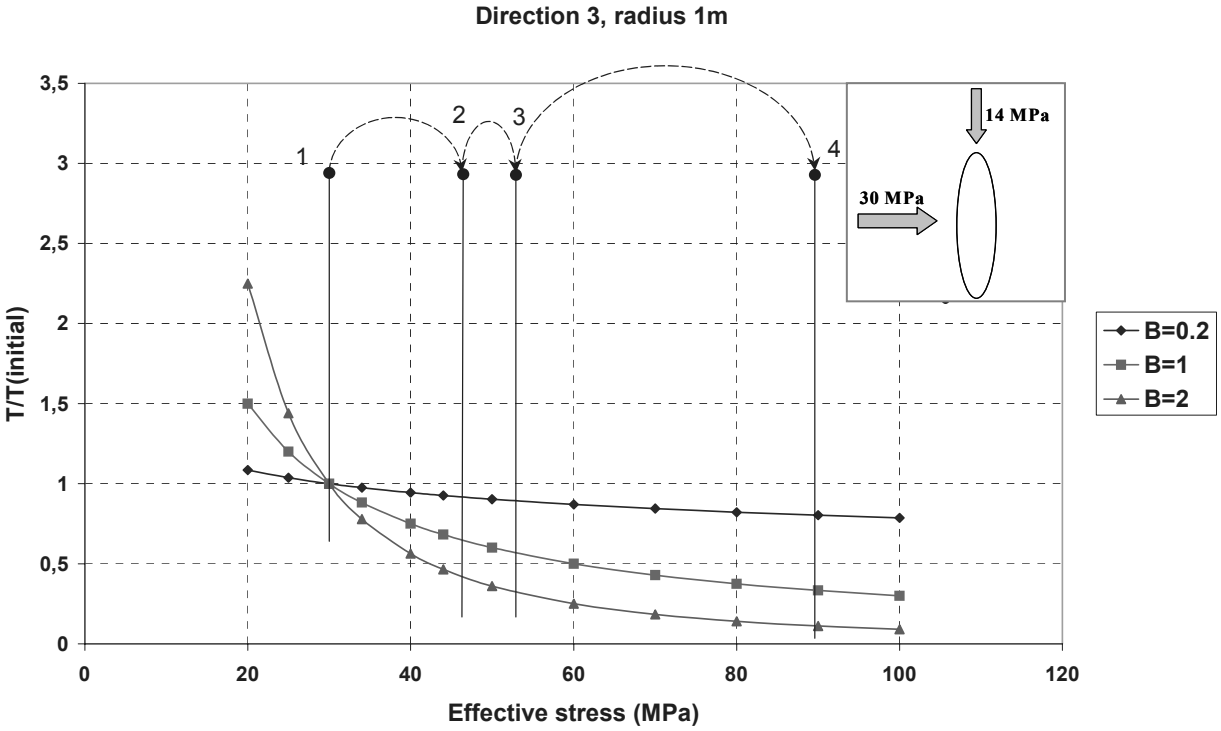

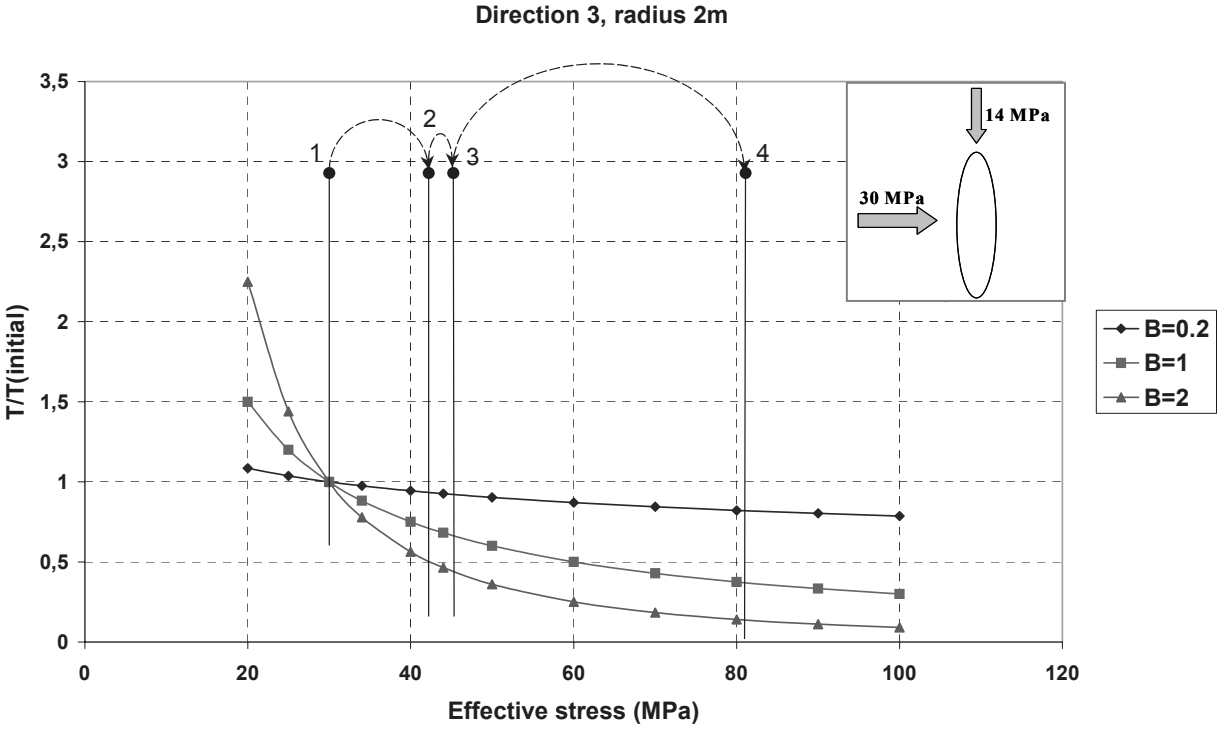

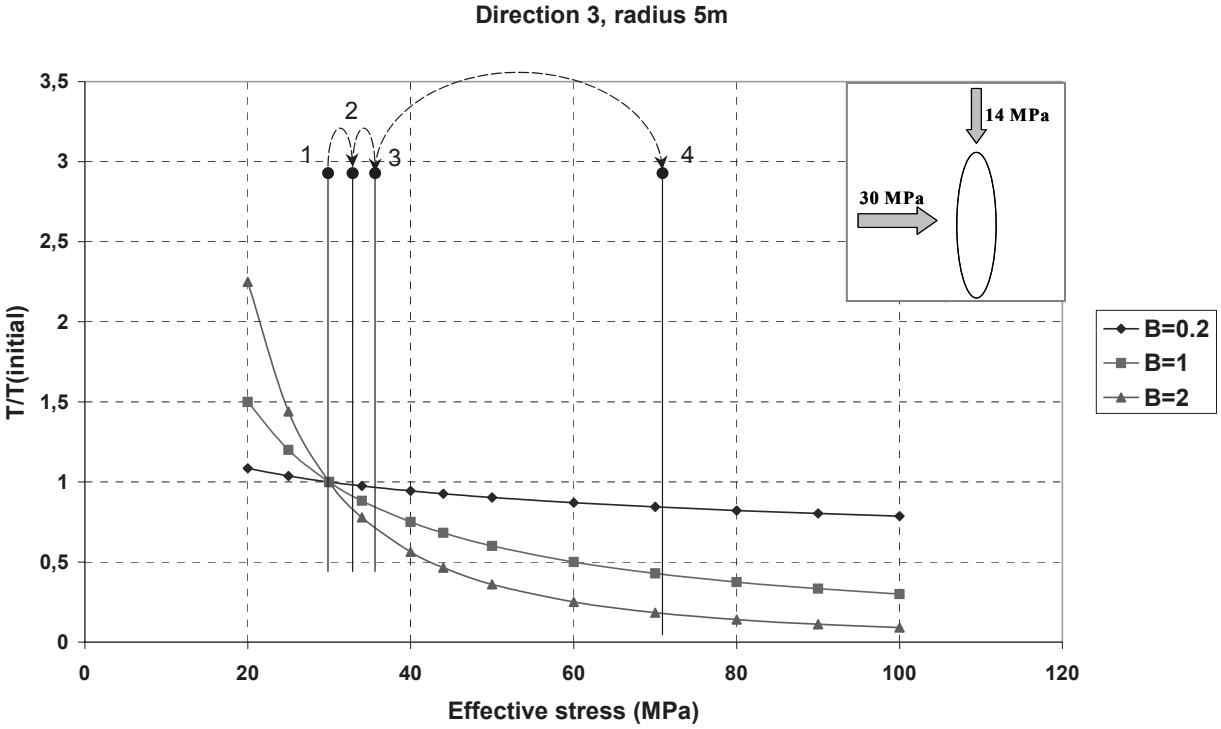
Direction 3, radius 5m
T/T(initial)
Effective stress (MPa)
1
2
3
4
14 MPa
30 MPa
B=0.2
B=1
B=2

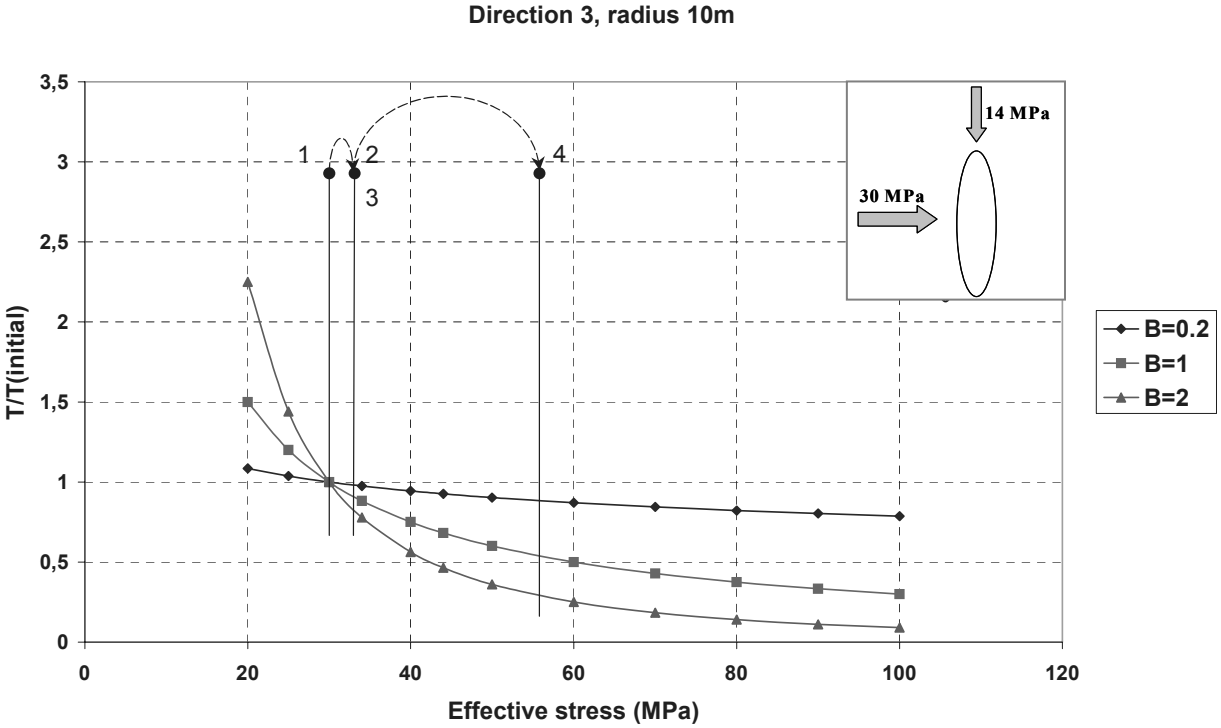
Direction 3, radius 10m
T/T(initial)
Effective stress (MPa)
1
2
3
4
14 MPa
30 MPa
B=0.2
B=1
B=2

Direction 1. Horizontal fracture where the intermediate principal stress acts as the normal stress to the fracture plane

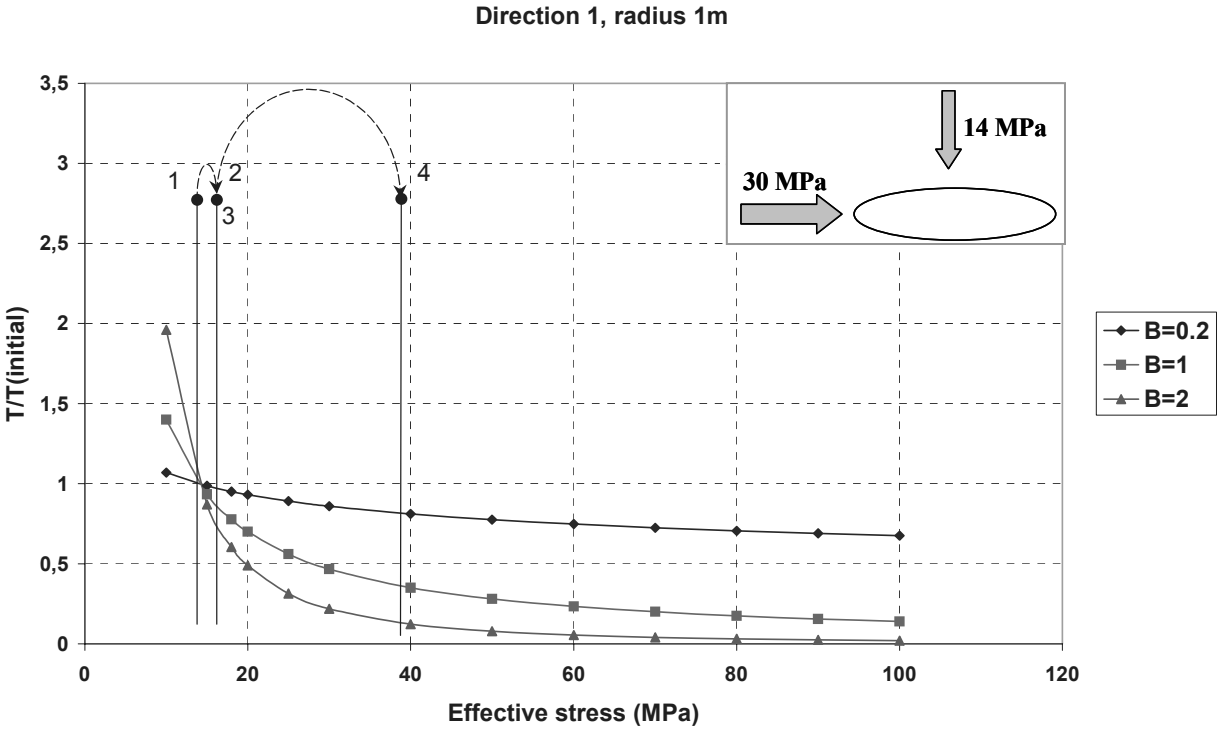

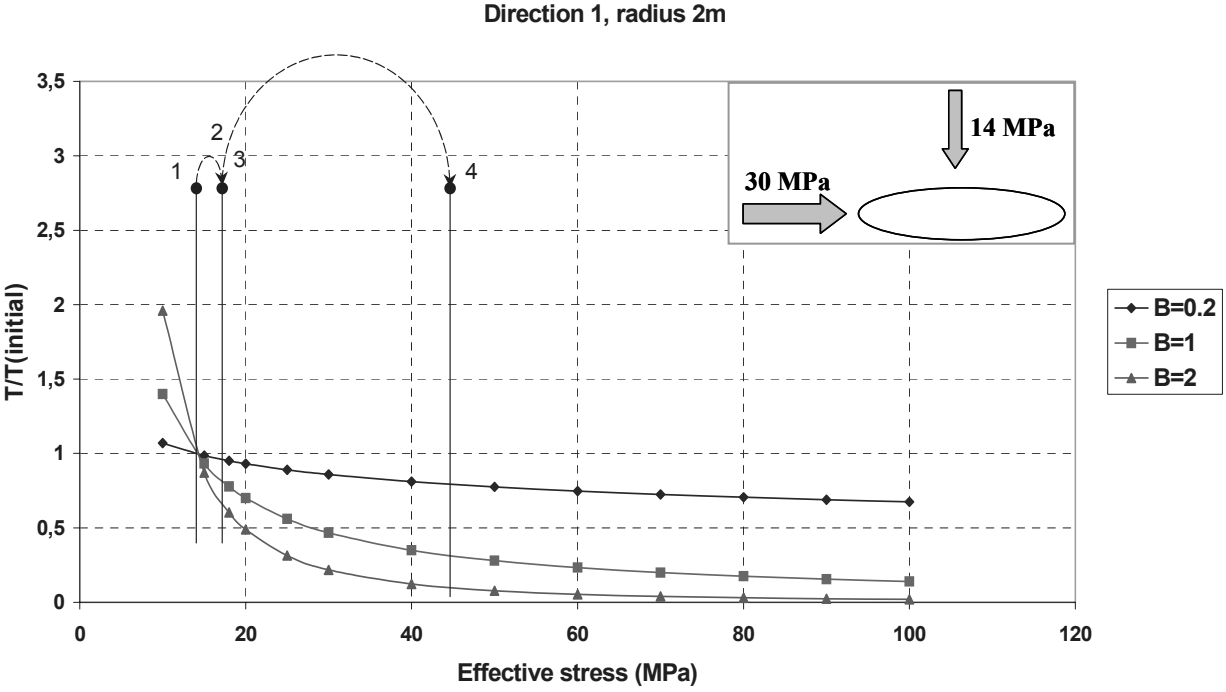

Direction 1, radius 5m

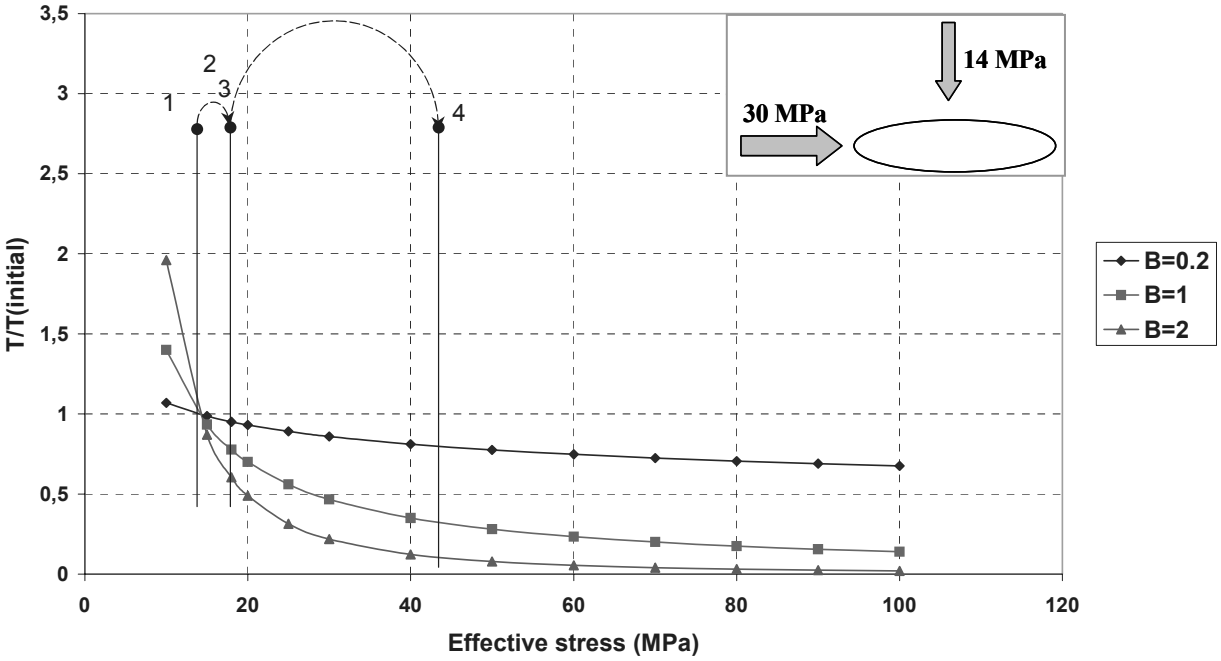

Direction 1, radius 10m

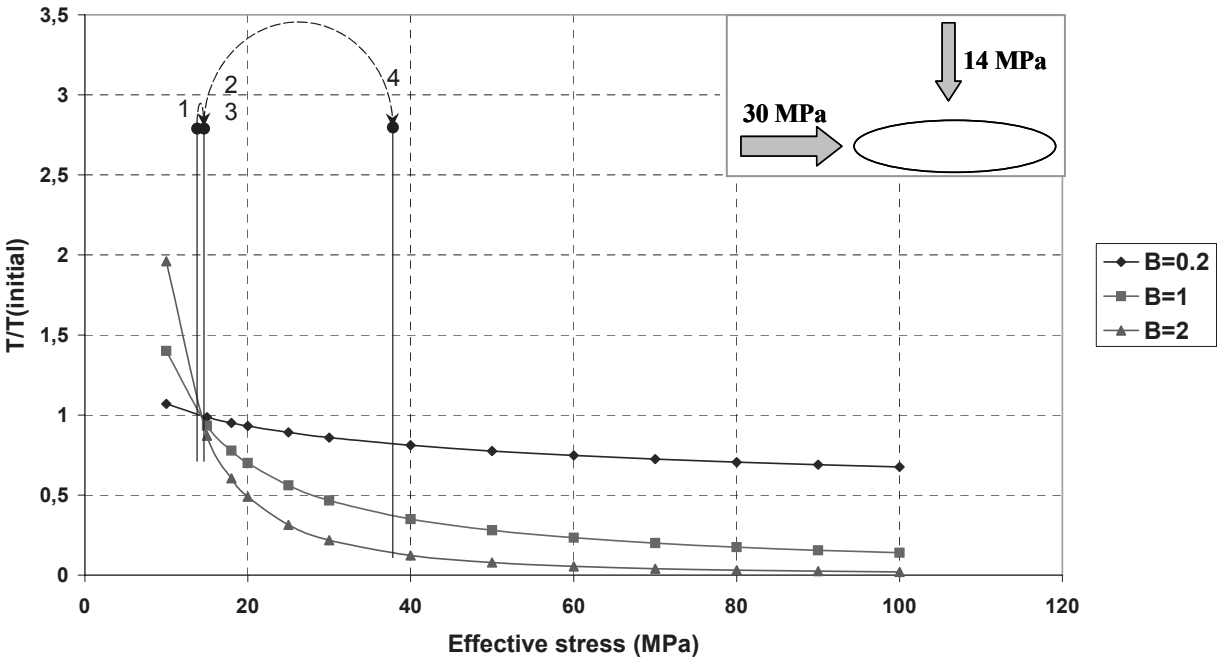

Direction 2. Horizontal fracture where the intermediate principal stress acts as the normal stress to the fracture plane.

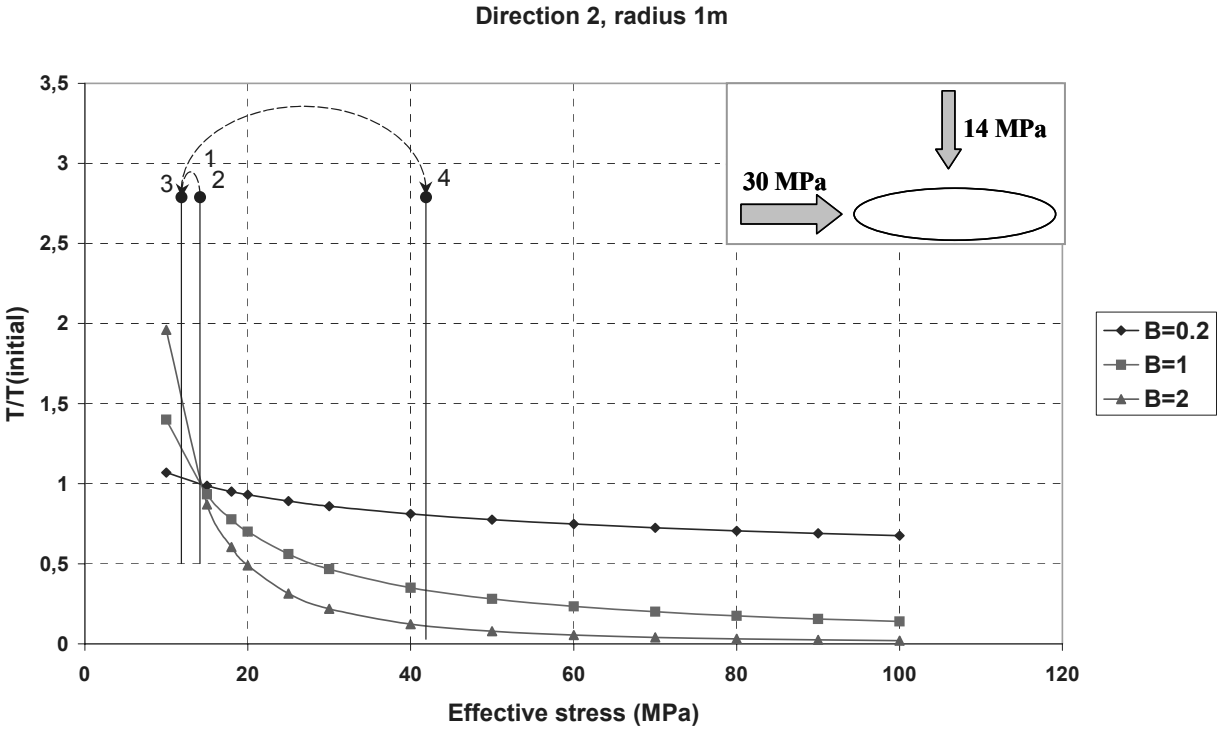

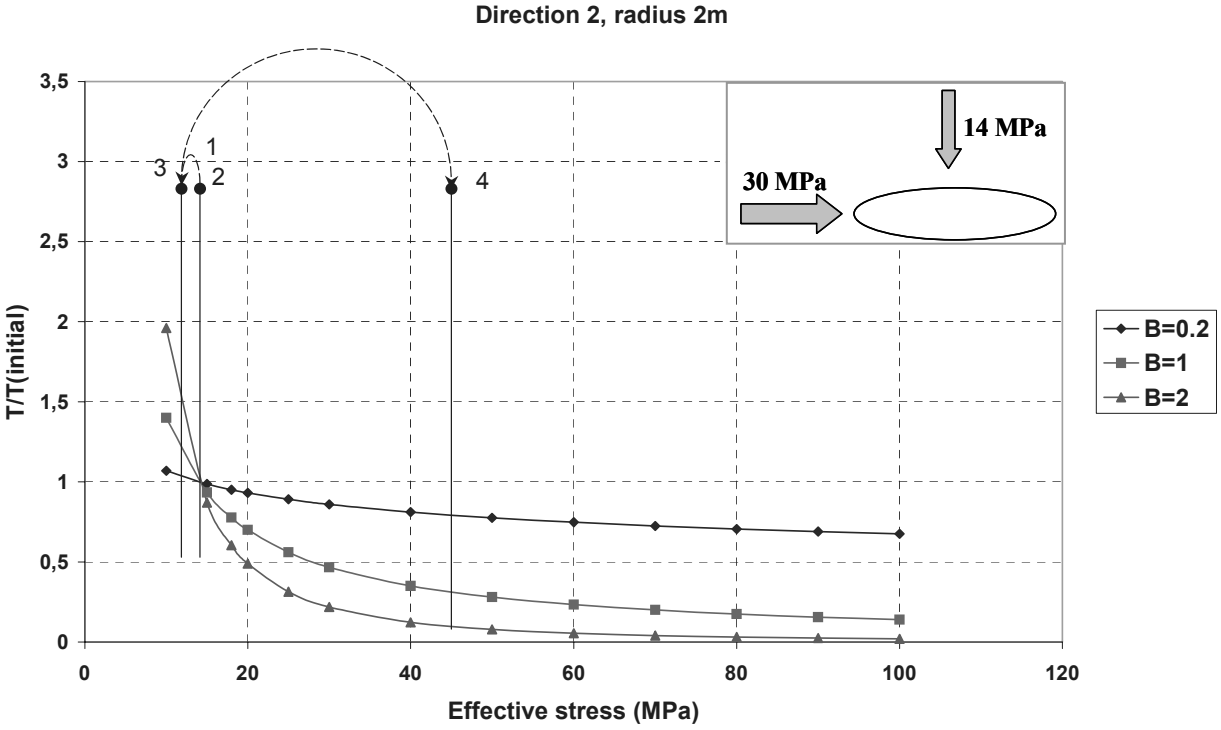

Direction 2, radius 5m

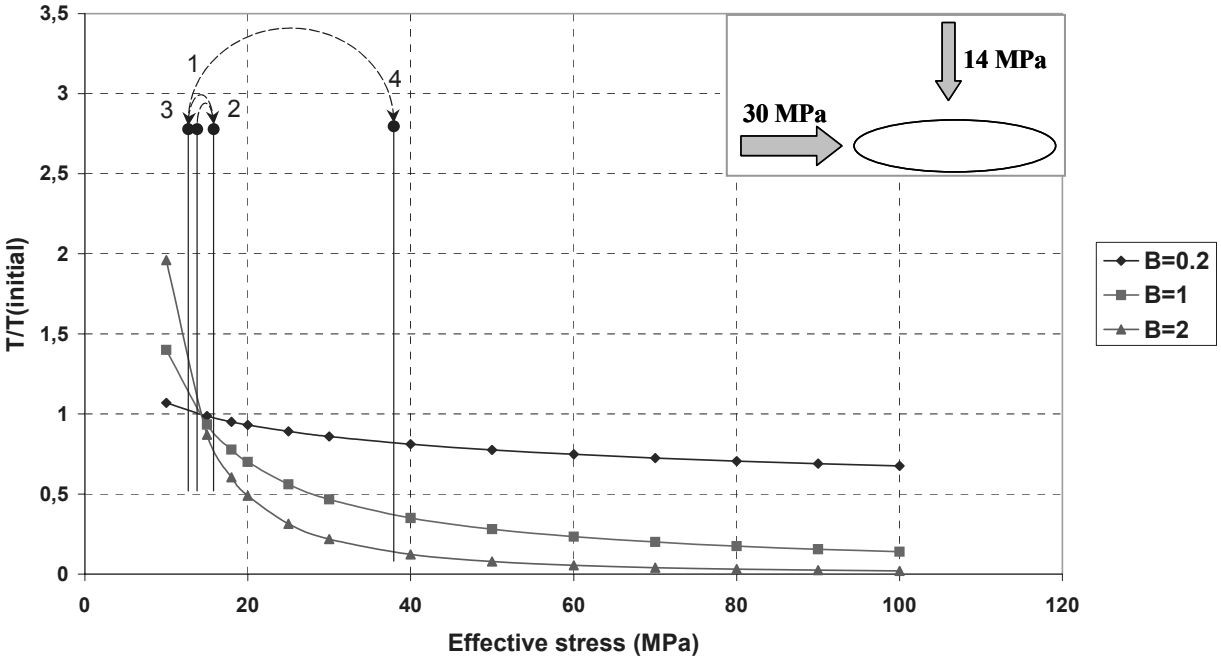

Direction 2, radius 10m

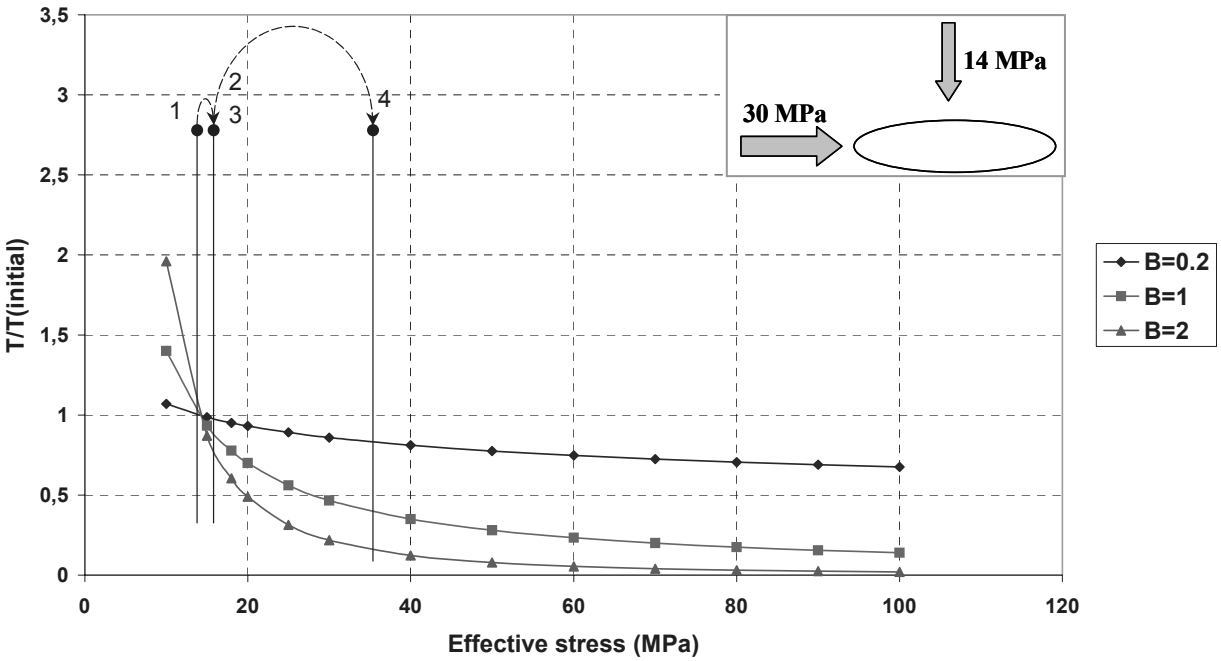

Direction 3. Horizontal fracture where the intermediate principal stress acts as the normal stress to the fracture plane

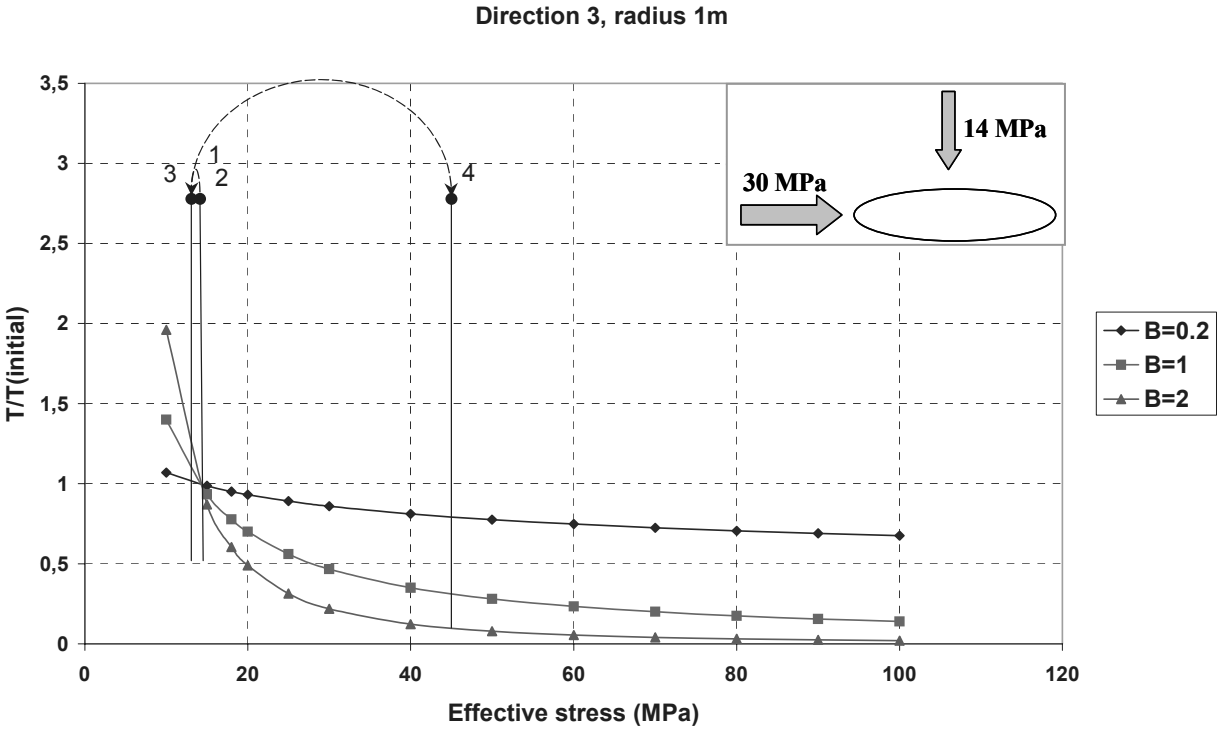

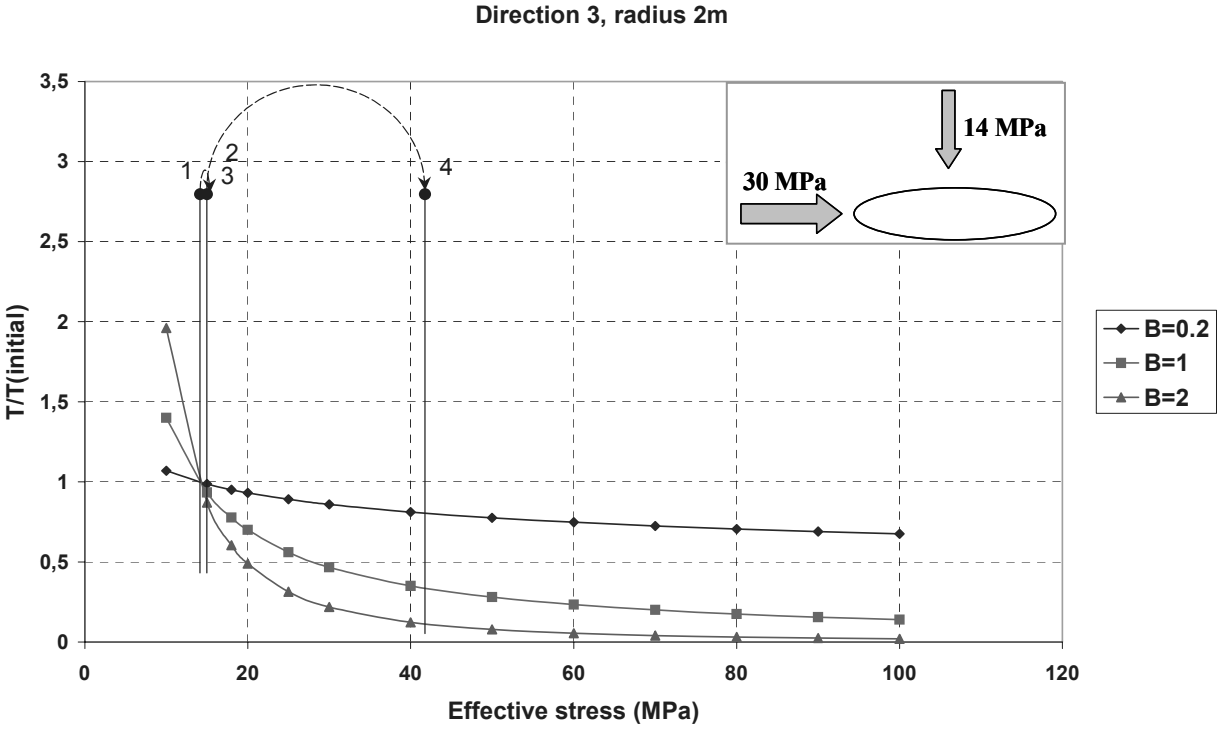

Direction 3, radius 5m

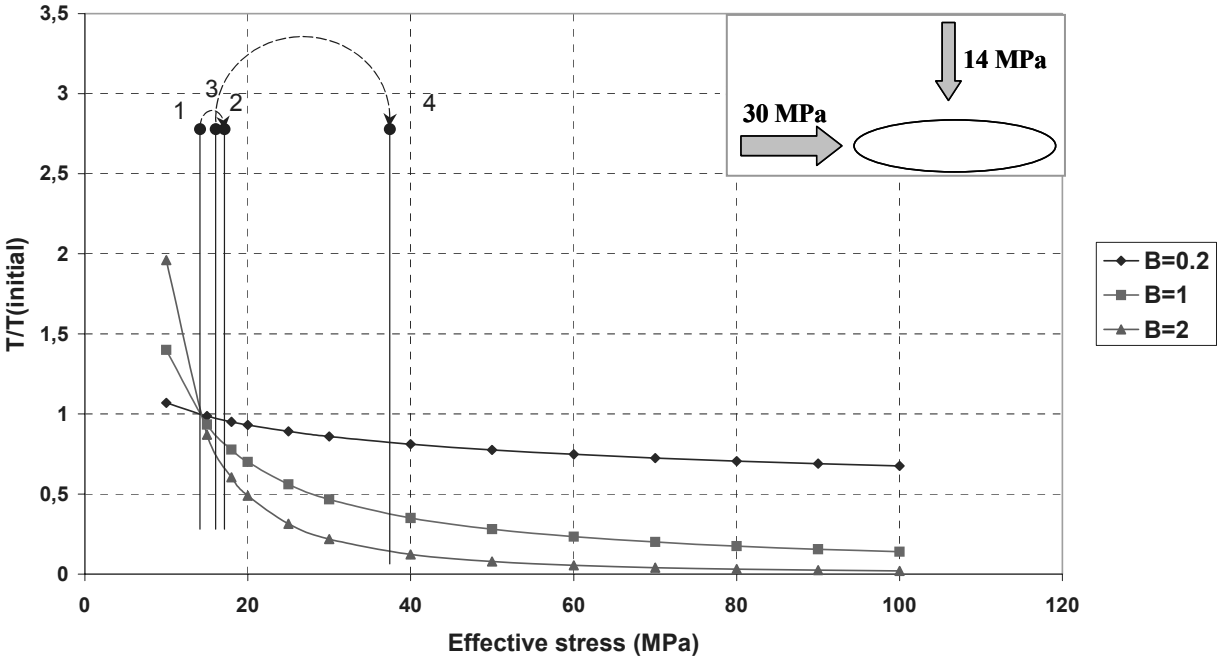

Direction 3, radius 10m

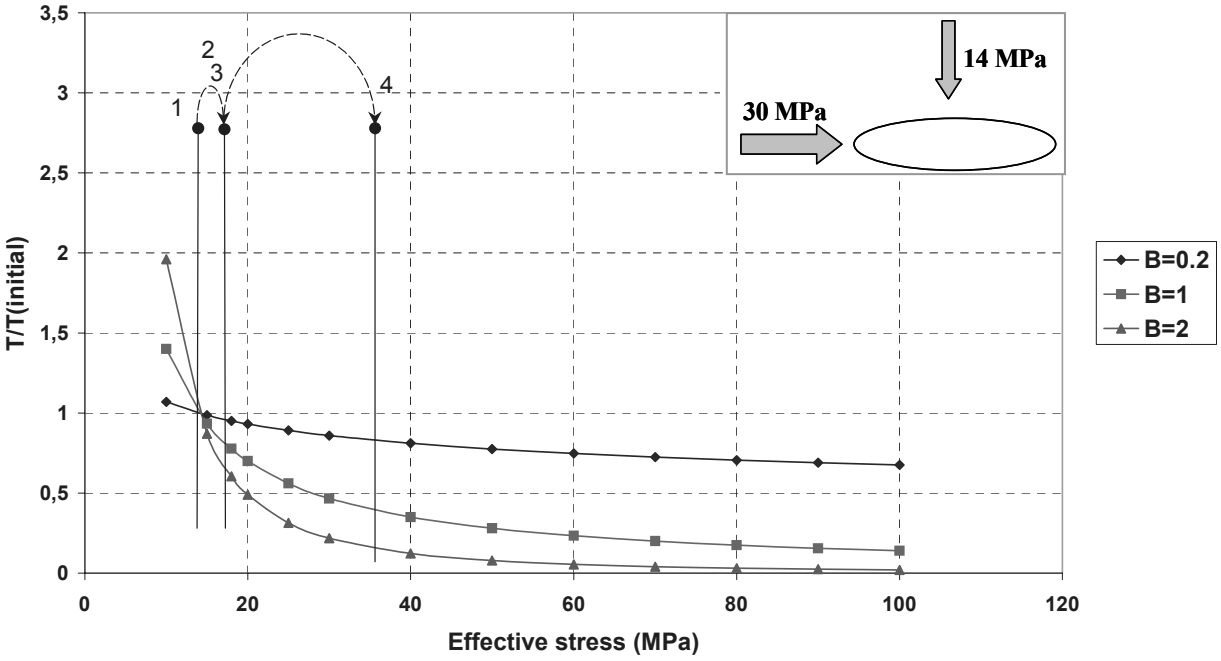

Direction 1. Vertical fracture that strikes parallel to the maximum principal stress.

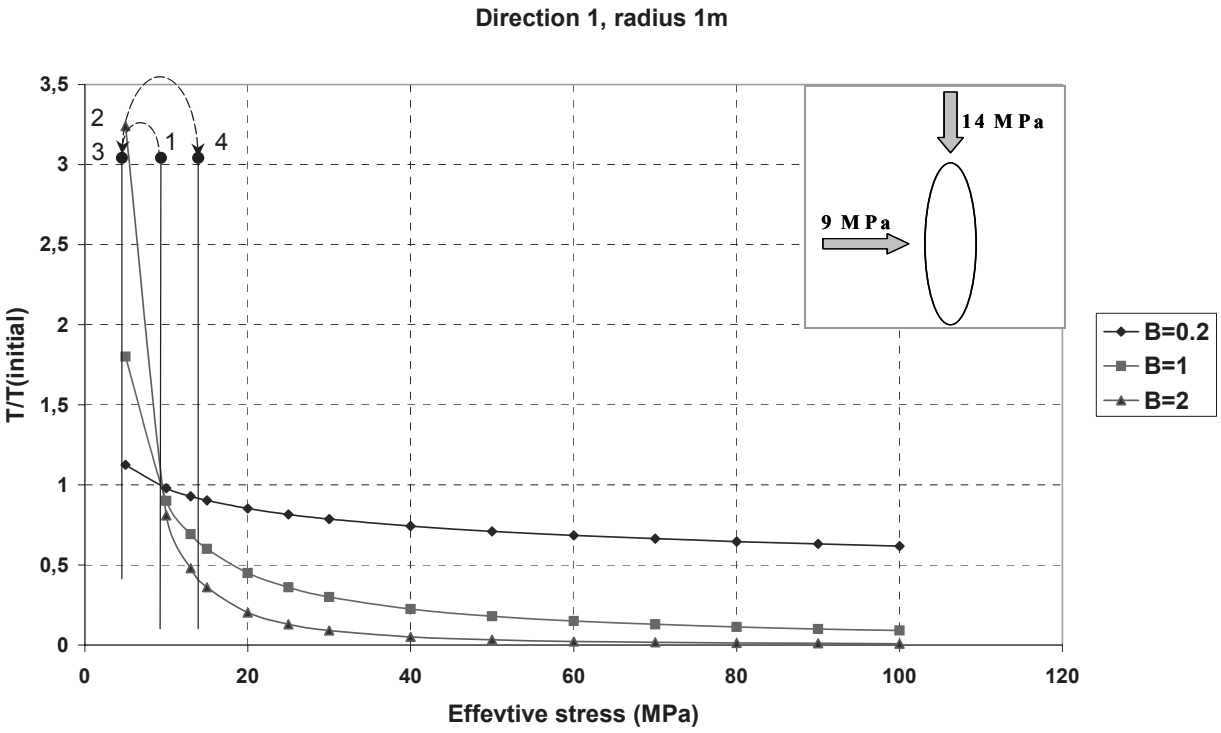

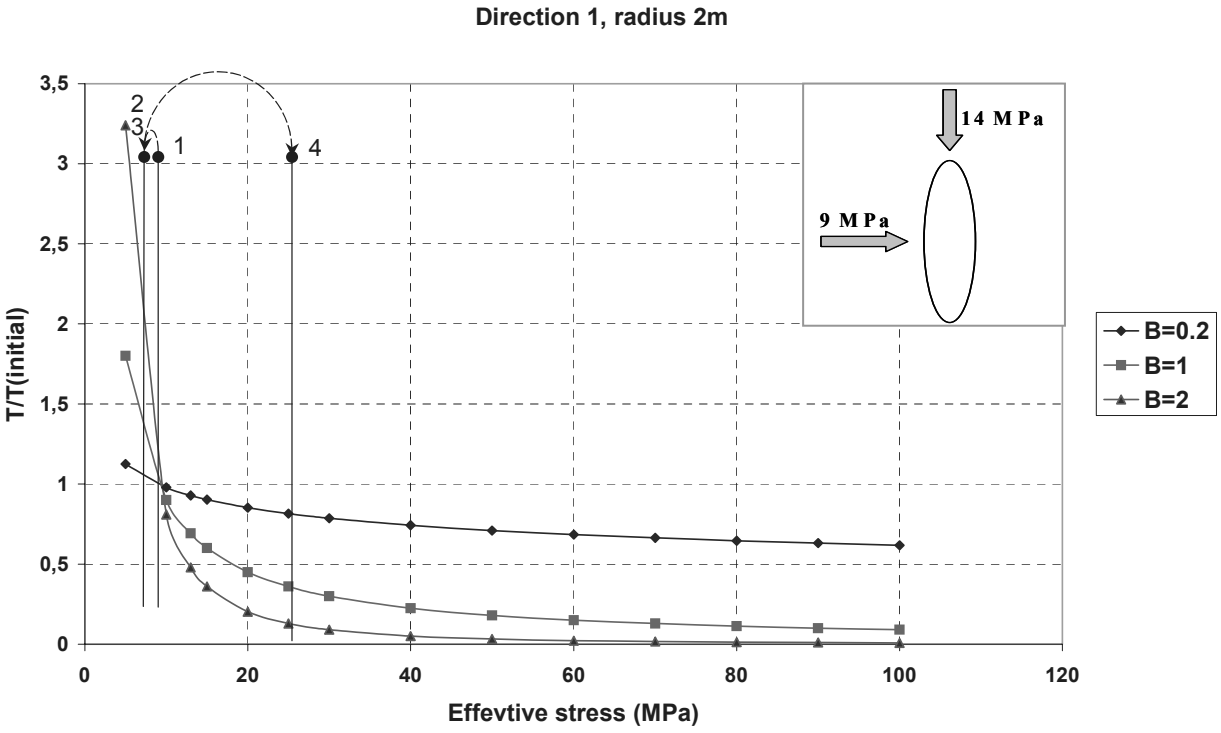

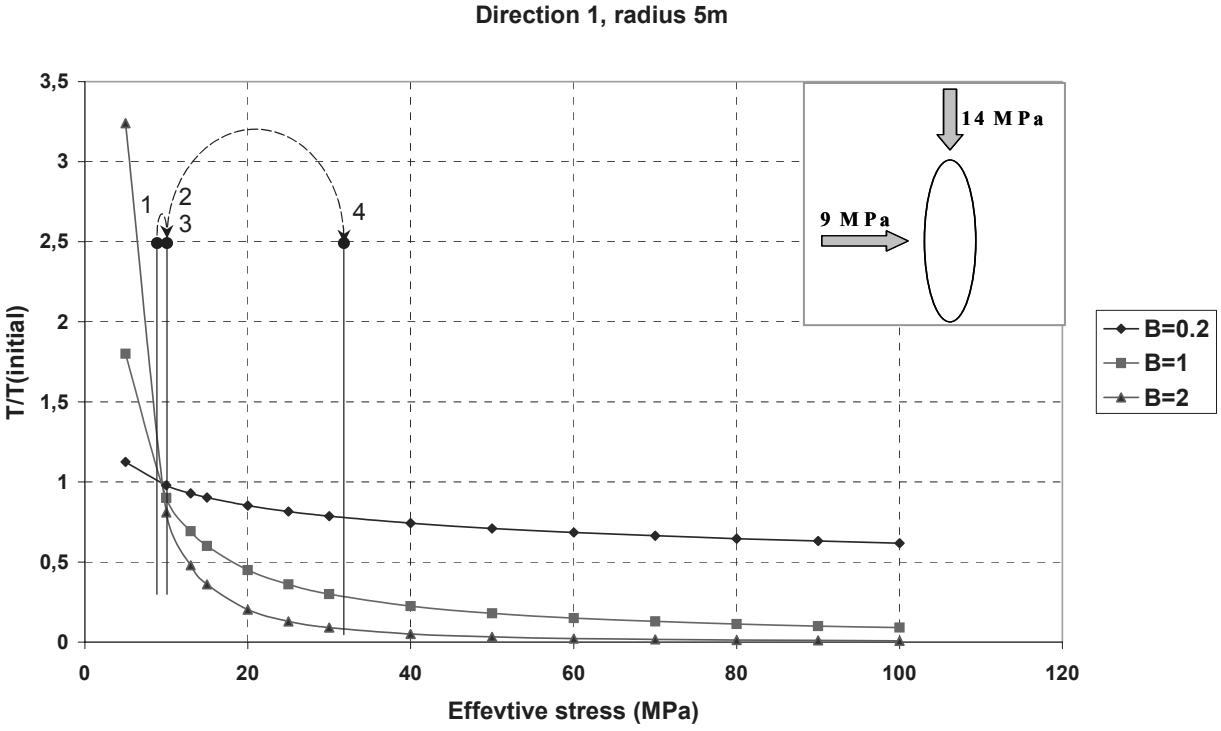
Direction 1, radius 5m
T/T(initial)
Effevtive stress (MPa)
14 MPa
9 MPa
1
2
3
4
B=0.2
B=1
B=2

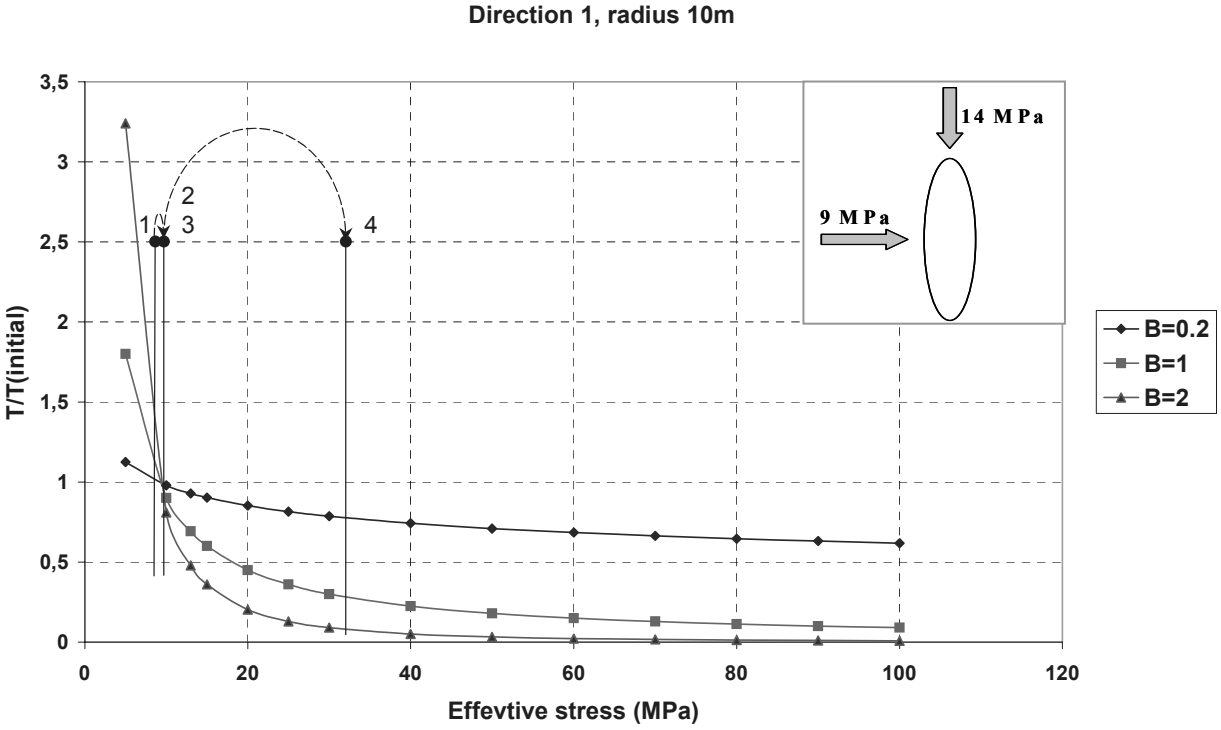
Direction 1, radius 10m
T/T(initial)
Effevtive stress (MPa)
14 MPa
9 MPa
1
2
3
4
B=0.2
B=1
B=2

Direction 2. Vertical fracture that strikes parallel to the maximum principal stress

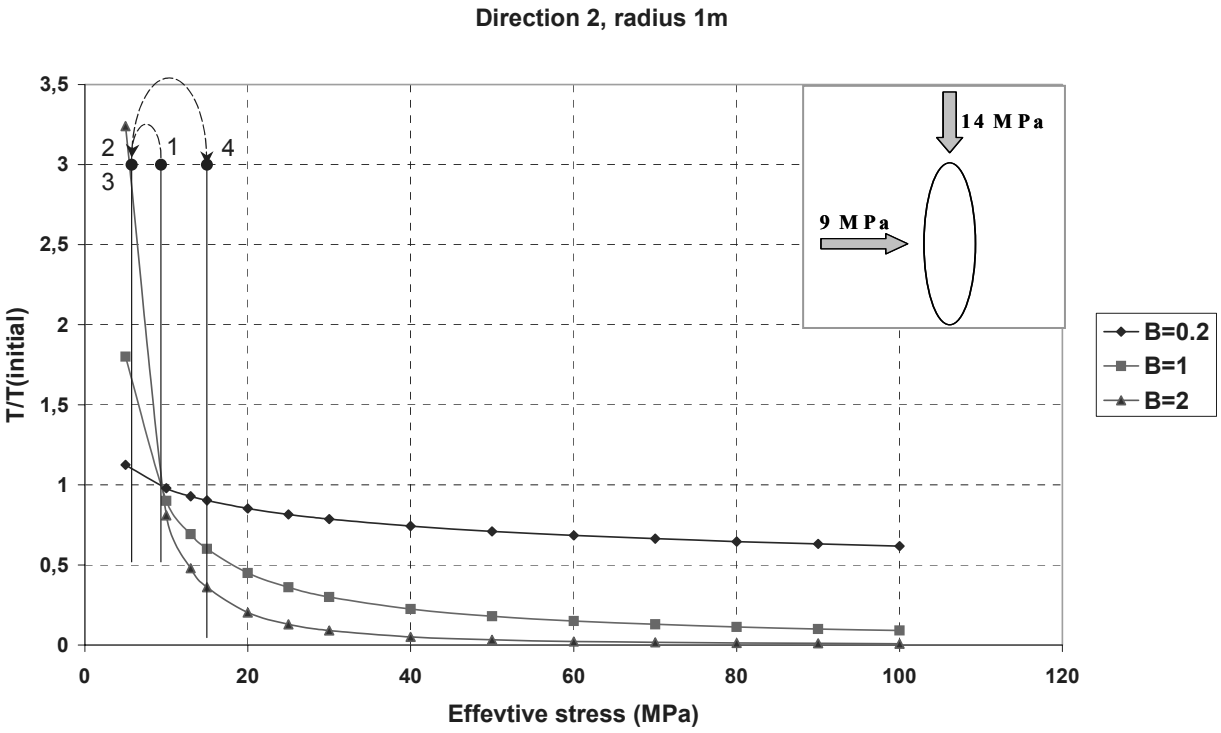

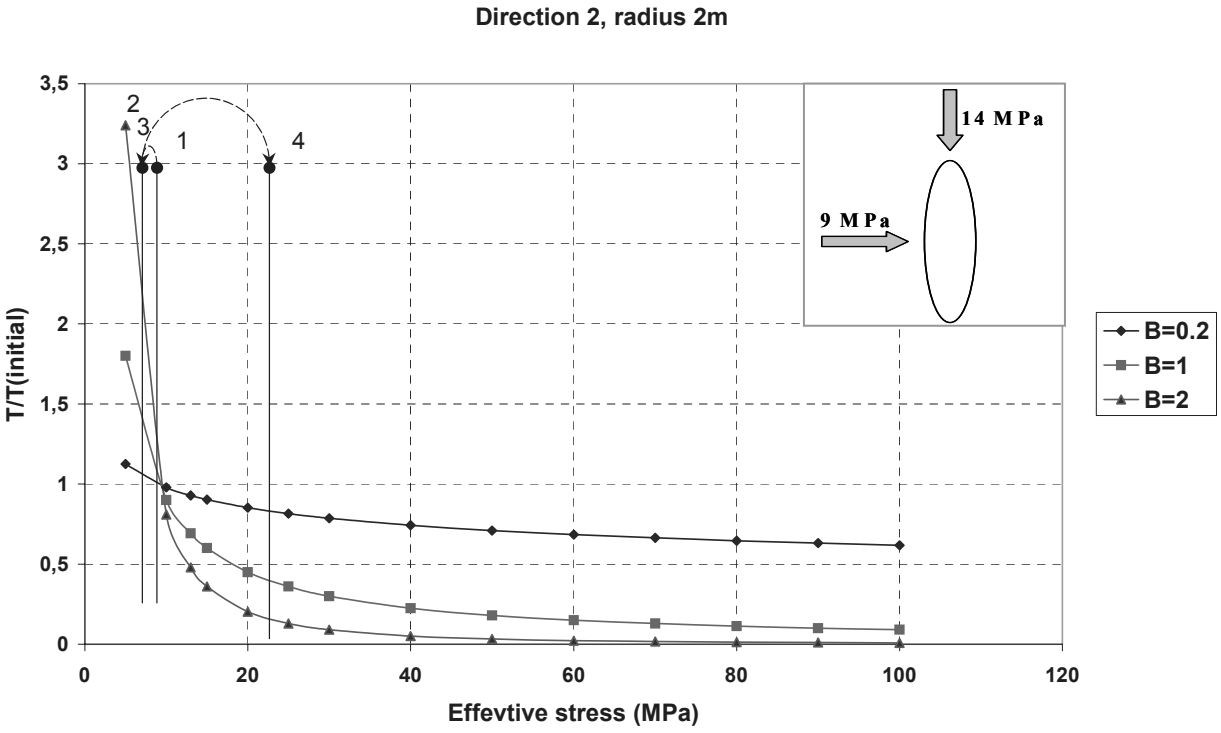

Direction 2, radius 5m

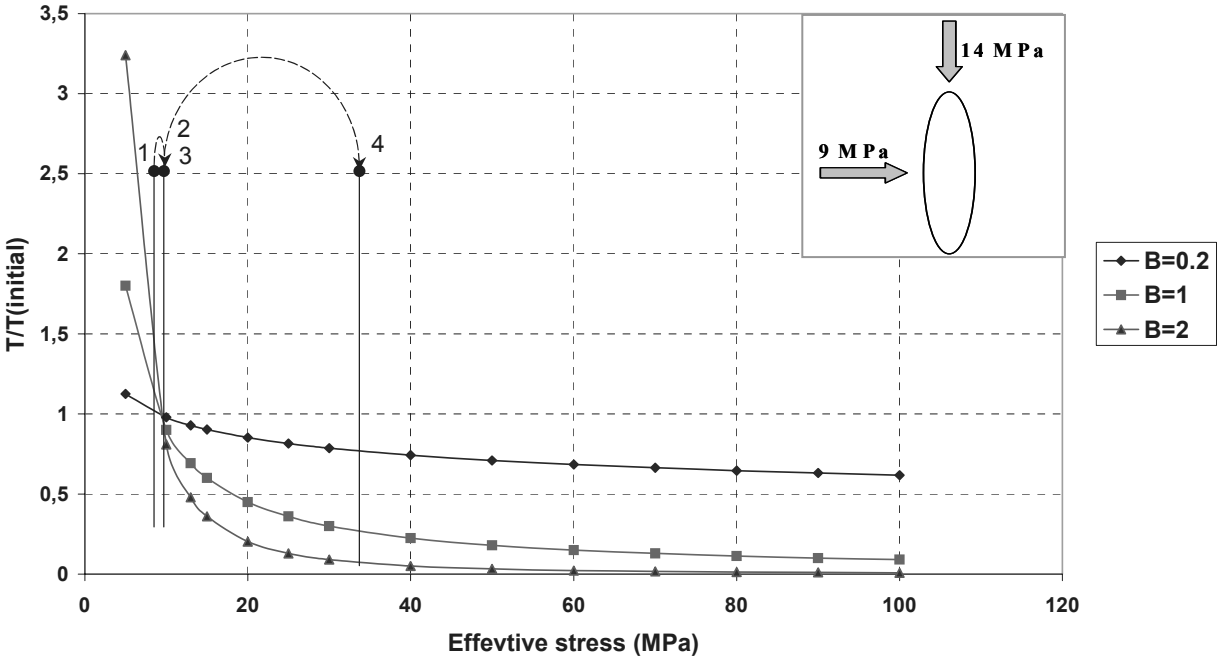

Direction 2, radius 10m

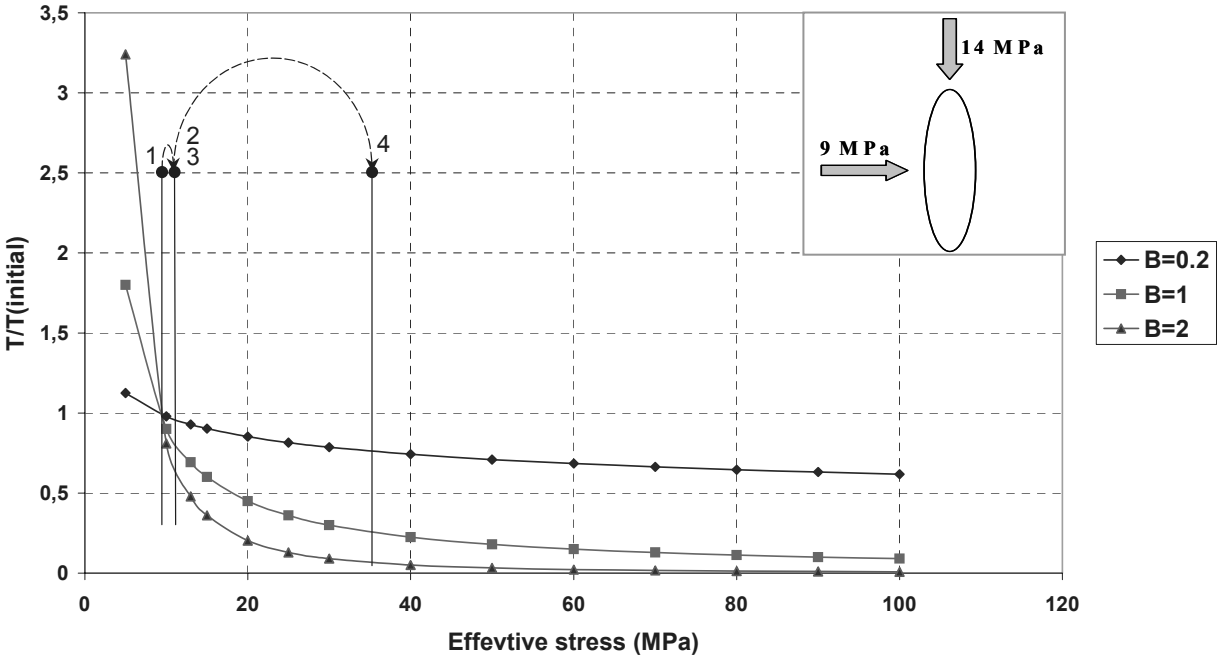

Direction 3. Vertical fracture that strikes parallel to the maximum principal stress.

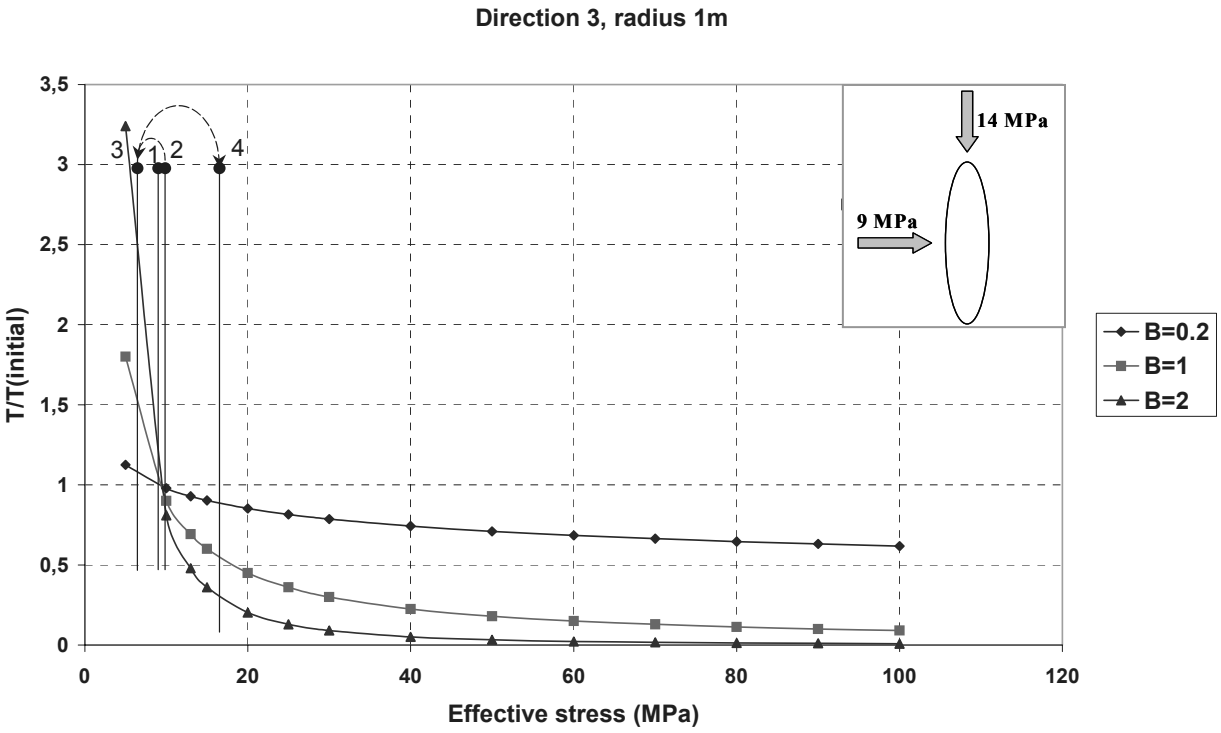

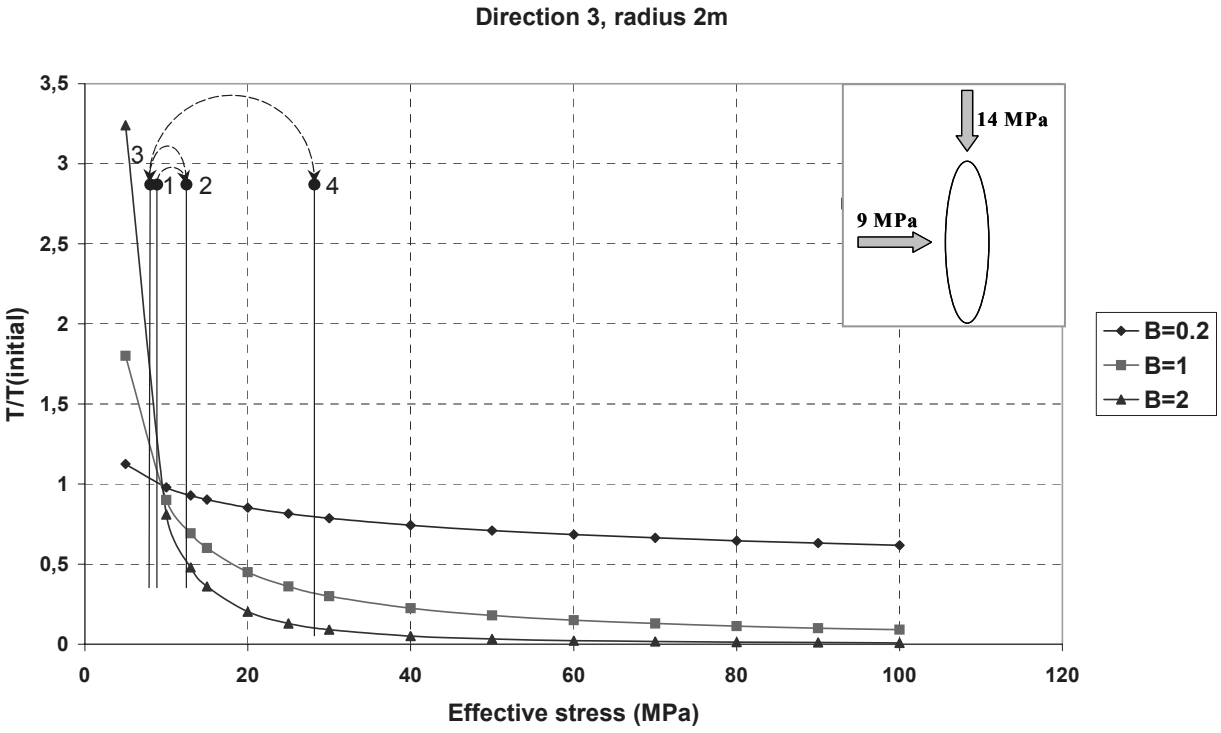

Direction 3, radius 5m

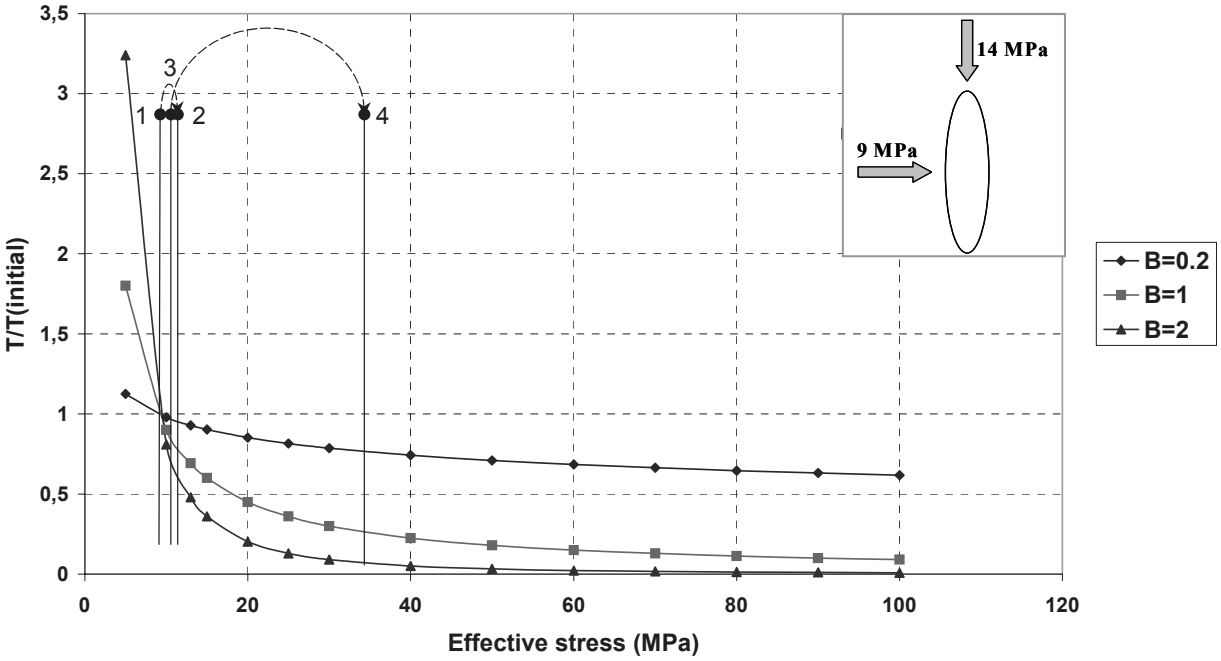

Direction 3, radius 10m